Assessment of the Thermal Efficiency, Structure and Fire Resistance of Lightweight Building Systems for Optimised Design

Aitor Amundarain

Doctor of Philosophy

The University of Edinburgh

2007

To aita Rafael, amatxo Maribel, Iker, Ioseba and Naiara.

Declaration

This thesis and the research described and reported within have been completed solely by Aitor Amundarain under the supervision of Professor Jose L. Torero and Dr. Asif S. Usmani. Where other sources are quoted, full references are given.

Aitor Amundarain
April, 2007

Abstract

The use of lightweight building systems is very controversial as existing knowledge about their performance is limited. Not enough research has been conducted to determine the suitability of these modern construction technologies and there is an ongoing controversy as to whether they are an appropriate replacement to traditional construction techniques. The most extensively used lightweight building systems involve the utilization of timber and steel as framing elements. The performance on both types of assemblies is regulated by applicable building regulations or regional laws. Compliance with law does not however preclude the need for their intrinsic characteristics and capabilities to be researched and eventually understood.

The prime objective of this study is to present a number of methodologies to assess lightweight external walling systems focusing on thermal efficiency, structure and fire performance, which are currently the main driving forces for this industry. Traditionally, these areas have been studied separately but there is a need to integrate them in order to get comprehensive solutions to the way these systems are designed. The drive to achieve improvements in one of these specific areas could potentially result in reduced effectiveness in the others. That is the reason why an integrative approach is recommended. These techniques are meant to be applied in the design phase of building projects so as to provide early quantitative information about the systems analyzed.

The methodologies described herein are then applied to real life light steel building solutions. Within this context, two different wall constructions are examined and conclusions made on their relative performance. The study

highlights the importance of having analytical and experimental solutions as a framework for further development. Two different approaches have been considered to assess thermal efficiency, structure and fire performance. On the one hand, a prescriptive approach has been employed to establish regulation compliance. On the other hand, a performance based approach is taken to actually understand and explain how these systems work in real life conditions. The outcome is a comprehensive set of tools to assure both industry and other stake holders.

The insulating properties of the structure need to be optimised in order to minimise heat loss. The process involves the definition of the type, quantity and arrangement of the constitutive materials to arrive at the most effective configuration. The standard methodology to determine the thermal performance is the quantification of a thermal transmittance coefficient commonly referred to as a U-value. These can be established using numerical tools or well defined experiments. The link between the two approaches has not been completely established, mainly due to poorly defined experimental boundary conditions. The need to build an apparatus capable of experimentally calculating the U-Value of lightweight building systems was therefore identified and subsequently implemented. A guarded hot-box that satisfies closely the criteria given by British Standards was constructed as an exemplar for quantitative assessment. The experimental results were then used to establish the validity and limitations of computer models. Three different commercial models were used, HEAT2, HEAT3 and ABAQUS as examples.

A well defined methodology for thermal performance assessment paved the way to shift focus to fire performance. Traditionally, fire performance is evaluated by means of large scale tests. Numerous studies have established the limitations of these tests as quantitative performance assessment tools. Therefore, for purposes of a systematic analysis, small scale experiments

and validated mathematical models have been advocated as a quantitative means to predict fire performance. The development of an engineering methodology for predicting the fire resistance of lightweight assemblies has been defined and a number of tests have been conducted to demonstrate its reliability. The results have been used to predict test behaviour and performance under real fire conditions. A full scale real fire experiment has been carried out in order to analyse the performance of lightweight external walls under the action of actual severe fire conditions. The results of the afore-mentioned tests were used to correlate with the predicted performance derived from the small scale tests.

Extensive knowledge about structural behaviour of lightweight construction systems under ambient conditions exists. There are a number of existing protocols that facilitate the design process of lightweight assemblies. Conversely, there is a lack of knowledge about structural performance under fire conditions. Given the well characterized evolution of the thermal field in the system a structural performance analysis could be conducted.

Publications

Conference Papers

Amundarain A., Torero J.L., Usmani A., Al-Remal A.M. Assessment of the thermal efficiency, structure and fire resistance of lightweight building systems for optimized design. THE THIRD INTERNATIONAL CONFERENCE ON STRUCTURAL ENGINEERING, MECHANICS AND COMPUTATION. SEMC 2007. Cape Town, South Africa (September 2007)

Rein G., Abecassis-Empis C., Amundarain A., Biteau H., Cowlard A., Chan A., Jowsey A.I., Reszka P., Steinhaus T., Welch S., Torero J.L., Stern-Gottfried J., Coles A., Lazaro M., Alvear D., Capote J.A., Ryder N.L., Mowrer F., Hostika S., Lautenberger C., Joyeux D., Kumar S. Round-Robin Study of Fire Modelling Blind-Predictions Using the Dalmarnock Fire Experiments. 5TH INTERNATIONAL SEMINAR ON FIRE AND EXPLOSION HAZARDS, Edinburgh, UK, (April 2007).

Amundarain A., Torero J.L., Usmani A., Al-Remal A.M. Light Steel Framing behaviour on fire: Fire Performance Test approximation and full scale real fire experimental results. THE STATE OF THE ART FIRE SAFETY CONFERENCE, Madrid, Spain (March 2007)

Amundarain A., Torero J.L., Usmani A., Al-Remal A.M. Light Steel Framing in Fire: Challenges for a New Technology. FIRE IN TALL BUILDINGS CONFERENCE 2006, Santander, Spain (October 2006)

Amundarain A., Torero J.L., Usmani A., Al-Remal A.M. Thermal Efficiency and Fire Performance of Light Steel Framing: Challenges for a New Technology. WORLD CONFERENCE ON ACCELERATING EXCELLENCE IN THE BUILT ENVIRONMENT – WCAEBE 2006, Birmingham, UK (October 2006)

Amundarain A., Torero J.L., Usmani A., Al-Remal A.M. Light Steel Framing: Improving the Integral Design. GLOBAL BUILT ENVIRONMENT CONFERENCE - GBEN 2006, Preston, Lancashire, UK (September 2006)

Acknowledgements

First of all I'd like to thank my supervisor, Professor Jose L. Torero for his support, valuable insight and patience. It has been a pleasure to work with somebody with such professionalism and personal skills. I would also like to thank my industrial supervisor Mr. Ahmad Mejbas Al-Remal for his incredible guidance, expert advice and kindness. This would not be possible without your help.

I would also like to thank Dr. Asif Usmani and my industrial supervisors, Mr. Domenic Tedesco and Mr. Bill Rutherford for their kindness and patience. Thank you also to Dr. Gerry Black for his time and support. This research was funded by Knowledge Transfer Partnership and is gratefully acknowledged. Thank you to Powerwall Systems Ltd for their support.

Thank you to the undergraduate students Ruth Bradley, Ross Byron, David Quinlan, Mary Ring and Fabrice Khan who have helped me with this research. Sorry for being such a persistent perfectionist but I cannot help it. Thanks also to Dr. Guillermo Rein, Alan Chan, Pedro Reszka and the rest of the Fire Group at The University of Edinburgh for helping me with my research and for all those good moments we have spent together.

Special thanks to my parents, brothers and my friends in Spain and London for their support in the last three years. And finally thank you Naiara for being that understanding and for the future.

Contents

List of Figures

List of Tables

Nomenclature

A	Area (m^2)
Bi	Biot number
C	Volumetric heat capacity (J/m^3K); C-Factor
c_p	Specific heat (J/kgK)
F	Force (N)
Gr	Grashof number
g	Gravitational acceleration (m^2/s)
H	Height (m)
HF	Heat Flux Meter
h	Heat transfer coefficient ($W/m^2.K$)
h_c	Convective heat transfer coefficient ($W/m^2.K$)
h_r	Radiation heat transfer coefficient ($W/m^2.K$)
k	Thermal conductivity (W/m.K)
L	characteristic length (m)
LSF	Light Steel Framing
m	mass (kg)
$\dot{m}$	mass flow rate (kg/s)
Nu	Nusselt number
Pr	Prandtl number
P	Pressure (N/m^2)
Q	Heat transfer rate (W)
q''	Heat flux (W/m^2)
r	Radius (m)
R	Thermal Resistance (m^2K/W)

R-Value	Total Thermal Resistance (m^2K/W)
Ra	Rayleigh number
Re	Reynold's number
T	Temperature (^oC) and (K)
t	Time (s)
TC	Thermocouple
U-Value	Thermal transmittance (W/m^2K)
V	Volume (m^3)
X, Y, Z	Rectangular coordinates
x	Length (m); thickness (m)

Greek letters

α	thermal diffusivity (m^2/s)
β	Volumetric thermal expansion coefficient (K^{-1})
δ	Thickness (m)
ε	Emmisivity
μ	Viscosity (kg/s.m)
ν	Kinematic viscosity (m^2/s)
π	pi
ρ	Density (Kg/m^3)
σ	Stefan-Boltzmann constant
τ	Thermal time constant
Δ	Change in
ϕ	Heat transfer rate (W)

Subscripts

a	Ambient, adjacent air
c	Convection; cold box
conv	Convection
crit	Critical
e	Environmental
f	Furnace
g	Gas
L	Lateral
lab	Laboratory
m	Metering box
max	Maximum
min	Minimum
net	Net
p	Pressure
r	Radiation; baffle
s	Surface; specimen
0	Initial conditions

Chapter One

1. Introduction

1.1. Background to the project

The use of lightweight building systems is very controversial as existing knowledge of their functionality is limited. More extensive research is required to determine the suitability of these modern construction technologies as a replacement for traditional construction techniques [1]. There are confronting opinions among architects who are reluctant to accept these new tendencies without sufficient supporting information and engineers who are pushing for a more manufacturing approach for the sector [2].

The most extensively used lightweight building systems involve the use of timber and steel as framing elements. These assemblies must comply with building regulations and provide a desirable performance. Even when fully compliant, their intrinsic characteristics and capabilities still need to be profoundly researched and fully understood. This will facilitate decision making when investigating potential improvements.

Potential improvements could be incorporated at any stage of the building life time. Experience has shown that they make an important impact when adopted at early stages [3]. This is why most of the efforts to achieve a more efficient construction technology are recommended at the design stage. This applies to aspects such as thermal efficiency, sustainability, fire performance, structural behaviour, sound transmission, vibrations, etc.

1.2. Objectives of the research

The objective of this study is to provide by means of quantitative methodologies a performance assessment of lightweight external walling systems focusing on thermal efficiency, structural and fire performance. These areas are currently the main driving forces for this industry and the

international research community. Traditionally, these areas have been studied separately but there is a need to integrate them in order to gain a comprehensive understanding of the way these systems behave, which will in turn lead to better design and construction. The drive to achieve improvements in one of these specific areas could potentially result in degrading the performance of another, hence the integrated approach.

These novel methodologies are meant to be applied in the design phase of the project so they provide quantitative information about the systems analyzed. They enable rationally-based modifications to these assemblies, which could then be incorporated to enhance the quality of the final product. These methodologies have been tested on actual lightweight construction systems and provided satisfactory results. They have proved to be sound and robust and in addition, are viable and cost effective. Figure 1 shows a flow chart describing how those methodologies must be applied.

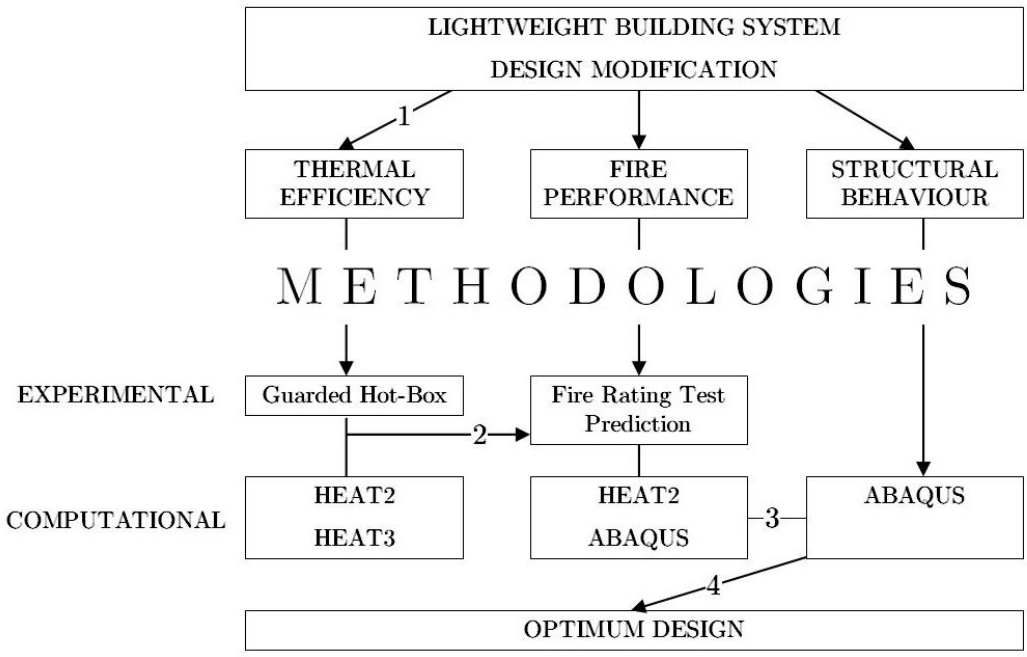

Figure 1: Methodologies to Assess Light Construction Systems - Flow Chart

1.3. Project Nature

The afore-mentioned methodologies have been implemented on a specific type of light steel framing (LSF) structures. Extensive conclusions have been drawn that establish the grounds to extend the use of these methods on any other lightweight construction technology. The motivation to find comprehensive solutions has pushed the project to focus the analysis on the most critical sections in this type of assemblies, external walls [4].

Lightweight external walls can either be load bearing or non-load bearing (infill walls). External load bearing walls are used in low rise buildings (up to a maximum of six storeys in most applications). Complete buildings, including roof and floor members, have been successfully built using LSF in a similar manner to timber framed construction [5]. Due to improvements in the way LSF is designed and its self containment they are being incorporated in low and high rise constructions as infill walls [6]. Partition walls are not analyzed in the present study due to extensive existing literature but their functionality could be assessed using the same tools presented in the following pages.

1.4. Outline of Chapters

Two different approaches have been considered to assess thermal efficiency, structural and fire performance. The first is a prescriptive approach that indicates the extent of compliance with building performance regulations. The second is a performance based method that demonstrates how these systems work in real life conditions. Together they form a comprehensive set of tools to inform both industry professionals and end users. Chapters 2, 3 and 4 include a preliminary introduction and a comprehensive literature review for each of the topics mentioned before.

Chapter 2

Lightweight Building Systems Thermal Efficiency

The insulating properties of the structure need to be maximized in order to reduce heat losses, through various alternatives affecting the type, quantity and arrangement of the constituent materials used. In order to find the most effective configuration, an apparatus capable of experimentally determining the U-Value [7] also known as thermal transmittance of lightweight building systems was designed and constructed. This relative property is defined by building regulations [8] and compliance is currently demonstrated mostly by computational means. A guarded hot-box that satisfies closely the criteria given by British Standards [9] was used to obtain experimental results and subsequently validate the detailed finite element computer modelling that was also undertaken.

Chapter 3

Lightweight Building Systems Fire Performance

Full scale Fire Rating Tests [10] are traditionally carried out to establish fire ratings that are meant to be satisfied by all construction elements. However, they are relatively too complex and time consuming to be conducted to promote understanding of performance or support design. As a more comprehensive and versatile alternative, small scale experiments and validated mathematical models have been used as a replacement means to predict performance [11]. The development of an engineering methodology for predicting the fire resistance of lightweight assemblies is suggested and a number of tests are conducted to prove its reliability.

Fire rating tests or small scale tests do not fully represent the conditions encountered in real fire scenarios, therefore methodologies involved in assessing real fire performance need to be validated for full scale real life fire scenarios [12]. Tests involving full scale fires are not normally viable

due to economical, environmental and safety reasons. During the course of this research, resources were made available for an experiment of this scale to be carried out in order to analyse the performance of LSF self contained walls under the action of actual severe fire conditions [13].

Chapter 4

Lightweight Building Systems Structural Behaviour

The structural behaviour of lightweight structures at ambient temperatures has been studied extensively by many research organizations. There are also a number of existing protocols [14;15] that facilitate the design process of LSF assemblies. Their validity is not questioned by this work but there is a lack of knowledge about structural performance of lightweight structures under fire conditions. The focus of this research has been on steel framed structures and computational work has been conducted to support the general understanding of the structural performance of these elements under fire conditions..

Chapter 5

Discussion of Results, General Conclusions and Further Work

The methodologies suggested in the previous chapters and the results obtained are commented on from an integrative viewpoint and general design conclusions are discussed. Further work is also suggested.

1.5. Introduction to Light Steel Framing

Light Steel Framing (LSF) is a novel construction technology that has been extensively used in cold climate countries due to its good thermal and structural behaviour. This modern building technology entered the British market a few years ago and it is gaining great popularity and credibility. The current tendency of the LSF industry is to transform the construction practice adopting a more off-site manufacturing approach [2]. This gives

versatility to the LSF production and consequently a solution for the lack of qualified work force.

Lightweight construction is a building technique based around vertical structural members called studs, which provide axial load-bearing capacity and stiffness to the structure. The studs are connected together by trusses or noggins in order to enhance structural resistance and control lateral deformation of the whole structure. The empty space left around the steel frame is usually filled up with thermal, acoustic and fire resistant insulation and finally covered by various sheathing materials. The stages in the assembly process of LSF structures are shown in Figure 2.

Figure 2: LSF Assembly Process

The popularity of LSF assemblies is increasing because they provide the following advantages [2; 16]:

- *Lower cost*. LSF walls are light weight compared to other assemblies, hence saving on foundation and handling costs. Steel prices are very stable. Steel is 100% recyclable and does not rot, nor allow growth of mildew. Design life is long and maintenance is rarely required.

- *Ease and quality of construction*. Manufacturer-controlled material properties eliminate grading and site quality checks. Geometry is very accurate. Members are cut to size with pre-punched assembly and service holes. Due to steel's uniformity and stability in dimension, there is little chance for gaps to form as a result of shrinking or warping. This will reduce the likelihood of air infiltration.

- *Stability and strength*. Steel is dimensionally stable which greatly reduces the need for movement joints. Strength of the assembly does not normally degrade with time.

Examples of LSF projects [16] are the Greenwich Millennium Village in London (low-rise and high-rise development), Ocean Terminal in Edinburgh (8 storey high flatted development) or Lancefield Quay in Glasgow (16 storey development and two storey marketing suite), which are shown in Figure 3.

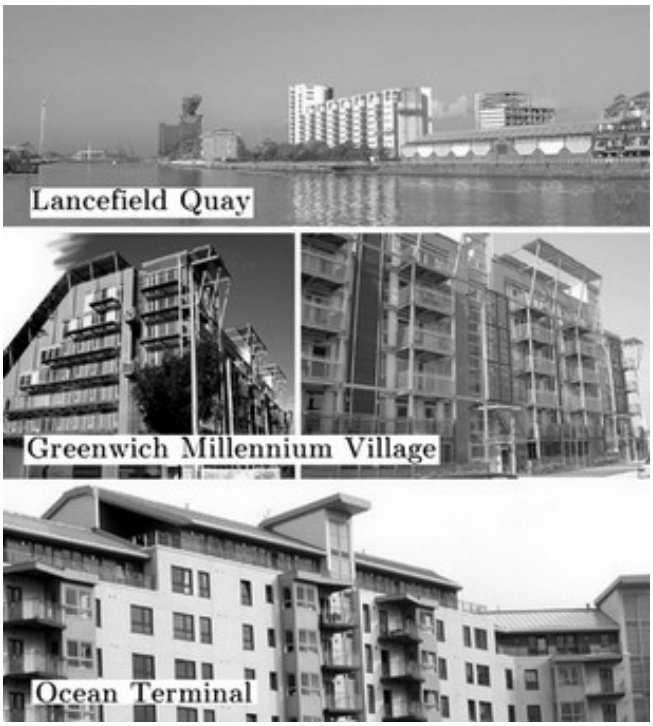

Figure 3: LSF Finalized Projects

The main disadvantage of this technology is based on durability issues. The durableness of this type of constructions has not been quantified yet because not enough time has passed from the construction of the first LSF units. This has pushed architects to still prefer traditional building techniques. With the on-going research on these building technologies, durability is proving to be acceptable because condensation and corrosion problems do not appear anymore. Architects, designers and society need to change their approach towards sustainable housing by accepting a limited life time for new constructions.

1.6. Reference System Descriptions

Two actual LSF systems known as New and Old System have been employed as a reference to verify the reliability of the various methodologies suggested in this research. They are appropriate and representative examples that serve to show the impact of different design considerations in the actual performance of the assembly. Figure 4 and Figure 5 show a sketch of these LSF walls. The existence of a drainable cavity in external walls is necessary [17] to take away any content of water that could accumulate within the wall due to diverse factors such as condensation, infiltration, etc. LSF constructions have traditionally been completed with brick work in the outer side of the external walls [18], however constructions with new insulating materials with impact absorption properties is being increasingly used.

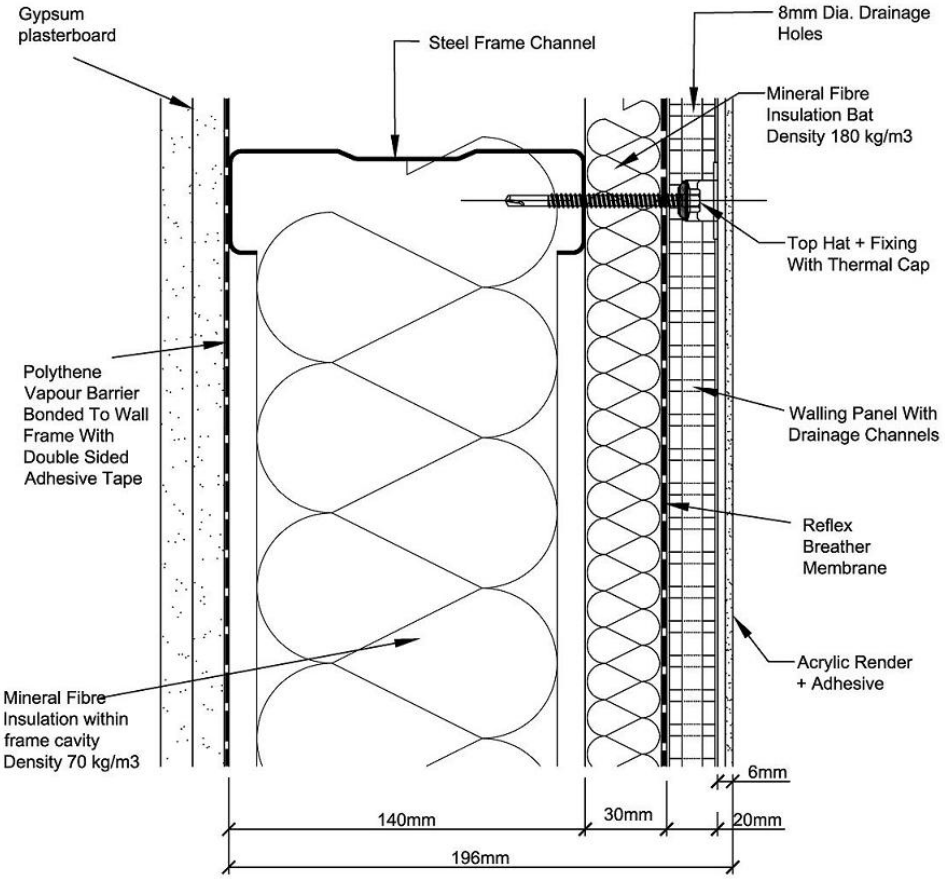

Figure 4: New System Frame Build Up

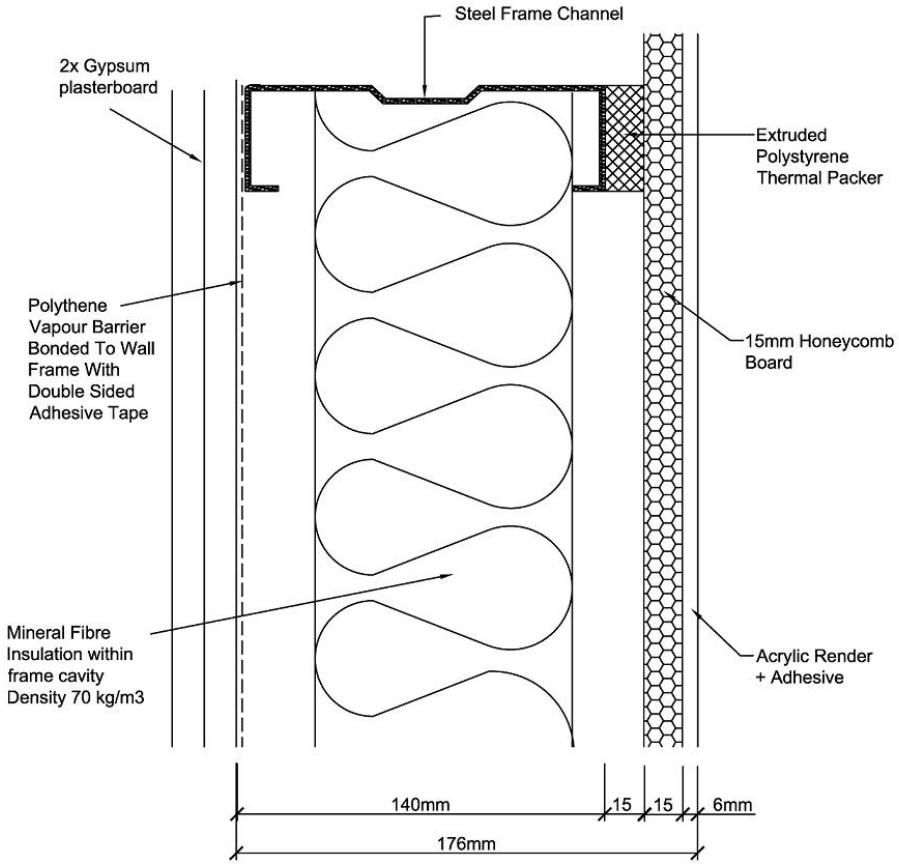

Figure 5: Old System Frame Build Up

Two overlapped layers of plasterboard [19] are fixed mechanically to the steel frame in the internal side of the assembly. This configuration is broadly used in the LSF construction market. These are 12.5 mm thick with a density of 650 Kg/m^3 at ambient temperature. Self screws [20] with a separation of 300 mm from each other are used to attach them to the frame. The generic thermal conductivity of the plasterboard at ambient temperature is 0.25 W/m·K.

The external surface is made of an aluminium honeycomb panel to which an adhesive and a render coat are applied. The reason why honeycomb panels are used is based on a reduction of the qualified workforce, which is needed in case of using bricks or other type of configurations. Mechanical

fixings with proprietary thermal caps at 600 mm separations have been used to fix it to the frame before applying the external coating. The thickness of the honeycomb is 15 mm in the Old System and 20 mm in the New System. They also differ in their functionality. The honeycomb in the New System has been drilled vertically and horizontally in order to generate a drainable membrane that works as a semi-ventilated cavity by itself in order to satisfy the requirements of the National House Building Council, NHBC [17]. The weight of the aluminium alloy per square metre of honeycomb is 2 kg in both cases and they are finished with a 0.5 mm layer of fibreglass.

The steel frames are built using C sections with an indent in the centre part of the web as shown in Figure 6. Galvanized steel [21] 1 mm thick has been used. The separation between studs is kept constant at 600 mm and noggins as bracing elements have been employed to provide lateral and torsional restraints to the assembly. These are placed at a height of 1500 mm as per manufacturer's standards. The thermal conductivity of the steel used is 60 W/m·K and the density is 7850 Kg/m^3.

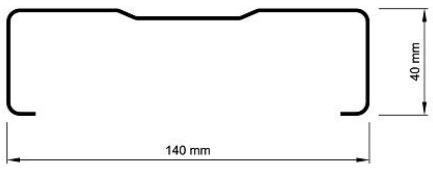

Figure 6: Steel Profile Cross Section

The frames are attached to the floor and ceiling using mechanical fixings that depend on the construction of floor and ceiling. Bats of mineral wool 120 mm thick and density 70 Kg/m^3 [22] are used to insulate the internal space left between the steel work in the New System, which also has an external layer of mineral wool 30 mm thick and density 180 Kg/m^3 [22]. This replaces the polystyrene strips [23] used in the Old System. The

thickness of the mineral wool used in the Old System is 100 mm with the same density as the New System. The thermal properties of the mineral wool vary with the density. The thermal conductivity at ambient conditions is equal to 0.033 W/m·K for the denser mineral wool and 0.031 W/m·K for the other.

The main difference between the Old and New systems is the substitution of a combination of polystyrene channels and a honeycomb panel in the former, for a self-drainable honeycomb panel and a thin layer of mineral wool in the later. This modification contributes to the improvement on the performance of the original LSF system as it is shown in further pages. One of the objectives of this research is to illustrate how slight modifications in the design influence the thermal efficiency, fire performance and structural behaviour so optimization can be achieved.

The thermal properties given above correspond to those required to understand the thermal performance of any external wall at steady state conditions. These are important for situations in which there is no variation of temperatures within the specimen analyzed such as Hot-box experiments. Additional information about thermal properties is needed for transient fire conditions. In addition there is a need to understand how these properties change with temperature, all of which is explained in further sections. The same applies to structural properties.

1.7. Software and Computer Modelling Tools

A preliminary analysis of various software packages was conducted to work out their convenience and reliability when applied to the conditions encountered in the experiments and in real life situations. These are listed in Table 1 and extensive information about their theoretical basis and

capabilities can be found in the respective manuals and the supportive references.

Software Package	Thermal analysis	Structural analysis	Non linearity	3D	Interface	Numerical Method
HADAPT [24]	Y	N	N	N	Linux	FEM
HEAT2 [25]	Y	N	N	N	Windows	FDM
HEAT3 [26]	Y	N	N	Y	Windows	FDM
TRISCO [27]	Y	N	Y	Y	Windows	FDM
ABAQUS [28]	Y	Y	Y	Y	Linux/ Windows	FEM

Y = yes; N = no; FEM = Finite Element Method; FDM = Finite Differences Method

Table 1: Software Packages Considered

All the software packages listed in Table 1 were subjected to assessment by solving a number of benchmarks that represent every thermal condition that could be encountered in the experiments. One, two and three dimensions, steady and transient, ambient and high temperatures situations were analyzed for the different software packages when solving the benchmarks and the following conclusions were drawn.

HADAPT [24] has proved to be a very accurate numerical model developed on FORTRAN. Non linearity and cavity radiation cannot be modelled, which limits its usage. In addition, any geometry and model modifications that can be easily implemented with other software packages require an extensive knowledge of FEM and code programming.

HEAT2 and HEAT3 [25; 26] have proved to be very accurate when solving ambient temperature problems in 2 and 3 dimensions respectively. The

solutions obtained from the benchmarks have been contrasted with other robust packages such as TRISCO and ABAQUS giving close results. The main disadvantage lays in the impossibility to model non linearity of material properties. This affects fire analysis but it is acceptable for Hot-box experiments where constant material properties are assumed.

ABAQUS [28] has been found to be the most robust software package and it is extensively used throughout the research. Non linearity of material properties can be modelled. Its only weakness is with regards to the inability to couple thermal and structural analysis when modelling cavity radiation. The analysis must be executed in two steps, an initial thermal analysis where the temperature for each of the nodes is calculated as a function of time, which is later used as an input for a subsequent structural analysis.

Chapter Two

2. Lightweight Building Systems Thermal Efficiency

2.1. Background to Thermal Efficiency

The world community is undertaking initiatives to reduce energy consumption and thereby greenhouse gas emissions. All the countries under the Kyoto Protocol [29] have agreed a target to cut greenhouse gases by 12.5% by 2008-2012 and move towards a domestic goal of a 20% cut in carbon dioxide (CO_2) emissions by 2010. With issues such as global warming, energy efficiency and affordable housing that are of paramount importance in this age, efforts to address these challenges through improvement of the construction technologies are essential. This is therefore stimulating new international directives, revision of national energy codes and the need to produce new building materials and products to achieve more sustainable building techniques.

Energy used in dwellings accounts for about 30% of all energy consumed in the United Kingdom [30] and a similar proportion of energy-related emissions of carbon dioxide to the atmosphere. This corresponds to 20 million tons of CO_2 released to the atmosphere per year as a result of the heating of buildings, which is equivalent to 17 billion pounds. By incorporating at the planning stage low-energy design elements into new build and refurbishment schemes, architects and specifiers have a unique opportunity to reduce a dwelling's energy use before construction even starts. The user aims to achieve a required indoor climate by minimising cost and energy consumption of the building.

External walls and their insulating value contribute to the overall energy performance of a home and represent approximately 25% of the total heat loss [4]. By improving the thermal insulating properties of the external walls, enhancements in construction sustainability can therefore be achieved. The thermal insulation of the building envelope can be characterised by several related parameters. The Thermal Transmittance

(U-Value) is extensively used in Europe, whereas the Total Thermal Resistance (R-Value) is commonly employed in America. These are reciprocal global properties of the building envelope.

The Thermal Transmittance is a measure of how much heat will pass through one square metre of a structure when the air temperatures on either side differ by one degree (W/m^2K). Therefore, lower U-Values or higher R-Values signify better levels of insulation. Environmental temperatures are considered for the analysis to account for the existence of potential thermal bridges, which cause higher rate of heat transfer by conduction in specific areas of the structure. This phenomenon is characteristic of lightweight building systems due to the specific thermal properties of the frame in opposition to those of the insulating materials.

When experimentally and computationally calculating these parameters, the existence of thermal bridges makes it difficult to establish average surface temperatures. It is necessary to move one step back and consider the temperatures of the gas phase and solid bodies around the internal and external surfaces for the analysis, which are directly influenced by the characteristics of the structure and the apparatus employed to asses the specimen. Despite the minimization of temperature determination errors, both convection and radiation heat transfer modes in and through the gas phase now need to be considered in order to get representative results.

The ability to make precise and reproducible measurements of the appropriate thermal performance property is essential to understand and improve the thermal efficiency of the existing and new construction technologies. Both experimental and computational work need to be coupled with real life conditions so comprehensive solutions can be suggested. The need to build an apparatus capable of experimentally calculating the U-Value of lightweight building systems was identified and

eventually implemented. A guarded hot-box that satisfies closely the criteria given by British Standards [9] was constructed, calibrated and a series of tests were conducted in order to validate the computer models suggested.

2.2. LSF Thermal Efficiency Literature Review

The USA was one of the first countries to start using LSF for residential purposes, which led to the need for categorising the thermal efficiency of external walls above a required minimum. R-values were then derived [31] using experimental tests for various configurations of lightweight construction systems. The test results could then be compared to theoretical values obtained by applying emerging analytical solutions that were being developed such as the ASHRAE zone method [32; 33]. This method has been improved throughout the years in order to increase its accuracy reaching levels around 2% [34; 35].

The main constraint of these ASHRAE based zone methods is the limitation in the number of design variations that can be considered. The number of modifications that could be implemented in the design is unlimited and the number of possibilities that the method offers is restricted therefore the aid of numerical modelling was identified by the research community and most of the studies conducted in the last few years have considered these computational techniques to predict the thermal performance of lightweight building systems.

Other countries such as Canada, the Scandinavian countries, continental Europe, Japan and recently the United Kingdom have adopted this modern construction technology and thermal efficiency has become one of the main driving forces within the industry. The international research community is making an important effort to improve the thermal

performance by means of design modification. The thermal efficiency is calculated experimentally by using the Hot-box method [9]. There are not many organizations worldwide that have an apparatus of such characteristics. However, the existing ones are actively researching the sustainability of lightweight construction systems. Most of the main organizations and most importantly, their unique facilities are discussed in the following paragraphs.

Kosny *et al* [36] and Williams [37] describe the characteristics of their rotatable guarded box at The Oak Ridge National Laboratory (USA) and the National Physical Laboratory (UK) respectively. Shah and Curcija [38] provide technical details about their guarded Hot-box at the University of Massachusetts (USA). Fazio *et al.* [39] also explains the design and development of a Hot-box built by the Canadian Centre for Building Studies. Goufeng [40] and Rose [41] explain the characteristics of their apparatus developed at the Division of Building Technology in Stockholm (Sweden) and the Department of Buildings and Energy at the Technical University of Denmark subsequently. All these institutions and some others are directly involved in the development of new international standards.

Comparative analyses have been carried out to determine the sustainability of LSF construction systems. CSSBI [42] monitored the natural gas consumption of six bungalows in Toronto with the same characteristics and specifications, three of which were LSF and the rest were timber framed. They showed that the average gas consumption for the LSF homes was 7% less than for the wood framed homes. The CARB [5] carried out a similar analysis in Maryland with bigger size properties and the results showed that the steel framed homes consumed 33% less energy than the timber framed houses.

As the industry started to become more involved with using calculations and tests for U-value determination, a set of standards were devised so accurate and benchmark results could be obtained for future reference. BS EN ISO 8990 [43] and BS 874 [9] relate to the Hot Box and its calibration. BS 7501 [44] relate to the conditions that the laboratory must satisfy for entitlement to execute Hot-box experiments.

Most of the facilities mentioned above are diverting their research towards the behaviour of doors and windows. However, extensive work regarding lightweight structures sustainability is still taking place. Kosny *et al.* [45;46;47] have investigated the performance of LSF external walls, trying to reduce the heat transfer though the steel across the wall. The steel frame creates a thermal bridge and various methods were analysed to try and limit this. These methods consider insulating sheathing, spacers between sheathing and stud flange (distance washers, ridges or dimples along the flange, furring strips), reduction in the area of the web of the steel stud (holes or slits in the web) and different shapes of stud and local stud insulation (composite foam and steel stud). Different configurations have been tested experimentally, and all the above methods were found to reduce the thermal conductivity of the steel leading to a reduction in the thermal bridging occurring through the walling systems. The influence on fire and structural performance when implementing these methods has not been analyzed yet.

Hoglund and Burstrand [48] analyzed the behaviour of slotted steel frames to reduce thermal bridges and increase the thermal efficiency of external LSF walls. Similarly, Elhajj [49] and Kesti and Makelainen [50] analyzed the same principals and eventually draw similar conclusions. The aim of this project is to actually develop methodologies to assist the understanding of those principals and to asses the lightweight structures similar to those presented in these papers. N. Suda *et al* [51] tested a

number of different configurations of steel stud walls. The tests used slit openings, Z shaped studs, varying thickness and spacing of the studs, and varying spacing of the screws to fix the plasterboard to the wall, which do not significantly affect the thermal performance of the walling system.

Doran and Gorgolewski [52] developed a method to analytically asses U-Values of light steel-frame constructions similar to the ASHRAE zone method [32] and the BS EN ISO 6946 Method [53]. The method was validated using BS EN ISO 10211-1 procedures [54] but once again, the same limitations apply with regards to the number of modifications that could be recommended in the design process. These are good tools for use in regulation compliance but not for research purposes as they do not provide accurate quantitative information about design optimization.

Kosny and Desjarlais [55] take the analysis of individual lightweight walling systems further and analyse the influence of thermal anomalies due to building envelope subsystems or intersections with other surfaces. They included the effects of subsystems such as corners, window and door openings, and structural joints with roofs, floors, ceilings, and other walls. Although the information included in this research paper is relevant for future design, it is not essential for the scope of this project.

As the use of LSF became more popular, their improved thermal efficiency started to become recognised in several industrial articles. CSSBI [42], LSFA [56], RUUKI [57] and SCI [58; 59] reported how LSF walling when compared to traditional methods proved to be cheaper, quicker to construct, less wasteful, more profitable, and more importantly, more environmentally friendly. Such bulletins proved LSF walling systems are having a positive impact on the market.

2.3. LSF Thermal Efficiency Project Objective

The insulating properties of the structure need to be maximized in order to reduce heat losses, though these alterations can affect the type, quantity and arrangement of the constituent materials used. In order to find the most effective configuration, an apparatus capable of experimentally calculating the U-Value [7] also known as thermal transmittance of lightweight building systems was designed and constructed. This intrinsic property is limited by building regulations [8] and compliance is currently demonstrated by computational means. A guarded hot-box that satisfies closely the criteria given by British Standards [9] was used to obtain experimental results and subsequently validate the detailed finite element computer modelling that was also undertaken.

2.4. Hot Box Specifications

The following identifies and discusses all of the components that were selected to build a Hot-Box apparatus in order to accurately evaluate the thermal efficiency of light weight building systems. The Hot-Box apparatus allows the specimens to be tested under steady-state conditions, enabling reliable results to be obtained. In order to determine suitable methods of testing with the Hot-Box, BS EN ISO 8990 [43] and BS 874 [9] were reviewed and their principles were discussed.

BS EN ISO 8990 is a European Standard that has been given the status of British Standard for use in the UK. BS EN ISO 8990 is the equivalent of two parts of BS 874, namely Part 3.1-Guarded Hot-Box method and Part 3.2-Calibrated Hot-Box method. Although the last revision of BS EN ISO 8990 is a more recently published standard, this is less specific as it combines the two parts of standard 874 into one summary document. It is for this reason that standard 874 has been chosen for use in developing a Hot-Box that will produce accurate results.

2.4.1. Standard Overview

BS 874 [9] describes a number of methodologies for determining the thermal insulating properties of materials. The methods relevant to the Hot-Box specifications are the ones for calculating the thermal transmittance or U-value. These are the Guarded Hot-Box method and the Calibrated Hot-Box method. The Hot-Box methods use a hot and a cold chamber, which are both five-sided boxes, between which a test element is placed. The basis of the Hot-Box method is to determine the heat flow through a certain area of the test element, and the appropriate temperature difference across it. The temperature distribution must be at equilibrium (steady-state conditions), for the test to be valid. The calibrated and guarded hot-box methods differ by the way in which the heat flux through the specimen is estimated, as shown in Figure 7.

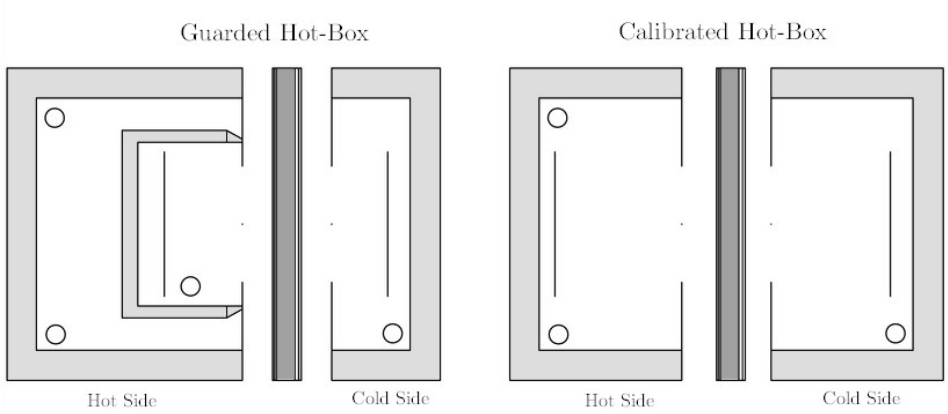

Figure 7: Calibrated and Guarded Hot-Box Methods

Figure 7 shows the Guarded Hot-Box apparatus, in which a hot inner chamber, known as the Metering Box, is surrounded by an outer chamber called the Guard Box. The Guard Box is maintained at the same temperature as the Metering Box to enable all the heat input to the inner box to pass through the test element, and not escape through the back and sides of the Metering Box. This allows a direct measurement of the heat flux through the test element. The guarded Hot-Box does not generally

require calibration but, due to the complexities of the apparatus design and operating procedures, checks with specimens of known thermal properties are advised to validate the method.

Figure 7 also shows the Calibrated Hot-Box, in which the heat input to the warm chamber is metered. In this method no outer guard box is provided, so corrections have to be applied to allow for heat flows through the sides and back of the hot chamber and at the edges of the test element. These corrections are determined by calibrating the apparatus with specimens of known thermal properties.

Both hot-box methods cover the same U-value and temperature range. The operational thermal transmittance range is between 0.1 and 15 W/m^2K. The operational temperature range is between -50 and 50 °C. These values are within the scope of the project. When thermal equilibrium is achieved, i.e. when the temperatures on each side of the test element and the heat flux through it are effectively constant, then the final measurements are taken.

2.4.2. Hot-Box Method Selection

It should be noted that with a suitable design, a given Hot-Box apparatus can operate in either mode, i.e. the inner metering box of a Guarded Hot-Box could be removed so as to work as a Calibrated Hot-Box. Although the calibrated hot-box offers a larger test area for a given size of test element, and has simpler control systems than the guarded hot-box, the decision to build a guarded hot-box has been made based on the following point stated in BS 874.

"To ensure that the heat flux through the test element is accurately determined in the calibrated hot-box, the heat exchange through the sides

and back of the metering box is measured and corrected for. This correction does not exceed 20 % of the total power supplied to the metering box."

Since the purpose of the apparatus is to test light weight external walls with similar, or possibly even lower, thermal transmittance than the walls of the metering box, then the heat loss through the sides and back of the metering box would be approximately 85%. This would mean that only 15% of the heat input would be transmitted through the test element, which is considerably lower than the limit of 80% specified by the standard. For that reason, the guarded hot-box method has been selected. Figure 8 shows the assembly process of the Guarded Hot-Box designed and built for this project and Figure 9 shows the finalized apparatus.

Figure 8: Guarded Hot-Box assembly process

Figure 9: Finalized Guarded Hot-Box

BS 874 states that the Guarded Hot-Box apparatus is capable of measuring the accuracy of test elements to ± 5 % for uniform thermal conductance. This occurs when no thermal bridges are created between the surfaces of the test element. However, in practise higher errors are expected for test elements due to a number of uncertainties involved in testing the Hot-Box, especially those of non-uniform conductance. The standard states that the determination of U-values below 0.5 W/m^2K requires high precision measurement, and therefore the results obtained in these tests may be less accurate.

Hot-box methods are intended for tests on large building elements such as sections of walls, roofs and floors, with a minimum specimen size of 1 m by 1 m. The thermal properties in light weight construction systems are not uniform and the surfaces are not isothermal (thermal bridging). As the temperatures measured on the specimen external surfaces do vary, characteristic environmental temperatures are deduced to account for this.

2.4.3. Guarded Hot-Box Constitutive Parts

All the constitutive parts were selected to satisfy BS 874 [9] and they are divided into two groups, structural passive components and active components. The structural passive components have been designed and built using the same LSF technology as the test elements being sampled. The active components are meant to influence, control and measure the thermal conditions encountered during the tests.

2.4.3.1 Structural Passive components

The structural passive components are represented in Figure 10. All surfaces of the structural components are of matt black finish, and have a total hemispherical emmisivity of at least 0.9. The lateral heat transfer between the metering box and guard box is controlled using a thermopile. This temperature measuring device is connected to a digital controller, which then relays a switch to the heater in the guard box. This system ensures that, as far as possible, the total heat supplied to the metering box passes through the test element and not through the sides and back of the metering box. The heat flow through the test element is in a direction normal to its faces, as the test element covers the open faces of the metering and guard boxes during testing.

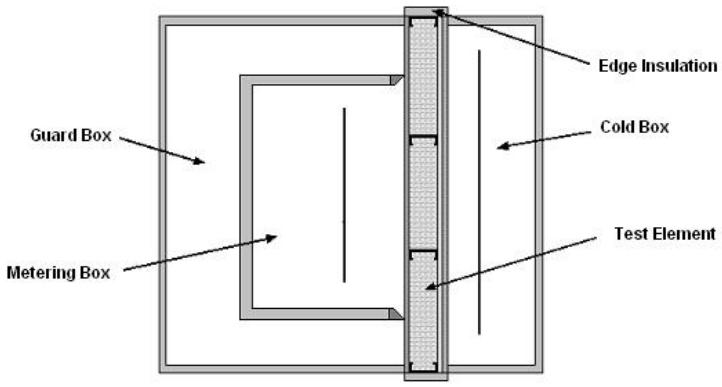

Figure 10: Guarded Hot-Box Structural Passive Components

When using natural convection during the test, the heat flux through the test element may be non-uniform around the perimeter of the metering box. This is due to natural convection in the metering box and forced convection in the guard box producing different air velocities, leading to varying convective heat transfer coefficients. To minimize this non-uniformity, the distance between the back of the metering box and the guard box is defined as 655 mm. There is also 250 mm either side of the metering box to aid forced convection inside the guard box, and enable the temperatures inside the guard and metering boxes to be closely matched.

- Metering box

The metering box is constructed using LSF members bolted with rivets. A 40 mm mineral wool layer and a 15 mm aluminium honeycomb layer then cover the interior of the LSF members. Four steel cables hooked to the ceiling of the guard box hang the metering box in position. Due to their configuration, they help the metering box to apply load towards the test element. The thermal conductivity of the mineral wool inside the metering box walls is 0.031 W/mK and the thermal resistance, neglecting the effect of the Honeycomb layer, corresponds to 1.29 m^2K/W. This complies with the recommendations given in BS 874 [9].

The area of the metering box is 1.258 m wide by 1.244 m high. Its depth is 800 mm and a baffle is used to ensure the air is distributed and circulated evenly. In addition, the baffle acts as a constant radiation surface of known properties. The metering box area is defined by the centre-line of the perimeter seal for calculation purposes. The linear dimensions of the metering box comply with the standard because they are larger than 1 m and greater than three times the maximum thickness of any test element. The maximum thickness of the test elements to be sampled is approximately 250 mm, but in the future if new LSF designs were

approved the test element could increase to 400 mm thick and still satisfy the standard.

In LSF construction, the steel studs of the test elements being considered are normally spaced at 600 mm centres therefore two vertical studs can be analysed within the width of the metering area, leaving a 300 mm space on either side of the studs. The surrounding steel frame of the metering box provides stiffness to the test element but will be neglected by the nature of the calculation. The metering box design will also be compatible with steel studs placed at 400 mm centres, leaving a 200 mm space on either side of the studs, which can also occur in LSF construction.

The open side of the metering box is provided with a perimeter seal to prevent air flow between the metering and guard boxes. This seal works when the test element is pressed against the metering box. The contact width of the seal is 24 mm to avoid significant contact and shielding effects on the test element caused by the perimeter seal and the edges of the walls of the metering box, thus complying with the recommendations given by the standard. The walls of the metering box are tapered from their full thickness down to the width of the seal using a Phenolic foam structure. Compressible foam rubber tape is then stuck onto the edge of this structure. The metering box overhangs the edge of the guard box slightly so that when the test element is pressed against the hot chamber, the weight of the metering box creates pressure that keeps the metering box tightly sealed against the test element.

The 24 mm contact width of the seal onto the test element corresponds to 2 % of the inner linear dimension of the metering area of 1200 mm, to satisfy the requirements of the standard

- Guard box

The guard box is constructed using LSF members bolted with rivets. A 120 mm thick mineral wool layer and an aluminium honeycomb layer cover the interior of the LSF members. The thermal resistance of the mineral wool inside the guard box walls is 3.87 m^2.K/W calculated from its thickness and its thermal conductivity (0.031 W/mK). This complies with the recommendations given in the standard.

The internal dimensions of the guard box are 1.94 x 1.94 x 1.56 m. Fans in the guard box supplement natural convection. The side widths of the guard space are measured as the distance between the outside of the metering box walls and the inside of the guard box walls. The side widths of the guard space are 250 mm, which is wider than the maximum thickness of the test element, and wider than the insulation around the outer edges of the test element, which is 150 mm. Both measurements comply with the standard. The external dimensions of the guard box define the size of the test element needed for sampling, and also the space required for building the Hot-Box apparatus.

An air-tight seal is used between the guard box and the surface of the test element. Compressible foam rubber on the edges of the guard box and cold box in conjunction with several clamping devices were used to hold the Hot-Box structure in place during tests. They were found to be satisfactory in creating an air-tight seal. As mentioned previously, steel cables hooked to the ceiling of the guarded box hang the metering box in position. As a precaution, three steel jacks have been positioned underneath the metering box in case the steel cables fail.

- Cold box

The cold box is constructed using LSF members bolted with rivets. It has been built using the same materials used for the guard box to comply with

the recommendations given in the standard. The internal height and width of the cold box are 1.94 x 1.94 m, which correspond to the internal dimensions of the guard box. This enables the test element to be sealed on all sides during the test. The internal depth of the cold box is 600 mm. Because thermal transmittance measurements will be made, a baffle is installed in the cold box to ensure the air is distributed and circulated evenly. Fans in the guard box supplement natural convection, and the direction of the forced air flow is in an upwards direction for vertical test elements. As with the guard box, an air-tight seal is created between the cold box and the surface of the test element using compressible foam rubber.

Temperature control inside the cold box is achieved using a cooling system, comprising of copper tubing connected to a cooled circulating medium. In this case, the circulating medium is water directly from a tap, but this could be upgraded in the future by using a water chiller. If such an upgrade occurred, then the cold box could be operational at temperatures approaching or below 0 °C. This is an extreme condition and would cause potential problems such as condensation and icing. A temperature of around 20 °C in the cold chamber and 50 °C in the hot chamber are expected, which complies with the recommendations given by the standard.

2.4.3.2 Active components

- Baffles

Baffles in the metering and cold boxes are parallel to the surface of the test element. They provide a radiating surface of near uniform temperature to radiate towards the test element. This is due to the baffle absorbing heat from the different parts of the metering and cold boxes, and emitting the heat as one source to the test element. In addition, they control the air

velocity inside the metering and cold boxes by creating a limited area through which the air can travel at any one time. This helps to keep the ventilation homogenous inside the metering and cold boxes.

The temperature of the baffle surfaces, recorded by various thermocouples, is used to deduce the radiation being transmitted to the test element. The distance from the baffles to the test element affects the convective coefficients inside the metering and cold boxes. Circulating fans are installed in the guard and cold boxes to assist natural convection. It should be noted that the air velocity influences the convective coefficients, and thus only limited adjustments to the air velocities are possible in order to keep the convection homogenous.

Where conditions of natural convection occur, the distance between the baffle and the test element has to be greater than 150 mm to satisfy the standard. The baffle is extended the full width of the metering box, and has gaps at the top and bottom to allow air circulation. The standard recommends that the vertical temperature gradient in the air stream should not exceed 1 K/m for test elements with a U-value up to 1 W/(m^2.K).

- Fans

Fans were installed throughout the Hot-Box to assist in the control of air velocity and reduce the air temperature gradient across the different chambers. Six A.C. fans were installed in the guard box, and another three in the cold box, which were connected to a mains power supply. Table 2 and Figure 11 show the specification of the A.C. fans.

Air Flow	160 m^3/h
Nominal Voltage	230 V (A.C.)
Frequency	50 Hz
Power Input	19 W
Nominal Speed	2650 /min
Temperature Range	-40 ^{0}C to 85 ^{0}C

Table 2: A.C. Fans Characteristics

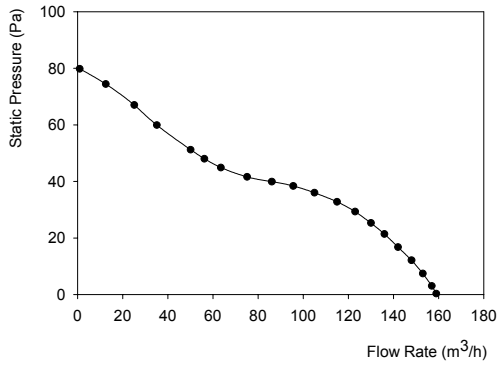

Figure 11: A.C. Fans Pressure/Velocity

In order to maintain a homogenous temperature distribution, a preliminary analysis was carried out to assess the best configuration of the fans and heater inside the guard box. Ten different configurations were analysed using 64 thermocouples to measure the air temperature. Figure 12 represents the optimum configuration inside the guard box to produce a homogenous temperature distribution. It was found that this configuration maintained a temperature difference in the guard box of 0.6 ^{0}C between the most extreme temperatures, which satisfies the standard.

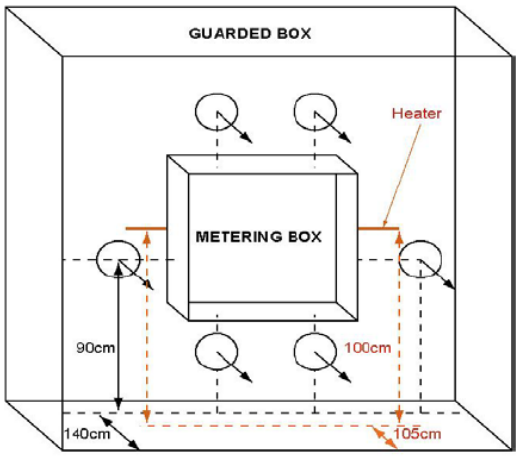

Figure 12: Optimum A.C. Fans/Heater Configuration

Three D.C. fans with variable speed were installed inside the metering box, and connected to a power supply unit. Table 3 and Figure 13 show the specification of the D.C. fans.

Air Flow	70 to 140 m^3/h
Voltage Range	8 to 12.6 V (D.C.)
Power Input	1.4 to 3.4 W
Nominal Speed	1150 to 2300 /min
Temperature Range	-20 ^{0}C to 65 ^{0}C

Table 3: D.C. Fans Characteristics

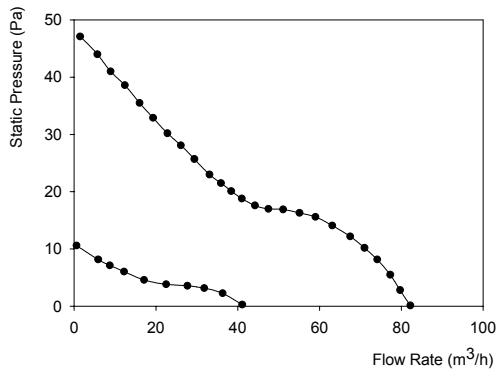

Figure 13: D.C. Fans Pressure/Velocity

If the D.C. fans are used, forced convection inside the metering box occurs. In this case, the distance between the baffle and the test element could be varied, along with the air velocity produced by the fans, to produce a suitable convective coefficient. This complies with the standard, which states that where higher air velocities are imposed across the test element by fans, it is permitted to gradually reduce the distance between the baffle and the test element to a minimum of 40 mm at an air velocity of 3 m/s or greater.

The fans and motors are installed inside the metering box. Therefore their power consumption needs to be measured, taking into account any phase angle. The amount of electrical energy consumed by the fans is equal to the summation of the kinetic energy leading to motion and the heat that they release. In further calculations, it must be added to the energy supplied by the heater.

- Heating elements

There are two tubular heaters within the Hot-Box apparatus, one in the metering box and the other in the guarded box. These are resistance wire heaters. A preliminary analysis was carried out to calculate the power they need to input into the system to achieve desired operation conditions. When considering a specimen with a U-value approximately equal to 0.3 $W/m^2.K$, a temperature difference between hot and cold chambers of approximately 30 $^{\circ}C$ and a testing area given by the dimensions of the apparatus, the following heat inputs are needed.

For the metering box heater:

$$\dot{q} = \frac{A_1(T_i - T_o)}{R_i + R_w + R_o} = \frac{1.5624 \times 30}{0.13 + \frac{1}{0.3} + 0.04} = 13.38W$$

For the guard box heater:

$$\dot{q} = \frac{A_2(T_i - T_o)}{R_i + \frac{x_1}{k_1} + R_o} + \frac{A_3(T_i - T_o)}{R_i + R_w + R_o} = \frac{21.56 \times 30}{0.13 + \frac{0.12}{0.031} + 0.04} + \frac{1.69 \times 30}{0.13 + \frac{1}{0.3} + 0.04} = 174.6W$$

Where:

A_1 is the total area of metering box onto test element = 1.5624 m^2

A_2 is the total area of guard box lateral walls = 21.56 m^2

A_3 is the total area of guard box onto test element = 1.69 m^2

T_i is the temperature of hot chamber = 323 K

T_o is the laboratory temperature = 293 K

R_i is the air thermal resistance of hot chamber = 0.13 m^2.K/W

R_w is the thermal resistance of specimen = $\frac{1}{U-Value} = \frac{1}{0.3}$ m^2K/W

R_o is the air thermal resistance of cold chamber = 0.04 m^2K/W

x_1 is the thickness of guard box walls = 0.12 m

k_1 is the thermal conductivity of guard box walls = 0.031 W/mK

There is no consideration for heat transfer through the back and sides of the metering box because it is kept at the same temperature as the guarded space. Therefore, all the heating input crosses the test element. Due to the characteristics of the calculations estimated to take place in the Hot-Box, and to the commercial products available in the market, two 1000 W tubular heaters were acquired and installed. In case greater heat input is required, the upgrading of the apparatus can be achieved through extra heaters.

The product of the average temperature gradient across the metering box walls, obtained from the thermopile, and the heat exchange coefficient for the metering box, provides an estimate of the correction to be applied to the heat input for the metering box. The heat exchange coefficient for the

metering box is calculated from its dimensions and the known thermal conductivities of its constituent materials. A reasonable estimate of the effective area of the sides and back of the metering box was obtained by taking an average of their internal and external areas. This value was taken as 5.28 m^2.

- Temperature measurement

Temperature measurement is of prime importance in Hot-Box methods. Due to their small size, low thermal mass and passive nature, thermocouples meet the standard requirements conveniently and cheaply over the range of temperatures of interest. Type T thermocouples fit well with the range of temperatures expected in the tests. They have a smaller temperature reading range than any other type of thermocouple, and therefore a greater accuracy over the same number of data points. Due to the stable alloy used in the thermocouple, they also have excellent repeatability. For the above reasons they have been chosen for this application. Thermocouples are made from calibrated wire which was certified by the supplier to comply with BS 4937 [60] to a specified tolerance of ± 0.4 %. Table 4 shows the specification of Type T thermocouples

Alloy materials	Copper vs. Constantan
Operating Range	-250 ^{0}C to 370 ^{0}C
Repeatability Range	-200 ^{0}C to 200 ^{0}C
Accuracy	$\pm$ 0.5 ^{0}C or $\pm$ 0.4 %

Table 4: Type T Thermocouples Characteristics

Representative hot face temperature measurements for the test element are taken 100 mm from the projected edge from the inside of the walls of the metering box. For surface temperatures, thermocouples are in close contact

with the surface for at least 25 mm from their junctions. They are taped securely to the surface, following isothermal paths where possible. The standard states that there must be a minimum of nine thermocouples on each face, uniformly distributed over the test area. However, preliminary tests have shown that using four thermocouples was more than sufficient to measure surface temperatures accurately.

Due to thermal bridging, the surface of the test element adjacent to the steel studs has a hotter temperature to the adjacent areas. The average surface temperatures are then determined on the basis of the proportionate areas of each region of the test element. Within each discrete region the variability of temperature was explored and it was found that placing the thermocouples in the middle of each region represented the average temperature accurately.

The difference in temperature of the test element between each side of the perimeter seal was determined from a number of measurements, taken at various points on the surface of the test element. The surface temperature measurements were made at points where similar thermal conductance occurred. In order to be outside the influence of the metering box walls, the measurements were made approximately 50 mm from the projected intersections of the surfaces of the metering box walls with the test element. This distance could be increased past 50 mm to take account of local thermal conductance variations.

Four thermocouples are also sufficient to measure the mean radiant temperatures of the metering and cold boxes emitted onto the surface of the test elements. The thermocouples have been appropriately distributed on the surface of each baffle to take account of their relative radiant influence on the test element. For the measurement of air temperatures in the metering and cold boxes there are another four thermocouples

positioned in the air spaces between the baffles and the test elements, uniformly distributed in relation to the test area. These thermocouples monitor the convection inside the metering and cold boxes. In the Hot-Box being tested, the distance between the test element and the baffle are around 180 mm. This means there is 90 mm either side of the thermocouple recording the air temperature, which satisfies the standard.

- Temperature control system

The temperatures inside the metering and guard boxes have to be kept as close to each other as possible so that lateral heat transfer is avoided. If the heater raises the temperature inside the metering box above that in the guard box, heat will dissipate through the metering box walls into the guard box. To avoid this, the AC heater inside the guard box is switched on to provide heat and balance the temperature difference. This is controlled by two monitoring systems, a temperature thermopile and a digital controller.

A temperature thermopile is a multiple junction thermocouple circuit with increased thermal capacitance, designed to amplify the output of the circuit and can be used to measure the temperature difference between two areas. In the Hot-Box system, it measures the average temperature differences between the metering and guard boxes. The conditions for equilibrium in steady state analysis can be satisfied in the hot side, using the thermopile and the digital controller discussed below. In the cold side, the water supplied to the system is constant and flows throughout the cold chamber therefore providing consistent temperatures.

The thermopile minimizes the lateral heat transfer through the sides and back of the metering box, which is limited by the standard to less than 10 % of the total power supplied to the metering box. The thermopile has at least one differential pair of junctions for each 0.25 m^2 of metering box

surface area. 22 thermocouple junctions have been provided in the thermopile, providing adequate differential pairs of junctions. Figure 14 shows the arrangement of the thermocouple pairs in the thermopile.

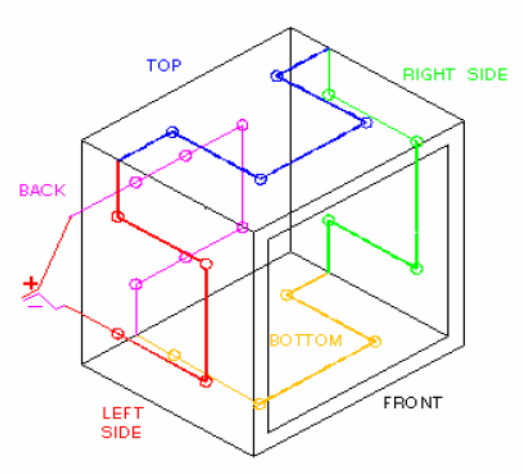

Figure 14: Thermopile Arrangement

The digital controller is connected to both the thermopile and the D.C. heater in the guard box. It displays the voltage output produced from the thermopile, and can be fixed to a desired value. If the voltage provided by the thermopile is below the set point, then the controller supplies voltage to the D.C heater. Similarly, if the voltage provided by the thermopile is above the set point, then the controller stops the power supply to the D.C heater. This allows the thermopile output to converge on the set point by means of regulating the temperature difference inside the Hot-Box. Table 5 shows the specification of the controller.

Accuracy	$\pm 0.5\ ^0$C
Resolution	$1\ ^0/0.1\ ^0$; 10 mV
Thermocouple Compatibility	Type T used
Output	Pulse

Table 5: Digital Controller Specifications

- Data logging

Type T thermocouples have been used in measuring the temperature inside the Hot-Box. The measurements have been recorded with a data logger that can be upgraded if necessary. The data logger selected is capable of housing 8 multiplexer modules, which were all capable of holding 40 channels of 2-wire thermocouples. Table 6 shows the specification of the data logger.

Datalogger Model	Agilent 34980A
Size	8 slot mainframe
Readings	Up to 3 000/second
Reading Accuracy	0.0015 %
Storage	Up to 500 000 readings
Multiplexer Module	AgilentMultiplexer 34921A

Table 6: Data Logging System Specifications

2.5. U-Value Experimental Definition

The experimental data obtained from the Hot-Box must be processed in order to provide quantitative information about the insulating characteristics of any light weight construction system assessed. The heat transfer mechanisms in both of the specimen surfaces are crucial for the definition of the thermal transmittance. Radiant interchange with other surfaces in the box and convective heat transfer at the air/surface interface are of relevant importance. The mean radiant temperature of the surfaces seen by the test element (baffles) characterized the rate of heat transfer by radiation. Convection is characterized by the surface and adjacent air temperature. The most characteristic temperatures to consider for the calculation of the U-Value are as follow.

T_a is the temperature of the air adjacent to the specimen (° C)

T_r is the temperature of the baffles (° C)

T_s is the mean surface temperature of the specimen (° C)

In addition it is necessary to know the heat flux density (ϕ / A) in W/m^2 and the emmisivity factor (E) in order to deduce the U-Value in each of the cases analyzed. The emmisivity factor depends on the emmisivity of the baffle (0.97 because it is painted matt black) and the emmisivity of the specimen surface. E is assumed to be 0.9 for lightweight construction systems [9].

The concept of environmental temperature (T_e) is introduced to group the radiation and convection heat transfer mechanisms occurring on the specimen surfaces into a single index. If the environmental temperature is to be deduced, a heat balance needs to be performed on either surface of the specimen. This is shown in the following equation.

$$\phi / A = Eh_r(T_r - T_s) + h_c(T_a - T_s) = \frac{1}{R_S}(Te - T_s)$$

Where,

h_r is the radiation coefficient (W/m^{2}K)

h_c is the convective coefficient (W/m^{2}K)

R_S is the surface resistance (m^{2}K/W)

Te is the environmental temperature (° C)

Therefore, $$Te = \frac{Eh_r}{Eh_r + h_c}T_r + \frac{h_c}{Eh_r + h_c}T_a$$

The radiation coefficient is proportional to the Stefan-Boltzman (σ) constant (5.67x10^{-8} W/m^{2}K^4) as indicated in the following equation.

$$h_r = 4\sigma T_m^3$$

Where $$T_m = 0.5(T_r + T_s)$$

The convection coefficient depends of the surface/air temperature difference, air velocity, and surface roughness and is difficult to predict. For natural convection a value of 3 W/m^{2}K is taken. It can be neglected for the purpose of the calculations as recommended by the standard [9], which simplifies the characteristic equation of the environmental temperature as follows.

$$Te = \frac{T_a \phi / A + Eh_r (T_a - T_r) T_s}{\phi / A + Eh_r (T_a - T_r)}$$

If Te_m is the environmental temperature in the metering box and Te_c is the environmental temperature in the cold box, the thermal transmittance of U-Value can be deduced from the following equation.

$$U - Value = \frac{\phi}{A(Te_m - Te_c)}$$

2.6. Hot Box Repeatability

The repeatability of the data obtained from the experiments was assessed by comparing the temperature readings obtained from experiments with identical settings. The overall temperature evolution inside the Hot-Box was very similar for each test undertaken. Due to the cooling system inside the cold chamber, the temperatures in that section have remained very stable during the tests. The repeatability of the readings in the hot chamber are within the expected error bars and as the more the power

input is increased inside the metering box, the more the repeatability reduces.

For a temperature difference of 40 °C between the hot and cold sides of the Hot-Box, the highest difference in the temperatures recorded in different tests by the thermocouples in the hot side can be up to 0.9 °C. This temperature difference corresponds to an error reading of 1.6 %. In the cold side, the highest difference in the temperatures recorded by the thermocouples can be up to 0.6 °C, which corresponds to an error reading of 2.9 %. This is because the temperature in the cold chamber is lower than in the hot one, so the error in the cold side is larger for the same temperature difference.

For a temperature difference of 45 °C between the hot and cold sides of the Hot-Box, the highest difference in the temperatures recorded by the thermocouples in the hot side can be up to 1.3 °C. This temperature difference corresponds to an error reading of 1.9 %. In the cold side, the same conclusions can be drawn as for the previous temperature difference as the cooling system is very stable and the same error was observed.

2.7. Thermal Efficiency Sensitivity Analysis

A sensitivity analysis has been conducted to determine how the input parameters affect the results obtained from both experimental and computational analyses. The most influential input parameters are obtained directly from the Hot-box experiments to feed further calculations. These are measurements of temperatures and heat. The output of these calculations is the U-Value (thermal transmittance), which characterizes the thermal efficiency of the lightweight construction systems as explained in previous sections.

The heat flowing through the specimen is equal to the DC power consumed by the tubular heater placed within the metering box after a correction for lateral heat transfer has been conducted to account for any temperature difference between this box and the guarded. This power is obtained multiplying the voltage drop between both ends of the heater by the intensity going through. The DC power supply unit is capable of keeping these parameters (voltage and intensity) constant throughout the duration of the experiments (around one week) with slight temporal variations up to 2%.

Hypothetical values of temperature and heat have been altered in this sensitivity analysis to observe what output would have been obtained. The U-Values that correspond to heat and environmental temperature variations of 2% above and below a number of reference values have been compared to determine the sensitivity of the system. This deviation factor has been selected to match with the variations of DC power supplied by the source. By doing so, a representative analysis of errors produced by the inherent properties of the equipment used, is conducted in parallel.

Ten different heat fluxes have been selected as reference values (7, 7.5, 8, 8.5, 9, 9.5, 10, 10.5, 11 and 11.5 W/m^2). Variations in the power equal to a 2% above and below each given reference heat flux have shown maximum variations in the U-Value of 3.7% when compared to each corresponding reference U-Value (base value). This analysis has been carried out for three temperature differences between the hot and cold environmental temperatures (20, 30 and 40 degrees Celsius). Considering the range of U-Values prescribed by building regulations, the error inherent to the process of monitoring heat fluxes is acceptable.

The same analysis has been conducted for environmental temperature variations. The temperature in the cold side has been kept constant and

equal to 20 degrees Celsius. The environmental temperature in the hot side has been modified subsequently 6 times (40, 45, 50, 55, 60, and 65 degrees Celsius). Variations in the environmental temperatures equal to a 2% above and below each given reference values have shown maximum variations in the U-Value of 3.5% when compared to each corresponding reference U-Value (base value).. This analysis has been carried out for three heat fluxes differences between the hot and cold environmental temperatures (7, 9 and 11 W/m2). The variations in the U-Value are even less than in the case of heat variations and therefore it is concluded that the monitoring devices do not provide much error to the analyses.

The same kind of analysis has been conducted to assess the sensitivity of the computer models and the results obtained are similar to the ones observed

2.8. Hot Box Calibration

In the first series of tests, the need to calibrate the hot box was identified. As the apparatus is a Guarded Hot Box, the calibration is not required by BS 874 [9] but recommended. The outcome expected from this experiment is a calibration factor by which the results of future tests will be multiplied in order to get accurate measurements. The calibration factor gives an idea of heat losses and imperfections of the apparatus and its constitutive subsystems, trying to minimise them. The duration of each individual test carried out to find the calibration factor was 14 days however the data used for the analysis corresponds only to the periods of the test when the standard was being satisfied.

The reference material selected for the calibration was Expanded Polystyrene (EPS) in block form which satisfies BS EN 13163 [61]. Three types of commercial EPS blocks were initially considered for the

experiment, namely EPS 70, EPS 100 and EPS 150. A decision was made to select the most convenient option for the purpose of the Hot Box calibration. This decision was based upon both the thermal conductivity and the thickness of the EPS, which is expected to closely match those of the test samples that will be tested in future. The decision process started by specifying the U-Value that is expected to be encountered in future experiments, which is likely to vary around 0.3 W/m^2.K. This value corresponds to that specified by Building Regulations for lightweight construction systems [8].

The U-Value is inversely proportional to the thickness of the test elements, which is likely to be between 200 and 300 mm for the lightweight specimens. The value of the convection and radiation coefficients was initially neglected in order to find the most convenient type of EPS block. EPS 70 was selected according to the preliminary assumptions as shown in the following lines. The thermal conductivity of EPS 70 [61] in W/mK is given by the following equation and it is used as a reference.

$$k_{PS70} = 0.025314 + 5.1743 \times 10^{-5} \times \rho + \frac{0.173606}{\rho}$$

Where ρ represents the density in Kg/m^3.

The density of EPS 70 is 15 Kg/m^3. The calculated thermal conductivity for that density corresponds to 0.038 W/m^2.K. A block of 125 mm thickness of that material has a thermal conductance (property similar to the U-Value that neglects the radiation and convection heat transfer in the specimen external surfaces) of 0.3 W/m^2.K. This value was close to the U-values expected for further LSF experiments, and that is the reason why EPS 70 was selected for the calibration of the Hot Box. Any other type of EPS would have meant thinner specimens that do not correlate with LSF conditions.

Two 2.4 x 1.2 x 0.15 m EPS blocks were sealed together along the 2.4 m edge with high strength glue. This was to ensure the two panels acted as one continuous sheet for the purpose of the calibration. The glue was given enough time to dry in order to ensure that its moisture content did not affect the test results. Due to the small amount of glue used, the effect of its thermal conductivity was negligible. The panels were positioned and secured to avoid any air infiltration through the cross section of the specimen.

The total dimensions of the calibration test specimen were 5.76 m^2 (2.4 × 2.4 m), which covered the whole space of the guarded box. The test element was orientated in a vertical position and the heat flow was perpendicular to its faces. The test area, or metering area, is defined by the centre-line of the perimeter of the metering box seal. This follows the recommendation given by BS 874 [9], specified as 1.565 m^2 (1.244 m × 1.258 m).

The thermal conductivity value obtained from the Hot Box test is compared to the theoretical value quoted before. This calculates a factor, known as the calibration factor, by which the Hot Box output differs from the expected value. This will then be added to future experiments as a correction to the thermal transmittance of lightweight walling systems. The calibration factor is influenced by both, convection losses due to infiltration and the intrinsic uncertainties in the determination of temperatures and heat fluxes produced by the sensing equipment.

2.8.1. Calibration Experiment Set up

A total of 40 thermocouples connected to 2 different data loggers were used for this test. The recommendation given by BS 874-3.1 sections 4.5.2 and 4.5.3 is that nine thermocouples should be placed in the air spaces,

baffles and on the surface of the test area however due to the temperature distribution homogeneity that has been observed in preliminary tests, a lower number of thermocouples have been used. Seven thermocouples were securely taped to the hot surface of the test element and another seven to the cold side as shown in Figure 15. There were also four thermocouples placed on each of the baffles and another four controlling the air temperature on both sides of the hot box. As the test area is 1.565 m^2, there was more than one thermocouple per 0.5 m^2 of test area, as specified in the standard.

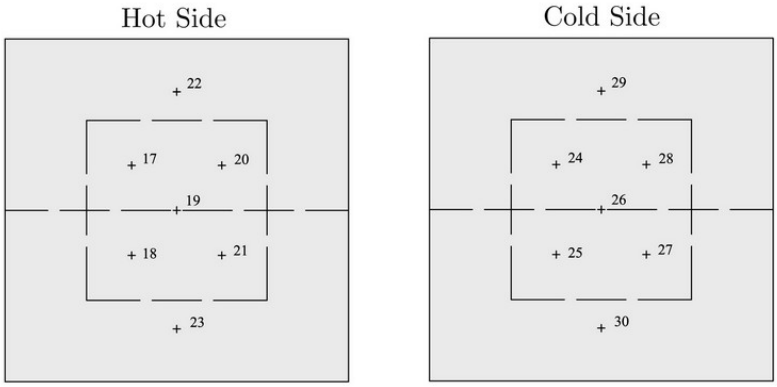

Figure 15: Test Specimen Thermocouple Distribution in Calibration Test

The remaining ten thermocouples were distributed around the air between the metering and guarded box, and also the section of the test element between those two boxes. Finally, there was a thermocouple for measuring the laboratory temperature as shown in Table 7. Distances from each thermocouple measuring air temperature to the test element satisfied BS 874-3.1 specification in section 4.5.3. When testing natural convection, this distance was kept to 100 mm. The position of these thermocouples is specified in Figure 16.

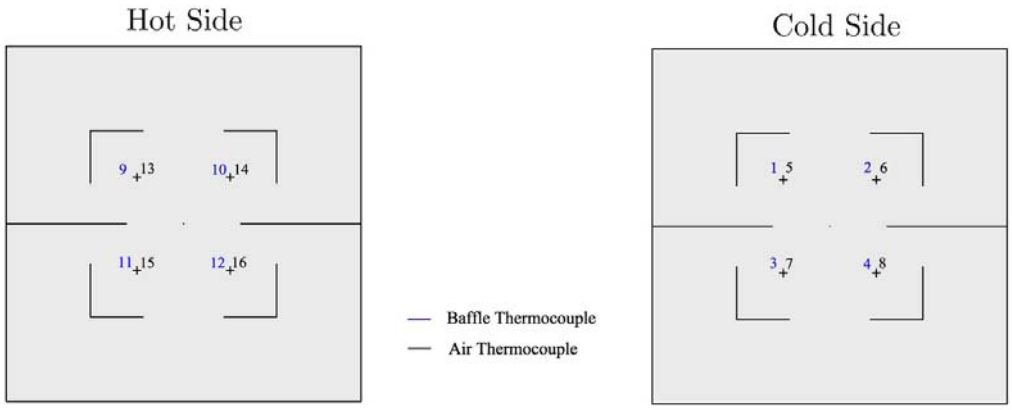

Figure 16: Thermocouples Position on Baffles and Air in Calibration Test

The position and the coordinates of the thermocouples in Table 7 are given, taking as a reference point the bottom left corner of the specimen. These are expressed as though the viewer were facing either the hot or cold face of the test element or, in the case of the air and baffle thermocouples, looking toward the inside of the guarded, metering and cold boxes. Representative hot face temperature measurement for the test element was taken at least 100 mm from the projected edge of the inside of the walls of the metering box, as can be noted in the drawing, satisfying section 4.2 of BS 874-3.1 [9].

HOT SIDE				COLD SIDE			
TC Number	Coordinates (mm)		Description	TC Number	Coordinates (mm)		Description
	X	Y			X	Y	
9	814	1465	Baffle hot	1	573	1616	Baffle cold
10	1585	1465	Baffle hot	2	1825	1616	Baffle cold
11	814	935	Baffle hot	3	573	784	Baffle cold
12	1585	935	Baffle hot	4	1825	784	Baffle cold
13	814	1465	Air hot	5	573	1616	Air cold
14	1585	1465	Air hot	6	1825	1616	Air cold
15	814	935	Air hot	7	573	784	Air cold
16	1585	935	Air hot	8	1825	784	Air cold
17	814	1465	Hot metering test surface	24	814	1465	Cold test surface
18	814	935	Hot metering test surface	25	814	935	Cold test surface
19	1200	1200	Hot metering test surface	26	1200	1200	Cold test surface
20	1585	1465	Hot metering test surface	27	1585	1465	Cold test surface
21	1585	935	Hot metering test surface	28	1585	935	Cold test surface
22	1200	2045	Hot guard test surface	29	1200	2045	Cold test surface
23	1200	350	Hot guard test surface	30	1200	350	Cold test surface

Table 7: Calibration Test Thermocouple Position

Four thermocouples measured the air temperature between the guarded and metering box; on its bottom, left, right, top and back side respectively. Throughout the experiment, the guarded space between the guard and metering boxes experienced forced ventilation. Natural convection has been allowed within the metering box. This simplifies the calculations, as there is no need to correct for the heat input induced by the DC fans. To satisfy Section 4.2 of BS 874-3.1 [9], the distance between the baffle and the test element in the metering box is 180 mm. One thermocouple was used to measure the laboratory temperature.

2.8.2. Calibration Test data

The calibration factor has been calculated for two different conditions (Test1 and Test2) and it has been found to be constant, as expected. The heat input into the system varied for the two tests and, therefore, the boundary conditions encountered were different. Figure 17 shows the temperatures obtained during Test1 where a lower heat input is imposed. The actual values of the temperatures in degrees Celsius measured in both of the tests are tabulated in Table 8.

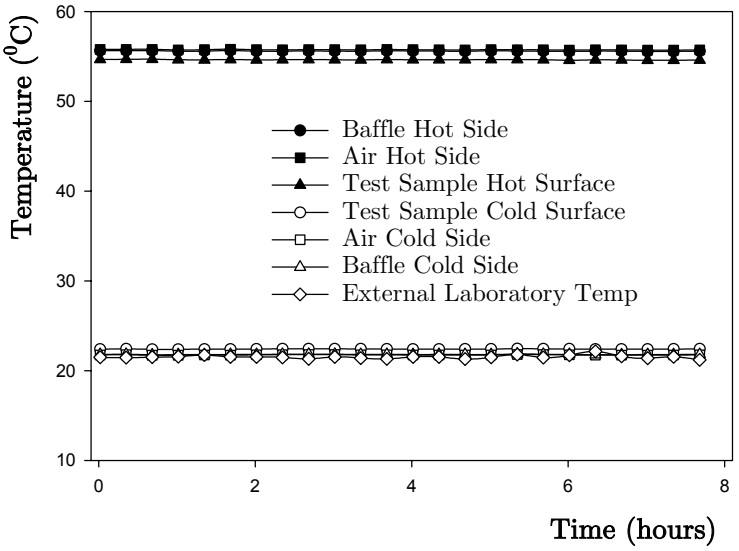

Figure 17: Calibration Test Temperature Evolution

Average Temperature	Test 1 Heat Input = 13.49 ±3% W		Test 2 Heat Input = 16.36 ±3% W	
	Hot Side	Cold side	Hot Side	Cold side
Air	55.74 ±5%	21.76 ±5%	64.04 ±5%	22.93 ±5%
Baffle	55.60 ±5%	21.81 ±5%	63.88 ±5%	23.00 ±5%
Specimen Surface	54.63 ±5%	22.41 ±5%	62.76 ±5%	23.72 ±5%
Environmental	**55.63** ±5%	**21.74** ±5%	**63.90** ±5%	**22.89** ±5%

Table 8: Calibration Test Experimental Data

As recommended in section 6 of the standard, if a measurement of thermal transmittance was to yield accurate results, the difference between the hot and cold air temperatures must be above 20 $^{\circ}$C in both tests. Figure 18 and Figure 19 show a close-up view of the preceding Figure 17.

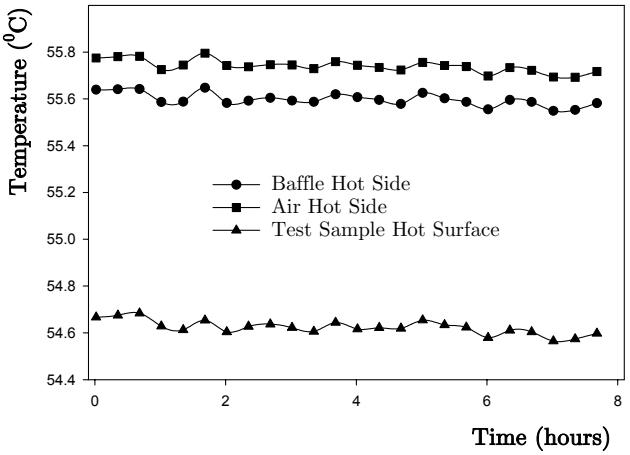

Figure 18: Calibration Hot Side Temperature Evolution

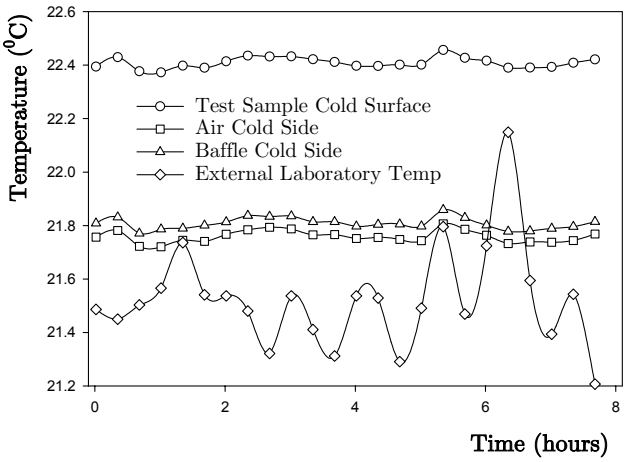

Figure 19: Calibration Cod Side Temperature Evolution

The standard states, in section 4.6, that when equilibrium has been reached any fluctuations in the average air temperature on the hot and cold sides of the metering area shall not exceed 1 % of the air-to-air

temperature difference between hot and cold over a period of at least 8 h. The air-to-air temperature difference between hot and cold sides for Test 1 was 33.98 ° C, so there is an allowance in the temperature fluctuation over a period of 8 hours of approximately 0.34 ° C. The temperature fluctuation in the air inside the metering box was 0.10 ° C and the cold box was equal to 0.02 ° C, both of which satisfied the prescribed condition. This is shown in Figure 20.

Similarly, the air-to-air temperature difference between hot and cold sides for Test 2 was 41.11 ° C, so there was an allowance in the temperature fluctuation over a period of 8 hours of approximately 0.41 ° C. This temperature fluctuation closely matched the fluctuation inside the metering box, and the fluctuation inside the cold box was equal to 0.177 ° C. Both of these satisfied the prescribed condition.

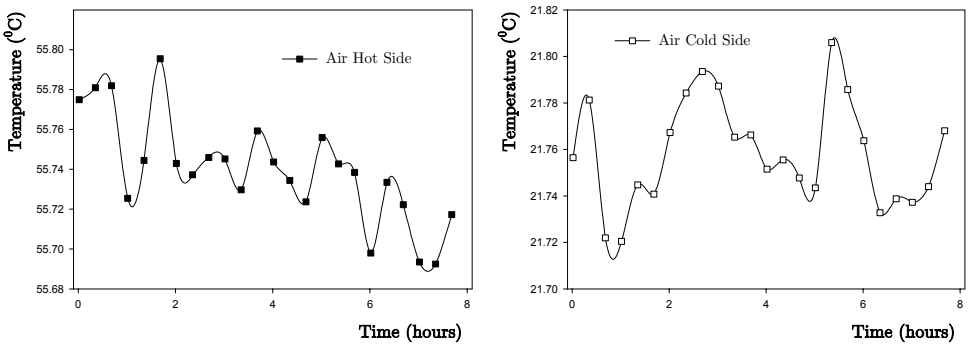

Figure 20: Calibration Test Air Evolution

The maximum vertical temperature gradient encountered during Test 1 in the metering box air was 0.65 K/m and 0.54 K/m for the baffle. In the cold box, the value of the vertical gradient corresponded to 0.18 K/m for the baffle and 0.18 K/m for the air. During Test 2 in the air of the metering box, the maximum vertical temperature gradient encountered was 0.78 K/m and 0.65 K/m for the baffle. In the cold box, the value of

the vertical gradient corresponded to 0.22 K/m for the baffle and 0.22 K/m for the air. These values comply with section 4.2 and 4.4 of BS 874-3.1 [9] where it is stated that up to 1 K/m temperature gradient is allowed on those sections.

The thermopiles connected to the digital controller have enabled the lateral heat transfer to be kept to a minimum. However, a small correction for lateral heat transfer has been applied in both of the tests. This correction has been carried out, following the recommendations given by BS 874-3.1 section 4.3. The average temperature gradient between the internal and the external side of the metering walls has been multiplied by the heat exchange coefficient of its constitutive materials. This heat exchange coefficient is calculated for the dimensions and the thermal conductivities of the metering wall materials.

For Test 1, the temperature in the internal side of the metering box walls was 0.13 $^{\circ}$C lower than the external temperature around it. This condition caused 0.76 W of heat to be transferred from the outside of the metering box to the inner space. For Test 2, the average temperature difference between both sides of the metering box is 0.60 $^{\circ}$C, but on this occasion the heat is transferred in the opposite direction and corresponds to 3.5 W, which is subtracted from the heat released by the tubular heater for the purpose of the calculation. As the standard prescribes in section 4.3.5, it is impractical to account for all of the lateral heat flow in the test element caused by surface temperature differences in the metering and guard box areas. Throughout the tests, these temperature differences have been kept to a minimum.

2.8.3. Hot Box Calibration Factor

As stated previously, the thermal conductivity value obtained from the Hot Box test is compared to the theoretical value quoted above, to calculate the Hot Box Calibration Factor. This will then be applied to future experiments, as a correction to the experimental U-Values obtained with the same apparatus and similar thermal conditions. The Hot Box Calibration factor to be applied in further experiments corresponds to the average of that calculated from Test 1 and Test 2 shown in Table 9, i.e. 1.183. This means that the Guarded Hot Box designed and developed in this research under calculates the actual value of any thermal property by 18.3%. This can be corrected by applying the Hot Box Calibration Factor.

Thermal Conductivity	**Test 1** **Heat Input = 13.49 ±3% W**	**Test 2** **Heat Input = 16.36 ±3% W**
Theoretical K_{EPS70}	0.038 W/m.K	0.038 W/m.K
Experimental K_{EPS70}	0.0321 ±5% W/m.K	0.0322 ±5% W/m.K
Calibration Factor	1.184 ±5%	1.182 ±5%

Table 9: Hot Box Calibration Factor

The experimental U-Value has also been calculated for both of the thermal conditions presented (Test 1 and Test 2), in order to certify the suitability of the EPS blocks selected. Environmental temperature approximations have been applied and the U-Values encountered after applying the Hot Box Calibration Factor are around 0.3 $W/m^2.K$ in both cases. This value closely matches building regulations [8] and it demonstrates that the selection was correct.

2.9. LSF Hot-Box Testing

One specimen that represents the New System was tested in the Guarded Hot-Box. The expected outcome from the experiment was a set of results with which to produce a consistent U-Value could be produced for a number of different boundary conditions. These boundary conditions are then inputted into computer simulations in order that those results can eventually be compared to the ones from the Hot Box experiments. This is done in order to validate computer models. Any difference found between the computer and experimental results gives an idea of software limitations as explained in the following pages.

The duration of each individual test carried out was 14 days. However, the data used for the analysis corresponds only to the periods of the test when the standard was being satisfied. The total dimensions of the test specimen being tested was 5.76 m^2 (2.4 × 2.4 m), which covered the whole space of the guarded box as shown in Figure 21. The test element was orientated in a vertical position and the heat flow was perpendicular to its faces. The metering test area is defined by the centre-line of the perimeter of the metering box seal following the recommendation given by BS 874 [9] giving a value of 1.565 m^2 (1.244 m × 1.258 m).

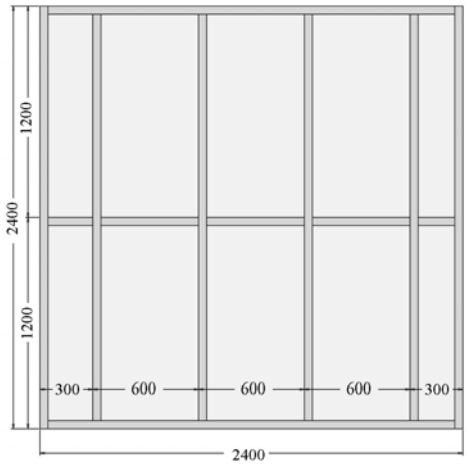

Figure 21: New System Specimen Geometry

A similar thermocouple arrangement to the Hot-Box Calibration was used for this test, having 40 thermocouples connected to 2 different data loggers. In this case, five thermocouples were securely taped to the hot surface of the test element, and six were taped to the cold side, as shown in Figure 22. In addition, there were three thermocouples placed across the steel stud section. This arrangement was used to compare information regarding the temperature evolution for the experimental data and the computer simulations. Two of those thermocouples were placed on the flanges, and the remaining one was placed on the middle of the web of one of the central vertical steel studs.

As in the calibration experiment, there were also the customary four thermocouples placed on each of the baffles, and another four controlling the air temperature on both sides of the hot box. The remaining ten thermocouples were distributed similarly to the calibration experiment around the air between the metering and guarded boxes, and also in the section of the test element between those two boxes. Finally, there was a thermocouple inserted for measuring the laboratory temperature as shown in Table 10. The position and the coordinates of those thermocouples were given taking as a reference point the bottom left corner of the specimen. These were expressed as though the viewer were facing either the hot or cold face of the test element or, in the case of the air and baffle thermocouples, looking toward the inside of the guarded, metering and cold boxes.

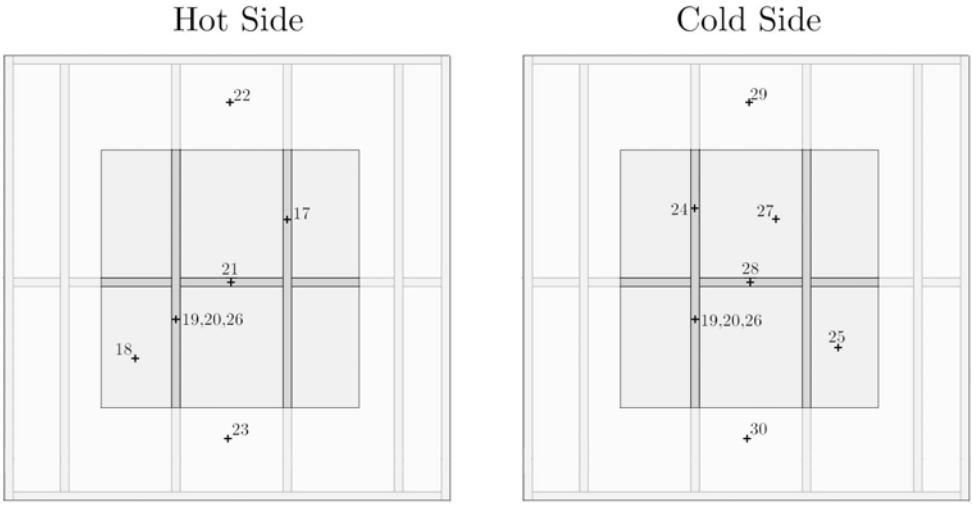

Figure 22: Test Specimen Thermocouple Distribution in New System Surfaces

HOT SIDE				COLD SIDE			
TC Number	Co-Ordinates (mm)		Description	TC Number	Co-Ordinates (mm)		Description
	X	Y			X	Y	
9	814	1465	Baffle hot	1	573	1616	Baffle cold
10	1585	1465	Baffle hot	2	1825	1616	Baffle cold
11	814	935	Baffle hot	3	573	784	Baffle cold
12	1585	935	Baffle hot	4	1825	784	Baffle cold
13	814	1465	Air hot	5	573	1616	Air cold
14	1585	1465	Air hot	6	1825	1616	Air cold
15	814	935	Air hot	7	573	784	Air cold
16	1585	935	Air hot	8	1825	784	Air cold
17	1525	1465	Hot metering test surface	24	925	1465	Cold test surface
18	700	935	Hot metering test surface	25	1720	935	Cold test surface
19	925	1070	Steel stud outer flange	26	925	1070	Steel stud inner flange
20	925	1070	Steel stud web	27	1350	1400	Cold test surface
21	1200	1175	Hot metering test surface	28	1200	1175	Cold test surface
22	1200	2045	Hot guard test surface	29	1200	2045	Cold test surface
23	1200	350	Hot guard test surface	30	1200	350	Cold test surface

Table 10: New System Test Thermocouple Position

Four thermocouples measured the air temperature difference between the guarded and metering box on its bottom, left, right, top and back side respectively. Throughout the experiment, the guarded space between the guard and metering boxes was forced ventilation. Natural convection has been allowed within the metering box just as in the calibration experiment. This simplifies the calculations as there is no need to correct for the heat input induced by the DC fans. To satisfy Section 4.2 of BS 874-3.1 [9], the distance between the baffle and the test element in the metering box was 180 mm.

2.9.1. LSF Test Data

The experimental U-Value has been calculated for three different conditions namely Test 1, Test 2 and Test 3. This has been found to be relatively constant, but the slight variations were due to varying boundary conditions in the tests. The heat input into the metering box varied for the three different tests (12.67, 15.35 and 18.43 W respectively) and therefore, the boundary conditions encountered were different. Figure 23 shows the temperatures obtained during Test 1, where the lowest heat input was imposed. The actual values of the temperatures in degrees Celsius measured in all of the tests are tabulated in Table 11.

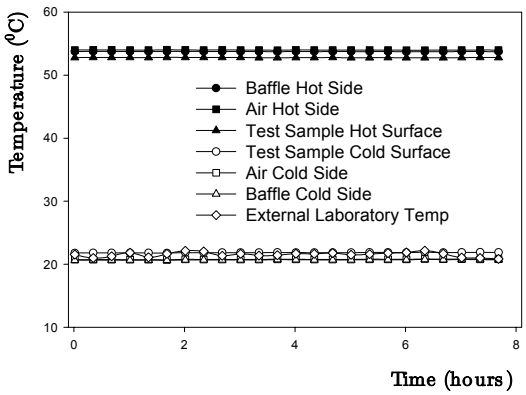

Figure 23: Test 1 New System Test Temperature Evolution

	Test 1		Test 2		Test 3	
	Heat Input = 12.67 W		Heat Input = 15.35 W		Heat Input = 18.43 W	
Average Temperature	**Hot Side**	**Cold side**	**Hot Side**	**Cold side**	**Hot Side**	**Cold side**
Air	53.98	20.77	60.79	20.67	70.45	23.39
Baffle	53.73	20.70	60.56	20.67	70.24	23.45
Specimen Surface	52.78	21.84	59.28	21.93	68.73	24.79
Environmental	**53.77**	**20.82**	**60.57**	**20.68**	**70.23**	**23.36**

Table 11: New System Test Experimental Data

As recommended in section 6 of the standard, if a measurement of thermal transmittance was to yield accurate results, the difference between the hot and cold air temperatures needed to be above 20 ^{0}C. Figure 24 and Figure 25 show a close-up view of the preceding Figure 23.

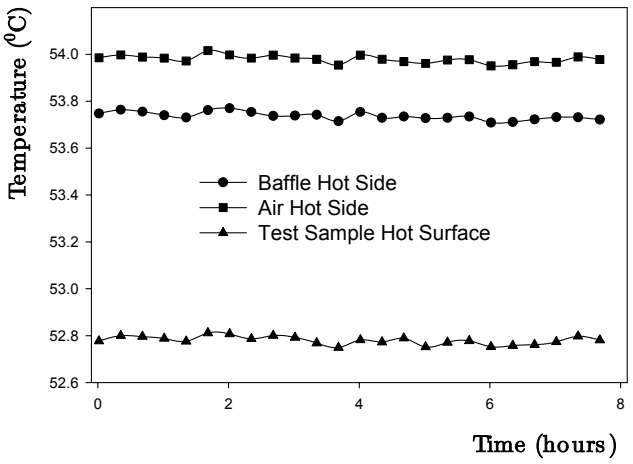

Figure 24: Test 1 New System Hot Side Temperature Evolution

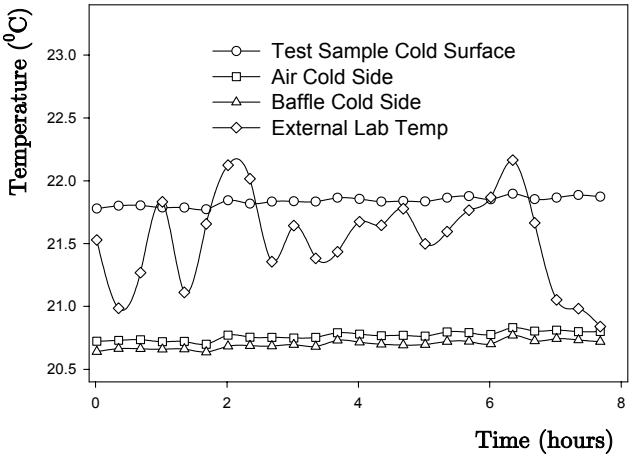

Figure 25: Test 1 New System Cold Side Temperature Evolution

The standard states in section 4.6, that when equilibrium has been reached any fluctuations in the average air temperature on the hot and cold sides of the metering area shall not exceed 1 % of the air-to-air temperature difference between hot and cold over a period of at least eight hours. The air-to-air temperature difference between hot and cold sides for the Test 1 was 32.95 $^{\circ}$C, so there was an allowance of approximately 0.33 $^{\circ}$C over the specified period. The temperature fluctuation in the air inside the metering box was 0.04 $^{\circ}$C and the cold box was equal to 0.08 $^{\circ}$C, both of which satisfy the prescribed condition. This is shown in Figure 26. Similarly, the air-to-air temperature difference between hot and cold sides for Test 2 was 39.89 $^{\circ}$C, so there was an allowance in the temperature fluctuation over the period of eight hours of approximately 0.40 $^{\circ}$C. The temperature fluctuation in the air inside the metering box was 0.17 $^{\circ}$C and the cold box was equal to 0.03 $^{\circ}$C. Both these conditions satisfy the prescribed condition. Finally, for Test 3, the air-to-air temperature difference between the hot and cold sides was 46.88 $^{\circ}$C, so there was an allowance in the temperature fluctuation over the period of eight hours of approximately 0.47 $^{\circ}$C. The temperature fluctuation in the air inside the metering box was 0.005 $^{\circ}$C, and the temperature fluctuation inside the

cold box was 0.42 °C. Both of these conditions satisfy the prescribed condition.

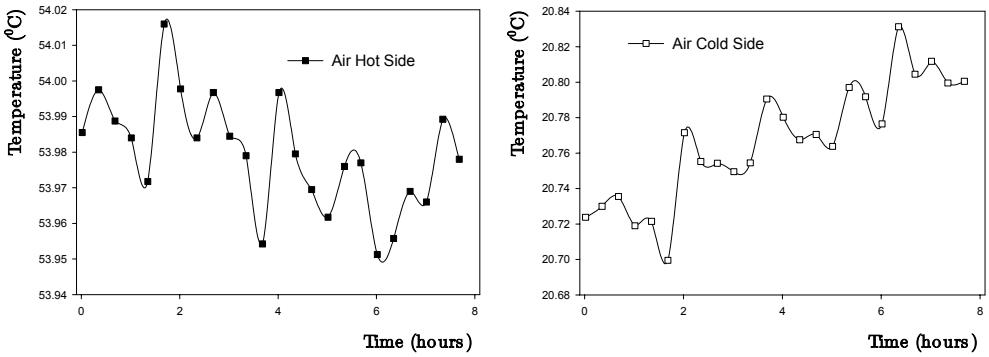

Figure 26: Test 1 New System Test Air Evolution

The maximum vertical temperature gradient encountered during Test 1 in the metering box air was 0.60 K/m and 0.52 K/m for the baffle. In the cold box, the value of the vertical air temperature gradient corresponded to 0.17 K/m for the baffle and 0.27 K/m for the air. Similarly, during Test 2, in the air of the metering box, the maximum vertical temperature gradient encountered was 0.80 K/m and 0.68 K/m for the baffle. In the cold box, the value of the vertical gradient corresponded to 0.19 K/m for the baffle and 0.21 K/m for the air. Finally, during Test 3 in the air of the metering box, the maximum vertical temperature gradient encountered was 0.92 K/m and 0.80 K/m for the baffle. In the cold box, the value of the vertical gradient corresponded to 0.24 K/m for the baffle and 0.25 K/m for the air. These values comply with section 4.2 and 4.4 of BS 874-3.1 [9] where it is stated that up to 1 K/m temperature gradient is allowed in those sections.

The thermopile connected to the digital controller enabled the lateral heat transfer to be kept to a minimum. However, a small correction for lateral heat transfer was applied in all of the tests. This correction has been

carried out following the recommendations given by BS 874-3.1 section 4.3. The average temperature gradient between the internal and the external side of the metering walls was multiplied by the heat exchange coefficient of its constitutive materials. This heat exchange coefficient was then calculated for the dimensions and the thermal conductivities of the metering wall materials.

For Test 1, the temperature in the internal side of the metering box walls was 0.22 ° C lower than the external temperature around it. This condition caused 1.28 W of heat to be transferred from the guarded to the metering space. This figure is then added to the heat released by the tubular heater to calculate the net heat flux emitted through the test sample. For Test 2, the average temperature difference between both sides of the metering box was 0.49 ° C, but on this occasion the heat was transferred in the opposite direction and corresponds to 2.86 W, which needs to be subtracted from the heat released by the tubular heater to calculate the net heat flux through the specimen. Similarly, for Test 3, the average temperature difference between both sides of the metering box was 1.18 ° C, with the heat again being transferred to the guard box. This value corresponds to 6.86 W, which needs to be subtracted from the heat released by the tubular heater to calculate the net heat flux emitted through the test sample. As the standard prescribes in section 4.3.5, it is impractical to account for all of the lateral heat flow in the test element caused by surface temperature differences in the metering and guard box areas however throughout the tests, these temperature differences have been kept to a minimum.

2.9.2. LSF Thermal Transmittance

A non corrected experimental U-Value was calculated for each of the three tests. The actual hot box results are multiplied by the calibration factor

(1.1831) to obtain an accurate value of the thermal transmittance named the Calibrated U-Value in Table 12.

	Test 1	**Test 2**	**Test 3**
	Heat Input = 12.68 ±3% W	Heat Input = 15.35 ±3% W	Heat Input = 18.43 ±3% W
Experimental U-Value	0.25 ±5% W/m^2.K	0.25 ±5% W/m^2.K	0.26 ±5% W/m^2.K
Calibrated U-Value	**0.29 ±5% W/m^2.K**	**0.29 ±5% W/m^2.K**	**0.30 ±5% W/m^2.K**

Table 12: New System Thermal Transmittance

The values of thermal transmittance and the temperature evolution through the steel work can be compared with the computer simulations to test their correlation. This enables the computer models to be validated so that they can test other systems and produce accurate U-Values. As mentioned previously, the calibrated U-Values are relatively constant, producing an average U-Value for the new system tests of 0.293 W/m^2.K, using the Guarded Hot-Box method.

2.10. Thermal Efficiency Computer Simulations

The empirical data obtained from the Guarded Hot-box experiments was used to assess the validity of 2-Dimensional computer models. The software package HEAT2 [25] was selected for this purpose. The reasons for this are that it has been proven to give accurate results, it is very flexible and it can be upgraded to HEAT3 [26] if more complex assemblies and potential improvements need to be modelled. The final aim is to calculate a correlation factor by which any 2-D computational calculation needs to be associated in order to predict a practical U-value.

HEAT2 and HEAT3 are based on the finite difference theory applied to heat transfer and therefore only rectangular cells can be used to discretize

the geometry. The size and shape of those can be varied to adapt to the characteristics of the element of study and the conditions of interest. The existence of a thermal bridge in any lightweight construction system influences how fine the cells must be in that section. Due to the thermal interactions in the area where the thermal bridges occur, it is necessary to increase the number of cells in that section.

The selection of representative models will allow the designer to obtain accurate and representative results. It is also recommended the implementation of sub models to study particular conditions. For instance, a representative 2D LSF model contains one steel profile, internal batt insulation and sheathing elements with a length equal to the distance between stud centres. The steel profile however is placed in the centre. Sub models have been produced to analyze particular conditions such as the heat transfers through the steel section when this is modified with slots.

A total of 45000 cells have been used for the general 2D models and a similar number for the sub models. The mesh is 3 times finer around the steel section than in the rest of the model. This was done using expansion points for the numerical grid. It was not necessary to conduct a sensitivity analysis because the modelling time for such a fine mesh in steady conditions was found to be acceptable (5 minutes). It is recommended to conduct such an analysis when more complex systems are modelled in case a reduction of computation times is necessary.

The boundary conditions selected for the analyses are either heat fluxes or air temperatures. It is recommended however the use of the later ones because these parameters are taken from Hotbox experiments and recording them involves reduced errors. Cavity radiation is accounted for in the analyses by calculating temperatures iteratively in each cavity

applying CEN/ISO correlations. The heat flow main direction within the cavities is selected automatically by the software package.

Steady analyses are conducted to calculate the thermal transmittance. The relaxation coefficient is kept equal to 1.95 and the stop criterion is selected to be a temperature difference between subsequent iterations (0.01 degrees Celsius). In case of further transient calculations, the same stop criterion is selected at time intervals characteristic of the process studied. The relaxation coefficient in transient calculations is selected to vary automatically through the simulations.

The most important output expected from the computer models is the thermal transmittance of the specimens assessed. This can be compared with the data provided by the Guarded Hot-box apparatus. The experimental temperature distribution within the specimens correlates with the computer models shown in Figure 27. The geometry, material properties and boundary conditions need to be specified in the computer models. Thereafter, steady state analyses are carried out to obtain the U-Value corresponding to each of the conditions analyzed. A comparative analysis between the computer and experimental results obtained previously is shown in Table 13.

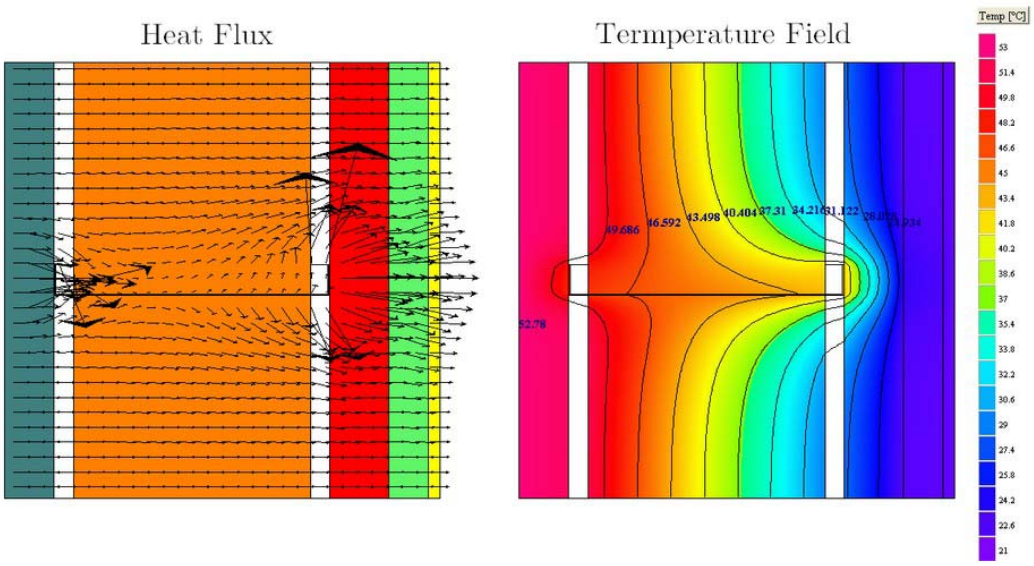

Figure 27: Computer Models for Thermal Efficiency

The first stage in the computer simulation is to calculate the specimen surface-to-surface thermal conductance. In order to do that, the surface coefficients are assumed to be zero and the boundary conditions are defined as the temperatures on the surface. By doing so, only conduction and cavity radiation are being considered. Convection and radiation in the external surfaces need to be considered when calculating the thermal transmittance by adding Rs_1 and Rs_2. Although convection and radiation coefficients can be calculated using analytical solutions, they have been approximated using the recommendations given by BS 6946 [62]. When calculating the computer based U-Values, the internal and external surface resistances are taken as 0.13 m^2K/W and 0.04 m^2K/W respectively when calculating the computer based U-Values.

	Test1		Test2		Test3	
	Experiment	Computer	Experiment	Computer	Experiment	Computer
Surface-to-Surface Thermal Conductance	0.26 ±5%	0.24 ±5%	0.26 ±5%	0.24 ±5%	0.27 ±5%	0.25 ±5%
Thermal Transmittance	0.29 ±5%	0.26 ±5%	0.29 ±5%	0.26 ±5%	0.30 ±5%	0.27 ±5%

Properties in $W/m^2.K$

Table 13: Experimental Vs. Computer Model U-Value Comparison

A good agreement between computer and experimental results has been found. When the surface-to-surface thermal conductance is compared between experiment and computer models, the maximum difference encountered is 0.02 W/m^2.K. When convection and radiation is considered in the gas phase, the thermal transmittance (U-Value) is deduced. When this property is compared between experiment and computer models, it is found that the computer results need to be increased 0.03 W/m^2.K. Similar conclusions were drawn by *Rose and Svendsen* [41] where they state that computer calculated U-Values must be raised by 0.04 W/m^2.K (more conservative approach) in order to make values safe for building design purposes.

The existing difference between those values is due to the following factors:

- Horizontal transversal studs are neglected in 2-D computational simulations
- The computer models take into account theoretical values for the thermal properties of the materials
- The computer models do not take into consideration the fixings
- The computer models neglect contact resistance between different materials
- The computer models idealize the geometry and do not consider irregularities
- Difficulties of experimentally determining convection and radiation coefficients
- 2D computational simulations are less representative than 3D simulations

2.11. LSF Thermal Efficiency Conclusions

The methodologies presented in this chapter have proved to be robust and it is concluded that building designers can rely on computer models to

calculate actual U-Values for lightweight construction systems. Some slight corrections and a good definition of the thermal properties need to be carried out if these computer models are expected to lead to representative results. It is recommended that the initial design modifications are assessed computationally so general conclusions about performance can be drawn. Thereafter, prototypes might be built and can be tested in the Guarded Hot-box apparatus designed, constructed and calibrated for that purpose.

Building regulations are becoming more restrictive and are targeting U-Values. Prescribing slight reductions in this parameter is a synonym of large savings in the residential energy bill and a decrement in the CO_2 emissions to the atmosphere. It has been proved by this research that using the correct methodologies and software packages lead to improved designs. This study however, does not account for other aspects such as assembly imperfections or reduced material qualities that are very influential for the thermal performance of the building system as a whole.

A more strict approach to be taken by building control authorities is necessary to tackle the problem of increasing CO_2 emissions every year. Integral measures need to be taken by the regulatory bodies, if more sustainable construction techniques are aimed. Controlling the assembly process and the thermal properties of the materials used in the construction of residential buildings will increase the quality of the final product reassuring the user and the environment.

The Hot-box experiment has proved to be a sound technique to determine experimentally the thermal transmittance of external walling specimens. It is also an experimental procedure recommended to analyze the interaction between the systems assessed with windows, doors, ceilings, corner configurations, etc. It is however not prescribed by building regulations the execution of such a test and compliance with current prescriptions is

demonstrated by computational means. These have proved to underestimate U-Values and therefore, it is recommended a redefinition of those regulations. The number of testing facilities around the world capable of conducting Hot-box experiments is rather limited and governments should be encouraged to increase those numbers.

In addition, national and international standards that apply to this type of measuring equipments are far too strict to be fully satisfied. A revision of their contents is recommended to lead to improved empirical tests. There are aspects included within these standards that are not highly relevant for the definition of the thermal transmittance. These aspects should be neglected or altered to simplify the experiments and facilitate their execution. Good examples of this are the prescribed laboratory conditions, the error bar suggested, etc.

Some other relevant aspects are omitted by the standards and their revisions should account for them in the modifications. For instance, the calibration of a Guarded Hot-box is not compulsory but recommended in the standards. This action is however extremely important to understand the existing errors of every particular apparatus and they can be accounted for in further tests. The calibration of these apparatus should be compulsory.

The sensitivity analysis conducted to the methodologies presented to in this chapter, has revealed the difficulty to measure the proposed modifications in the prescribed U-Values. Building regulations have reached a limit where only marginal reductions in the thermal transmittance can be prescribed. These slight reductions are difficult to be measured using the existing methodologies and techniques because the current experimental error bars are even larger than the modifications proposed. A different approach from the regulatory bodies is recommended

such a determination of new thermal efficiency monitoring technologies or building control actions as mentioned before.

The execution of Hot-box experiments is rather time consuming. Their cost however is marginal and prescribing the execution of these tests would not be an economical difficulty, which could be assumed by the construction companies. The opposite happens with the fire rating test that is explained in the following chapter. In that case, cheaper and reliable methodologies capable of approximating the outcome obtained from the full scale test are necessary and they are developed and recommended.

The final outcome of the thermal efficiency methodologies is the value of the thermal transmittance (U-Value) that gives an idea of heat loss for any lightweight construction configuration. In addition to that, and more importantly, this property is inputted in the following methodologies to analyze the performance of these systems in fire, which are presented in subsequent chapters. This contributes to an integrated approach to design lightweight construction systems, which is the main goal of the project.

Chapter Three

3. Lightweight Building Systems Fire Performance

3.1. Background to Fire Performance

Full scale Fire Rating Tests [10] to measure the fire resistance of walling systems are intended to be satisfied by all construction elements. They are however too expensive and time consuming to be conducted in a regular basis, therefore small scale experiments and validated mathematical models have been advocated as a replacement means to predict performance [11]. The development of a novel engineering methodology for predicting the fire resistance of lightweight assemblies is suggested and a number of tests are conducted to prove its reliability.

Fire rating requirements do not fully represent the conditions encountered in real fire scenarios. Therefore, all methodologies involved in assessing real fire performance need to be validated for full scale fire scenarios [12]. Tests involving full scale fires are not normally viable due to economical, environmental and safety reasons. However, an experiment of this nature has been carried out in order to analyse the performance of LSF self contained walls under the action of severe fire conditions [13].

3.2. LSF Fire Performance Literature Review

A limited number of research studies regarding the performance of LSF under fire conditions have been conducted in the past. Some of these have been selected as sources to compare experimental results and modelling techniques in this project and they are listed in the following pages. Two main topics have been reviewed in the existing literature for the purpose of this project, firstly behaviour of LSF system in the Fire Rating Test [10] and secondly, performance in real life conditions.

The study conducted by Feng *et al* [63] investigates the thermal performance of cold-formed steel assemblies in which fire is only present on

one side (furnace). This experimental and numerical investigation was initially conducted over eight small sized steel stud panels, which included various profile geometries, lipped or unlipped channels, various gypsum board configurations and the presence or absence of batt insulation. The finite element modelling tool ABAQUS was used to analyse the results and this was found to give reasonable results but lacked information on properties of materials used. It was found that the shape of the stud cross-section does not have a critical effect on the temperature distributions in the assembly and if the width of the lips of the steel section is short, their effect on temperature distribution can be ignored. It also established that the presence of insulation in the wall cavity is a key factor effecting steel temperatures. They conclude to say that without insulation in the wall cavity, poor fire performance will result.

Sultan [64] tested LSF non-insulated, unloaded, gypsum board protected walls using a one-dimensional heat transfer model. This study involves comparisons between the temperatures found at various positions of the assemblies with temperatures predicted for the same locations using the model. Fire resistance ratings are assessed and compared again between the predicted and measured values. It is found that the predictions are reasonably accurate however, some of the limitations of using computer models to predict fire performance are revealed. Determining how convective coefficients change throughout the experiment is essential, especially in the first stages of the fire rating test. Imperfections that might appear in the specimen should also be considered if accurate results are expected. This applies especially to the gypsum board that is no longer in place when 600^0C is reached, although the models assume that it remains until overall failure occurs. Further work is also identified with regards to wall cavity insulation and the addition of structural load to the specimens.

Kodur and Sultan [65] carried out a study to analyze factors that influence the fire resistance of gypsum protected load-bearing steel stud walls. A detailed experimental study was conducted to evaluate the fire resistance of 14 full-scale steel stud wall assemblies. It was concluded that the type of batt insulation used had a significant effect on the fire resistance (mineral wool insulation provided a higher fire resistance compared to glass fibber insulation, but a lower than cellulose fibber insulation). The number of gypsum board layers was found to have a significant effect on fire resistance of loadbearing steel stud walls. Double layers provide a much higher fire resistance than single layer protection. Stud-spacing, load intensity, gauge thickness of studs of single and double row steel stud configurations were also analyzed.

The study conducted by Lee *et al* [66] is a very broad experimental investigation of low and high strength light gauge steels. Three steel grades are used at six different thicknesses varying from 0.4 to 1.2mm, and are subjected to elevated temperatures up to 800^0C. This experiment is to investigate the deterioration of the mechanical properties of the light gauge steels and therefore determine reduction factors. The properties considered are yield strength and modulus of elasticity. Yield strengths at various temperatures and strain levels are found and physical equations are formed to calculate modulus of elasticity. A stress-strain model for elevated temperatures is also developed on the basis of a Ramberg-Osgood formulation [67]. A comparison is made between the stress-strain model mentioned before and an experimental stress-strain curve, which shows that the model was viable for light gauge steels at elevated temperatures.

Feng *et al* [68] produced numerical results of cold-formed thin-walled steel studs under non-uniform high temperatures with different slenderness to find the ultimate failure loads. These results were then compared with predictions achieved using Eurocode 3 Part 1.3 [69] and Lawson's limiting

temperature method [70]. It was established from these comparisons that using Eurocode 3 for the predictions was a suitable way but Lawson's method cannot viably be used. Also the failure mode established was reported to be local buckling but this was not the case at high temperatures. Due to thermal bowing the failure mode changed from local buckling to a combination of local, flexural and bi-axial buckling. Additionally the length of the column had an effect on the state of the column throughout the test. At non-uniform high temperatures the strength and elastic modulus of the steel was reduced for short columns and only in long columns would the thermal bowing effect become problematic.

Buchanan *et al* [71] produced a detailed study on loadbearing walls and their performance when exposed to fire. This study was used to investigate the strength, stiffness, deflections and pressure effects of cold formed steel. Heat transfer modelling is applied for the calculation of the temperature of the steel framing according to the standard ISO 834 [72] time-temperature curve, and three full scale furnace tests are carried out to assess the analytical predictions. From all tests it is found that the main failure mode of the LSF systems is buckling of the compression flange on the ambient side of the wall assembly. The heat transfer model and the furnace tests show the thermal deflections of the LSF to an acceptable degree of accuracy and highlight the fact that when thermal deflections take place, any rotational restraints present are superseded. The research paper suggests that LSF walls with low levels of axial load may perform better in fire tests than in actual fire situations because frictional restraints and redistribution of load can enhance the test result. There are limitations to this work and they have put forward that another model should be used with finite element integrated to help predict steel temperatures and evaluate structures. This could then be used to calculate failure times for design principles.

Feng and Wang [73] produced a comprehensive study predicting lateral deflections and failure times of full-scale cold-formed thin-walled steel structural panels under load and exposed to fire conditions. They determined the effects of thermal bowing deflection to check the relative merits of using Eurocode 3 [74] to perform design calculations for axially loaded steel studs under non-uniform temperature distributions. They determined that the fire resistance of steel panels is affected by thermal bowing deflection and they also suggest that Eurocode 3 could be used for design calculations if modified accounting for LSF.

Alfawakhiri and Sultan [75] developed an analytical thermal-structural model for loadbearing LSF walls. In their investigation six tests took place to generate a model comparing temperatures with deformations and numerous trends were found relating the two factors. All tests included two layers of gypsum board and the specimens failed due to loadbearing capacity. It was found that using cavity insulation might reduce the fire performance of LSF systems. This is because the batt insulation slows down heat transfer through the wall producing a concentration of high temperatures in the exposed flange, which in turn causes buckling. In the case of non-insulated LSF systems, the failure mode observed is compressive failure of the cold flange, with the wall buckling away from the furnace. Alfawakhiri *et al* [76] also produced a review paper about some fundamental analyses that study the variation of the mechanical properties of cold-formed steel under fire conditions. Thermal properties of sheathing materials can also be found in this document and more importantly, some of the drawbacks of the current practice.

Feng and Wang [73] performed eight tests on the resistance of loadbearing steel structural panels. Two tests were conducted at ambient temperatures to deduce the carrying capacity of the LSF system, with the other six

exposed to a standard fire state on only one side. The investigation was proposed using two different lipped channels for the wall sections and varying loads for each. At ambient temperature the failure mode for both channels was located around the top service hole of the specimen. For the six tests under fire conditions the results were very different. The primary failure mode was flexural-torsional buckling. Lateral deformations caused by thermal bowing at high temperatures were found. In addition, the insulation in the wall completely burnt through and this had major effects on the steel panels. It was concluded that the thickness of the steel panels was proportional to the failure time in the fire resistance test.

All methodologies involved in assessing real fire performance need to be validated for full scale fire scenarios. A full scale fire test took place at BRE's facility at Cardington [77], which consisted of two experiments where LSF performance was tested. The experiments were tailored to produce results that could be incorporated into the building regulations for fire safety. Special attention was paid to the performance of LSF separating elements such as walling systems and floors.

In the first test, the floor consisted of pre-fabricated cassettes, whereas in the second it was made out of floor joists. Bracing was used in both of the specimens for added support. The fire destroying the end wall upset the outcomes of the first test and this resulted in the termination of the fire. All building regulations such as integrity, stability and insulation were still met even after the upset. It should be noted from this experience that the weakest component of a system should not have an effect on the system as a whole. The second test alternatively had the advantage of knowing before hand the dangers of the fire breaking affecting specific areas so the form of failure encountered in this case was different. This happened due to vertical deflection because the plasterboard from the ceiling fell on the floor below exerting extra pressure. This shows the importance of using

adequate fixing elements when framing with lightweight construction systems.

Zhao *et al* [78] investigated the performance of lightweight steel frames in fire to improve design efficiency, quantifying the structural benefits provided by the use of sheathing and glazing elements. A numerical analytical calculation method capable of predicting the behaviour of lightweight steel frames under load and non-load bearing conditions and a set of harmonised design rules to be used in European standards were developed. This research was articulated by evaluating the mechanical performance of cold formed steel at elevated temperatures and confirming the behaviour of cold formed steel members and assemblies at room temperature conditions. They also assessed the fire behaviour of fully engulfed lightweight steel studs, and the fire behaviour of steel studs maintained by boards with fire on one side. Finally, they verified the fire behaviour of floors and wall-floor assemblies.

As the use of LSF became more popular, its behaviour under fire conditions started to become recognised in several industry articles. The SFA [79; 80; 81] published a design guide where expected fire ratings are expressed as a function of the number of gypsum boards layers used to sheath the steel frame. SCI [82] also published a design guide in which detailed information about performance of cold formed steel at elevated temperatures and protection to LSF walls, floors, beams and columns is provided.

3.3. Fire Rating Test Prediction

Full-scale tests to measure the fire resistance of walling systems are expensive and time consuming therefore small scale experiments and validated mathematical models have been advocated as a replacement

means to predict performance. Construction companies, architects and fire safety engineers have, in recent years, requested means to establish fire-resistance ratings on an engineering basis. With the advent of performance-based codes and performance-based fire safety engineering, small scale fire resistance tests and validated fire-resistance models have become essential. This paper summarizes the development of an engineering methodology for predicting the fire resistance of lightweight construction systems.

The objective of this section is to illustrate the results obtained from three series of tests in which two different configurations of cold-formed steel walls were subjected to defined heating conditions. The results express a quantitative comparison between the two different configurations tested. The heating conditions intend to simulate the scenario encountered during the Fire Rating Test as described by BS 476 [10]. The translation from the current tests to the larger scale BS 476 and to realistic fire scenarios is achieved with the aid of computational models.

3.3.1. Fire Rating Prediction Methodology

A full scale fire resistance test following BS EN 1365-1:1999 [83] was previously executed over a reference LSF system (Old System). Both the temperature evolution in the most critical section and its actual fire rating are taken as a reference when assessing subsequent assemblies. The incident heat flux evolution imposed over the specimen in order to get that temperature evolution has been calculated experimentally. This heat flux evolution can be corrected and applied over any other systems. By understanding how other systems would react to those corrected heat fluxes, fire rating can be closely approximated. The correction applied over the heat flux evolution takes into consideration the thermal properties of the system analyzed.

This approach is based on the approximation of the heat fluxes that appear in the fire rating test, which are a function of the thermal properties of the specimen. Figure 28 shows two different systems rated following the fire resistance test. The sample on the left is a thermally thin sample and the one on the right is a thermally thick sample (more insulating). If the temperature in the laboratory (T_{lab}) is assumed to be the same in every experiment and the insulating properties of the lateral walls of the furnace do not change from test to test, for the same internal temperature evolution (T_f), the lateral heat loss (Q_L) is equal in both of the experiments represented.

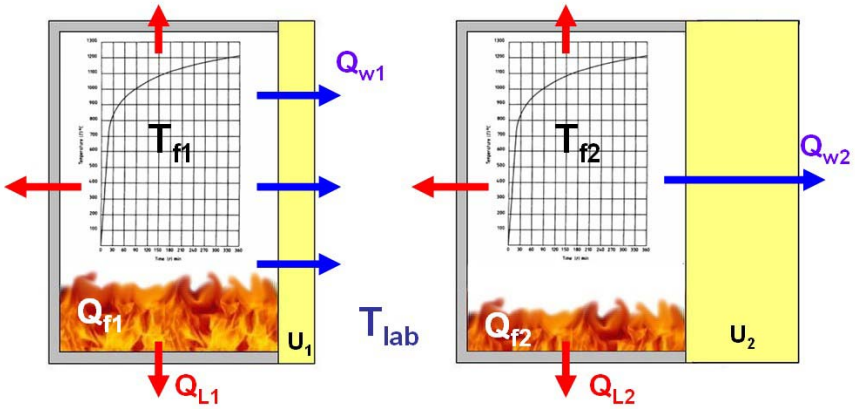

Figure 28: Thermally Thin and Thermally Thick Samples in Fire Rating Test

Due to the weak insulating properties of the specimen on the left (thermally thin), if the temperature distribution within the furnace (T_f) follows the same logarithmic evolution, the heat injected into the furnace (Q_f) must be much greater in the thermally thin specimen than in the thermally thick. This difference affects the amount of heat going through the analyzed specimen (Q_W). The heat going through the specimen is proportional to the heat injected into the furnace and the constant of proportionality depends on its thermal properties (U-Value or thermal

transmittance). The thermal transmittance is a property that changes with temperature and can be calculated experimentally and approximated with the aid of computational models. This methodology is expressed by the following set of equations.

$$T_{f1} = T_{f2} \rightarrow Q_{L1} = Q_{L2}$$

$$Q_{f1} >> Q_{f2} \rightarrow Q_{W1} >> Q_{W2}$$

$$\textit{If not phase change: } Q_{W2} = Q_{W1}\ (U_1/U_2)$$

The amount of heat going through the analyzed specimen (Q_W) is also known as the net heat flux. This quantity is related to the incident heat flux as it is shown in the following heat balance. A further analysis of those concepts is explained in subsequent pages.

$$\dot{q}''_{inc} = \dot{q}''_{NET} + \dot{q}''_{conv} + \dot{q}''_{rad}$$

The same furnace is assumed to be used for the prediction of the fire rating test, therefore any of those two magnitudes (net heat flux and incident heat flux) can be used indistinctly when applying this methodology. This is because of the negligible difference in the convection and radiation heat fluxes encountered when testing different specimens. Although the use of the net heat flux is recommended, the only requirement is to be consistent in their use by only taking one of them as a comparative magnitude between different systems.

This is true for those situations in which there is no constitutive materials changing phase or melting. In these cases, a correction is needed to take into account for the convective heat lost through the openings left in the sample tested. This heat flux methodology has proved to be robust and sound. One of the advantages is that it could be applied to other construction technologies.

3.3.2. Fire Rating Test Standard Review

The main standard that applies to the Fire Rating Test is the BS 476 [10] and the most important sections to be considered are:

- Part 20 : Method for determination of the fire resistance of elements of construction (general principles)
- Part 21: Methods for determination of the fire resistance of loadbearing elements of construction
- Part 22 : Methods for determination of the fire resistance of non-loadbearing elements of construction

BS 476 [10] provides means of quantifying the ability of an element to withstand exposure to high temperatures, setting criteria by which the loadbearing capacity, the fire containment (integrity) and the thermal transmittance (insulation) functions can be adjudged. A representative sample of the element is exposed to a specified heating regime and the performance of the test sample is monitored on the basis of criteria described in the standard. Fire resistance of the test element is expressed as the time for which the appropriate criteria have been satisfied.

The fire resistance of the test construction shall be assessed against one or more of the criteria for loadbearing capacity, integrity and insulation, whichever are relevant to the elements used in practice:

- Loadbearing capacity: specimen fails to support the test loading
- Integrity: when collapse or sustained flaming on the unexposed face occurs or the criteria for impermeability are exceeded
- Insulation: either the mean unexposed face temperature increases by more than 140 °C above its initial value or the temperature recorded at any position on the unexposed face excess of 180 °C above the initial mean unexposed face temperature

BS EN 1365-1:1999 [83] was also considered for the realization of the experiments. This standard gives a detailed explanation of how to execute fire resistance tests for loadbearing construction elements and its first part focuses on walls.

3.3.3. Fire Rating Test Failure Criteria

A benchmark has been selected in order to illustrate the applicability of the methodology presented before. The subsequent steps in the testing procedure are applied to help the reader with the understanding of the methodology. The selected system is a load-bearing external wall exposed to an external fire and the failure criterion is loadbearing capacity. The critical temperature and section when failure happens is calculated by executing a reference full scale test. If an infill wall was selected, the failure criteria would be different and the critical temperature would also change accordingly.

A specimen that corresponds to the 'Old System' and represents an external load-bearing wall assembly was subjected to a test according to BS EN 1365-1:1999 [83], to determine its fire resistance performance. The sample was subjected to heating conditions that intended to simulate an external fire. Figure 29 shows the temperature evolution throughout the duration of the test. The criteria that determined the failure after 38 minutes of exposure of the structure was the Loadbearing capacity. Special attention is paid to this failure mechanism because it is likely to be the determining mechanism however the other failure criteria are also taken into consideration.

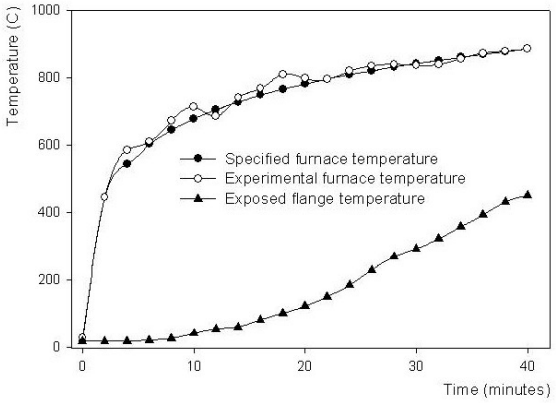

Figure 29: 'Old System' Fire Rating Test Temperature Evolution

The most critical section of the wall when loadbearing failure happens is the exposed flange, which is the nearest to the exposed surface (render). Local buckling induced by thermal expansion is the most common failure mechanism. The previous graph shows the temperature reached by the exposed flange when the failure occurred was 450 °C. None of the three series of tests described in this document have used load bearing specimens. Due to the fact that the critical temperature corresponding to loadbearing failure is known, the results obtained are extrapolated to those conditions and conclusions can be drawn. When loadbearing and non-loadbearing tests are carried out, it is expected that for the same kind of structure, failure under loadbearing conditions might occur at earlier stages. This is due to a reduction of the strength and elastic modulus of the steel at elevated temperatures.

The critical section changes when analyzing infill walls. These systems do not carry load and they do not fail due to load-bearing capacity. This is due to the fact that the systems can expand freely with no vertical restriction. Local and global buckling might occur due to high temperatures in the steel sections, which might lead to integrity failure. However, this mechanism is difficult to predict by means of the proposed methodology therefore the main failure mechanism considered when

analyzing infill walls is insulation. The temperature in the unexposed surface of the walling system is taken as the critical condition to compare different assemblies.

3.3.4. Fire Rating Prediction Experiment Set-up

A number of specimens have been built and subjected to severe heat fluxes. The heating element used to replicate the standard fire rating test furnace is a ceramic radiant panel with no enclosure fuelled by a mixture of propane and air, which is shown in Figure 30. Due to its nature, the heat flux reaching the exposed face of the test element could be varied either by altering the distance from the panel to the sample or by changing the flow of propane.

Figure 30: High radiation panel and representative test sample

The specimens consist of a surrounding steel frame that keeps its constitutive materials in place and a vertical stud that has been fitted in the centre of the frame, in which temperature readings have been recorded. Type K thermocouples attached to the steel members by silver soldering and adhesive tape have been used as temperature probes. The size of the sample has varied throughout the execution of the experiment. A critical size in which the temperatures of the thermocouples on the central stud are affected by the lateral steel frame has been avoided.

The systems analyzed correspond to the Old and New Systems as described in the introduction section. In the 'Old System', polystyrene strips are sandwiched between the external flange of the studs and the honeycomb to create a drainable cavity in order to satisfy NHBC requirements [17]. In the 'New System' sample the polystyrene has been substituted by a layer of mineral wool sheathing. The honeycomb layer from the New System is perforated creating a drainable cavity by itself. This option reduces the size of the cavity and it is expected to improve the behaviour under fire conditions.

One test sample of each system was built for the first series with the dimensions as shown in Figure 31. In the second series, three specimens of each system were built, the size of which had been reduced. In the third series, one test sample of each system was built. All the specimens were heavily instrumented with thermocouples and heat flux meters.

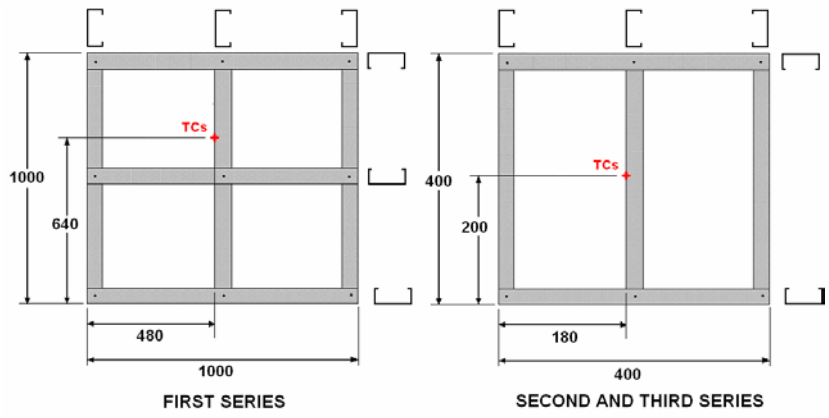

Figure 31: Fire Rating Prediction Test Sample Dimensions (in mm)

The fire performance assessment of these light weight steel systems represents a transient problem and the main thermal properties needed for the computer models are the thermal conductivity, the specific heat and the density of the materials involved. Two of those properties are

represented by the volumetric heat capacity C [J/(m^{3}K)] which is the product of the density [kg/m^3] and the specific heat [J/KgK]. The value of those properties at ambient temperatures is explained in previous chapters and their variation with temperature is illustrated in later.

Type K thermocouples (TC) with fibre glass insulation have been used to record temperatures. Fibre glass is capable of withstanding high temperatures without affecting the readings. Thermocouples are attached to the steel members using a combination of silver soldering, adhesive tape and mechanical fixings. They are positioned in the centre of the specimen where it is assumed that all the heat is transferred perpendicular to the sample and lateral heat transfer can be neglected. Information about its location can be found in Table 14. The ambient air temperature in the general vicinity of the test construction throughout the heating period is measured using a type T thermocouple.

Several thin skin calorimeters and a calibrated incident heat flux meter have been used to record the heat flux evolution throughout the duration of the tests. Their location was selected so as not to influence the heat transfer through the centre part of the specimen where the temperatures are being recorded and thus the heat flux meters have been placed in the bottom corners of the samples as shown in Figure 32.

New System	Old System
External surface (Coating)	External surface (coating)
TC between honeycomb and mineral wool sheathing	TC between honeycomb and polystyrene strips
External Flange (Coating)	External Flange (Coating)
Middle of the Web	Middle of the Web
Internal Flange (Plasterboard)	Internal Flange (Plasterboard)
Internal surface (Plasterboard)	Internal surface (Plasterboard)
Laboratory temperature	Laboratory temperature

Table 14: Thermocouple Position

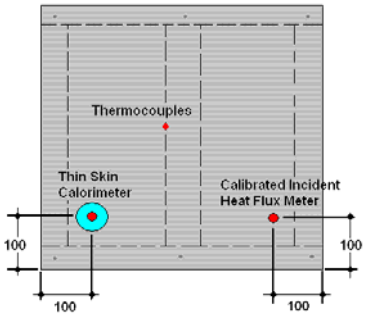

Figure 32: Heat flux meters position

3.3.5. Heat Flux Readings

Every sample has two heat flux meters in the exposed surface as shown in Figure 32. One of them is a calibrated Schmidt-Boelter radiometer [93] that needs water circulation for cooling purposes. The other one is a thin skin calorimeter built following ASTM E459 [86]. The later comprises a 2 mm thick copper disc with a diameter of 20 mm tightly fitted into a flat bottomed hole drilled into a 40 mm diameter plasterboard cylinder. Detailed information about these sensors can be found in further pages. The plasterboard cylinder is embedded on the wall surface. The dimensions of the plasterboard cylinder are 12.5 mm thickness and 40 mm diameter. The thin skin calorimeters have been calibrated taking the readings from the Schmidt-Boelter radiometer as a reference.

The reason why thin skin calorimeters have been used in this experiment is that they are also employed in the Dalmarnock Fire Test that is described later in this chapter. By understanding how these sensors work, heat flux readings can be easily obtained in a full scale fire scenario. This is therefore a bench scale analysis of sensors that are later used in other applications.

The thin skin calorimeters have been mounted in both the 'Old System' and the 'New System' and an energy balance satisfying the following

equation has been conducted. The various terms in this equation have been calculated as explained in further pages. The convective coefficient has been calculated using Nusselt correlations and the radiation term has been calculated taking the temperature of the surroundings as ambient.

$$\dot{q}''_{inc} = \frac{1}{(1-C)}\left[\rho\delta c_p \frac{dT}{dt} + \varepsilon\sigma(T_S^4 - T_0^4) + h_{conv}(T_S - T_g)\right]$$

The value of the C-Factor has been established experimentally for several incident heat fluxes. This factor has been found to depend on the temperature of the copper disc and this is shown in Figure 33.

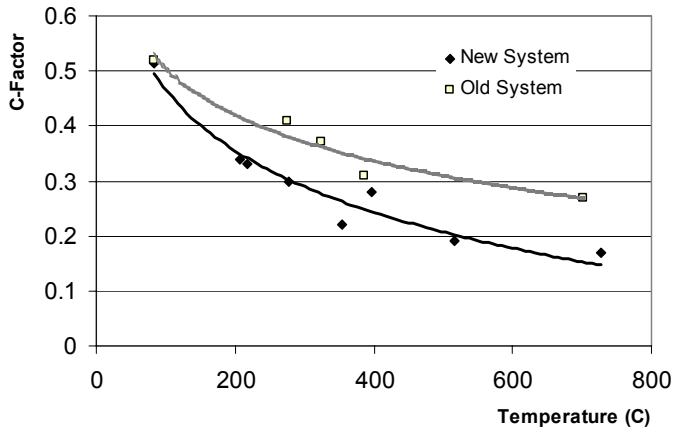

Figure 33: Thin Skin Calorimeter Calibration Factor

3.3.6. External Fire Rating Replica

The first and second series were intended to show the dependence of specimen size and variable heat flux on the temperature evolution in the critical parts of the systems analyzed. The third series is intended to provide actual data to realise a comparative analysis over the two systems examined when subjected to an external fire. This replicates a situation in

which the external side of the specimen (coating) is placed facing the furnace and the plasterboard faces the laboratory.

One specimen of the 'New System' and another of the 'Old System' were exposed to certain heating conditions in the first series. Smaller specimens were exposed to the same conditions in the second series of tests. The temperature evolutions encountered for that specific heat flux were found to be relatively similar therefore it was concluded that the size used for the second series was adequate and any subsequent specimen should be built accordingly. This is shown by Figure 34.

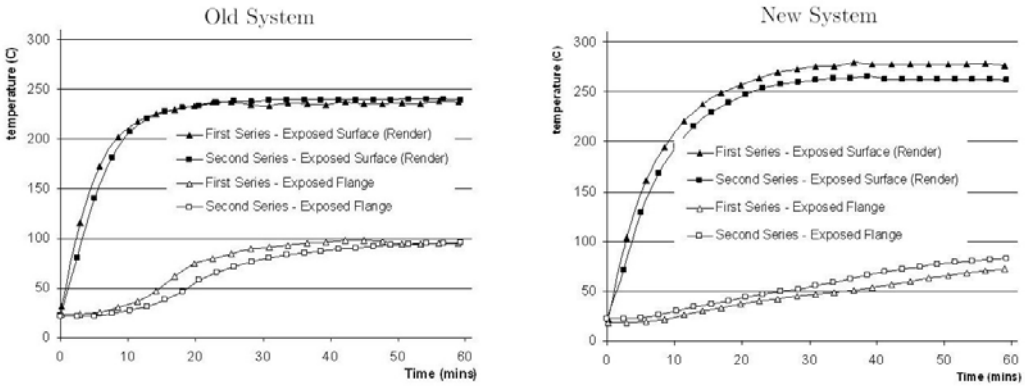

Figure 34: Comparative Temperature Evolution for Same Heat Flux and Different Specimen Dimensions

The second series also analyzed the influence of incident heat flux variations on the temperature evolution at several points of the specimens. It was found that varying the propane flow was not an adequate alternative due to the difficulty in fully controlling the opening of the valves. Modifying the distance at which the specimen is located from the radiant panel proved to be a more satisfactory way to control the incident heat flux. Figure 35 shows a graph where the incident heat flux is expressed as a function of the distance between the radiant panel and the test sample.

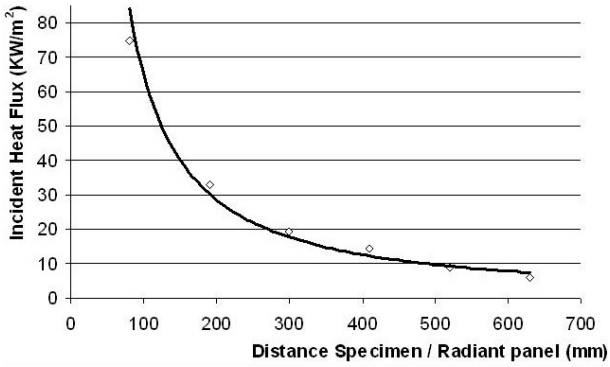

Figure 35: Variation of Heat Flux with Horizontal Distance from Radiant Panel

None of the specimens used for the execution of the experiments were loaded however due to the fact that the temperature corresponding to loadbearing failure is known (450 ° C in the exposed flange), the results obtained are extrapolated to those conditions. One representative specimen of each system was exposed to a number of constant heat fluxes. For each of those heat fluxes, the specimens were left until reaching steady temperatures on the critical section (exposed flange). By doing that, the maximum temperature in that critical point for each particular heat flux was determined experimentally. Additionally, the method by which the steady conditions were reached was recorded and characterized mathematically. Figure 36 and Figure 37 shows the temperature distribution for each system throughout the duration of the test.

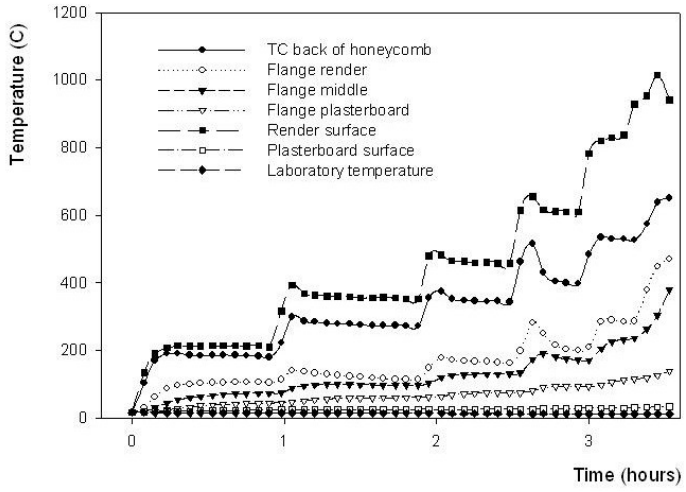

Figure 36: 'Old System' Fire Rating Prediction Temperature Evolution

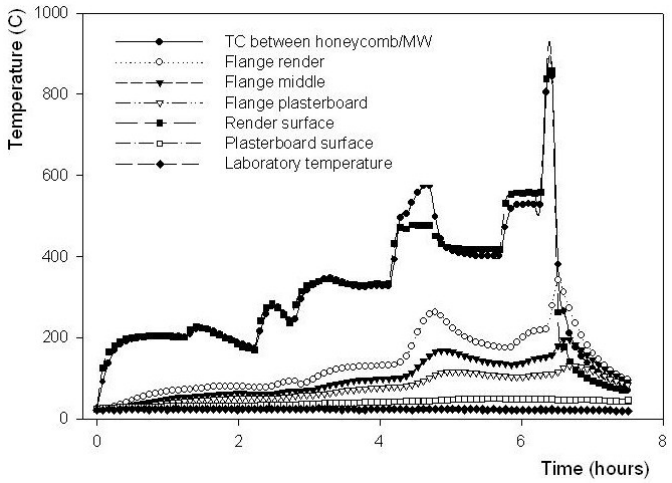

Figure 37: 'New System' Fire Rating Prediction Temperature Evolution

It is observed in both of the experiments that at a surface temperature of around 400 °C, the aluminium within the honeycomb starts oxidizing exothermically. Aluminium at ambient conditions is covered by a thin layer of aluminium oxide. This covering layer brakes when an incident heat flux such as those encountered in fire condition is applied. These irregularities induced in the surface allow the interior bulk of aluminium alloy to get into contact with oxygen producing immediate oxidation and a large amount of heat to be released (exothermic reaction). This is a chain reaction that continues if the incident heat flux is increased.

This corresponds to a heat generation source within the systems that lasts for a short period of time. This chemical oxidation releases a large amount of heat as it detailed later in the text. In addition the mineral wool binding agent begins to evaporate and burn at a temperature of 250 $^{\circ}$C. This combustion releases heat that affects the interiors of the systems. The actual fibres can withstand more than 1000 $^{\circ}$C without melting however when the temperature rises above 250 $^{\circ}$C the binder evaporates in the exposed zones and the fibres remain intact as their inbuilt cohesiveness and layering keep them together ensuring that the material retains its rigidity.

The duration of the test was different for each of the configurations as shown in the previous figures and several events happened throughout the experiments. They were recorded and are presented in Table 15 and Table 16.

Time (hours)	Distance from heater (mm)	Incident heat flux (KW/m2)	Action / Event
0.0	630	5.00	Heating starts.
1.0	410	14.31	The sample is moved closer to the radiant panel
1.9	300	19.34	The sample is moved closer to the radiant panel
2.5	190	33.61	The sample is moved closer to the radiant panel
3.0	100	78.5	The sample is moved closer to the radiant panel. Beginning of spalling. The TC recording the surface temperature came off (5mm away from surface).
3.3	70	N.A.	The sample is moved closer to the radiant panel
3.5	70	N.A.	The propane flow is interrupted and the sample is allowed to cool down.
3.6	70	N.A.	End of data logging

Table 15: 'Old System' Fire Rating Timeline

Time (hours)	Distance from heater (mm)	Incident heat flux (KW/m2)	Action / Event
0.0	630	6.04	Heating starts.
1.3	630	6.04	Propane flow readjustment, which produces change in heat flux. Initial heat flux rise. After the pick, heat flux drops
2.2	520	8.86	The sample is moved closer to the radiant heat panel. The propane flow is adjusted and there is a rise in the heat flux. After the initial pick there is a drop in the incident heat flux. Propane bottle is replaced (no effect in test)
2.8	410	14.40	The sample is moved closer to the radiant panel.
4.2	300	19.35	The sample is moved closer to the radiant panel.
4.7	300	19.35	The render starts producing spalling. The TC recording the surface temperature came off (5mm away from surface)
5.7	190	33.06	The sample is moved closer to the radiant panel.
6.3	100	74.68	The sample is moved closer to the radiant panel.
6.3	100	74.68	Interstitial fire within the honeycomb
6.4	100	74.68	The propane flow is interrupted and the sample is allowed to cool down.
7.5	100	74.68	End of data logging

Table 16: New System Fire Rating Timeline

The heat transfer mechanisms considered in the gas phase around the specimens are radiation and convection. The heat transfer mechanisms within the specimens vary depending on each configuration. The polystyrene channels in the Old System melt rapidly leaving an empty space in which radiation and convection occur. This is not observed in the New System as the polystyrene channels have been substituted by mineral wool. If the fixings do not fail, the mineral wool stays in place and conduction is the governing heat transfer mechanism.

The convective coefficients have been calculated from the experimental data by applying the following Nusselt correlations that describe external free convection flows in vertical pates.

$$h_{conv} = \frac{Nu_L \cdot k}{L}$$

$$Nu_L = \left\{ 0.825 + \frac{0.387 Ra_L^{1/6}}{\left[1 + (0.492/\mathrm{Pr})^{9/16}\right]^{8/27}} \right\}^2$$

$$Ra_L = \frac{g\beta(T_s - T_{lab})L^3}{\alpha\nu}$$

Properties evaluated for $T_f = \frac{1}{2}(T_S + T_{lab})$

Where,

Nu_L is the Nusselt number

Ra_L is the Rayleigh number

Pr is the Prandtl number

k is the conductivity of the air in W/mK

L is the characteristic length in m

g is the gravity in m/s^2

ρ is the inverse of the temperature at which the properties are being evaluated in K^{-1}

α is the thermal diffusivity in m/s^2

υ is the kinematic viscosity in m^2/s

T_S is the surface temperature in K

T_{lab} is the laboratory temperature in K

3.3.7. 'Old System' External Fire Rating Characterization

The experimental temperature reached in the exposed flange of the Old System was recorded and it is plotted as a function of the incident heat

flux in Figure 38. The red dots represent the maximum temperatures in the exposed flange when the steady temperature distribution is reached. The trendline that connects those points is exponential and characterizes the heat radiated over the exposed flange, which in reality is proportional to the temperature to the power four on the back of the honeycomb (when the polystyrene strips have melted).

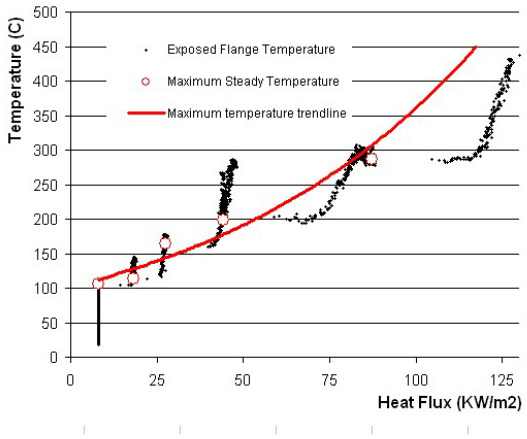

Figure 38: 'Old System' Experimental Exposed Flange Temperature Evolution

The temperature in the exposed flange depends on convection and radiation within the space left by the melted polystyrene. Radiation from the back of the honeycomb to the exposed flange is the most influential form of heat transfer however re-radiation from the flange and convection in both the back of the honeycomb and over the exposed flange have been taken into consideration. After determining the maximum temperature on the exposed flange for each heat flux, it is required to calculate how this temperature is reached. The lumped capacitance method (in the steel section) is used in order to approximate the temperature evolution and the following equation is used to approximate the temperature rise.

$$T_i = T_{\max} - (T_{\max} - T_{\min})e^{-\tau t}$$

Where

T_i is the approximated temperature in °C

T_{max} is the maximum steady temperature for each heat flux in °C

T_{min} is the initial temperature in °C

t is the time in seconds

τ is the thermal time constant

The thermal time constant is a non-dimensional parameter that symbolizes the time in a transient temperature change rate for a structure. This parameter is characterized by the following equation.

$$\tau = \frac{h_{total} A_s}{\rho V c}$$

Where

h_{total} is the heat transfer coefficient (including convection and radiation) in W/m^{2}K

As is the area in m^2

ρ is the density in Kg/m^3

V is the volume in m^3

C is the specific heat in

C, ρ, V and A_s are assumed to be constant throughout the duration of the experiments. Therefore, the thermal time constant varies proportionally to the h_{total} coefficient. This coefficient takes into consideration both convection and radiation, which are dependant on the temperature, and ultimately on the incident heat flux. The variation of the h_{total} coefficient as a function of the heat flux is shown in Figure 39. The convective proportion of h_{total} has been calculated using the approximation presented before and it does not change significantly with incident heat

flux variation (around 12.5 W/m^{2}K). The radiation has been calculated using the following estimation [92].

$$q_{rad}'' = \varepsilon\sigma(T_s^4 - T_{sur}^4) = h_r(T_s - T_{sur})$$

$$h_{rad} = \varepsilon\sigma(T_s - T_{sur})(T_s^2 - T_{sur}^2)$$

where

T_s is the temperature on the flange in $^\circ$C

T_{sur} is the temperature on the back of the honeycomb in $^\circ$C

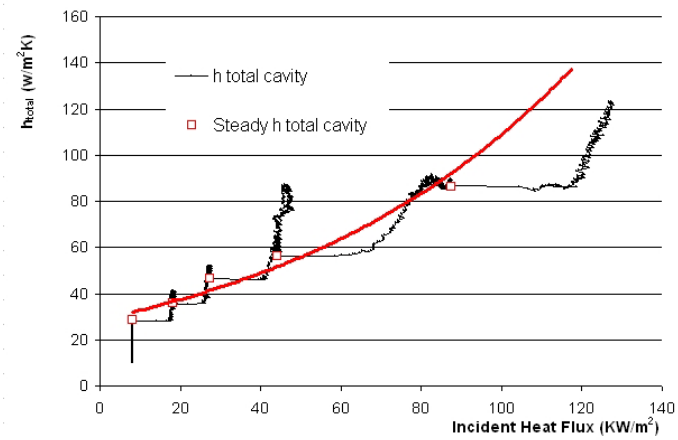

Figure 39: 'Old System' Internal h_{total} evolution

The coefficient h_{total} varies exponentially as shown by the trendline in Figure 40. Consequently, the thermal time constant is expected to follow the same pattern. When the variation of the thermal time constant as a function of the incident heat flux was determined, the same coefficients that characterize the previous trendline have been applied and adjusted.

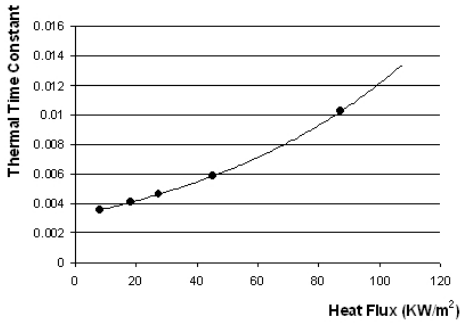

Figure 40: 'Old System' Thermal Time Constant

The analytical solution found for the Old System that characterizes both the maximum critical temperature (exposed flange) and the thermal time constant for each characteristic incident heat flux is as follows:

$$Tcrit_{\max} = 101.43 \times e^{0.0127 Q_{inc}}$$

$$\tau = 3.2 \times 10^{-3} \times e^{0.0133 Q_{inc}}$$

Where,

$Tcrit_{max}$ is the maximum temperature to be reached in the exposed flange (steady state conditions) in $^{\circ}$C

Q_{inc} is the incident heat flux in KW/m^2

τ is the thermal time constant

By using the previous mathematical model, both the maximum temperature in the exposed flange and the thermal time constant can be approximated for any incident heat flux as shown in Figure 41. The error bar between the experimental and approximated temperature on the exposed flange is acceptable. This model could be applied in the opposite direction. Starting from the temperature rise in the exposed flange, the incident heat flux can be closely approximated. This approach has been used to work out the incident heat flux evolution in the full scale fire

resistance test and the result is shown in Figure 42. The incident heat flux is assumed to grow lineally at the early stages of the full fire rating test where less than 100 °C were recorded on the exposed flange (the honeycomb strips have not melted completely). This linear approximation is acceptable because the exposed flange temperature is not really affected by such small incident heat fluxes.

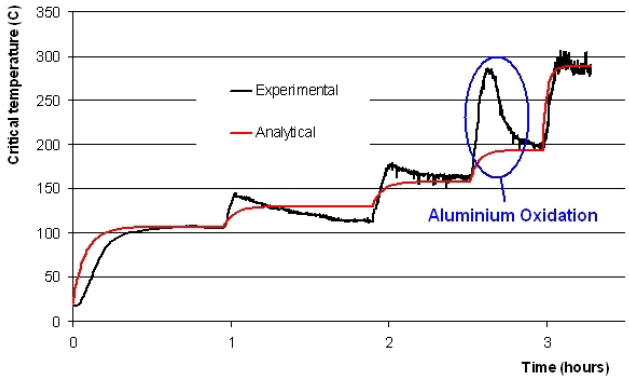

Figure 41: 'Old System' Exposed Flange Temperature - Experimental vs. Analytical Solutions

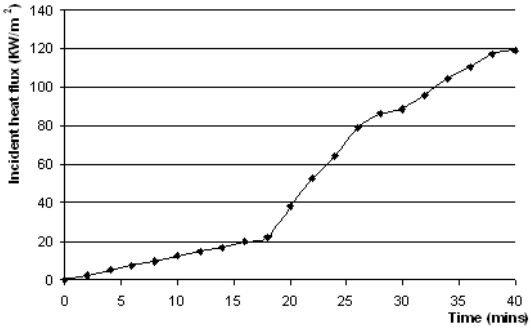

Figure 42: Incident Heat Flux Evolution in 'Old System' Fire Rating Test

When this heat flux evolution is applied over other systems, a correction for convective heat losses is recommended. This is due to the fact that when the polystyrene channels have melted, some convective heat is lost into the ambient environment through the gaps left in the system. This does not happen in the New System where gaps are not created and the

heat is either contained within the system or travels through. That convective heat loss has been calculated and it is proportional to the incident heat flux as shown in Figure 43. Figure 44 shows the corrected incident heat flux evolution in the full scale fire rating test to be applied over other systems.

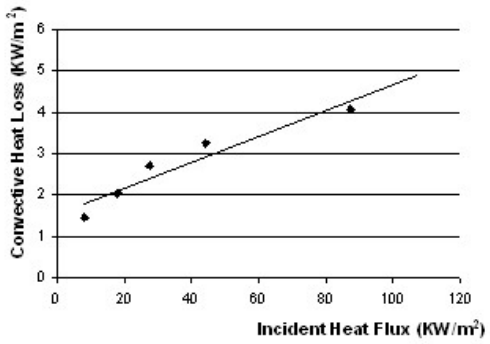

Figure 43: Convective Heal Loss through Gaps in 'Old System'

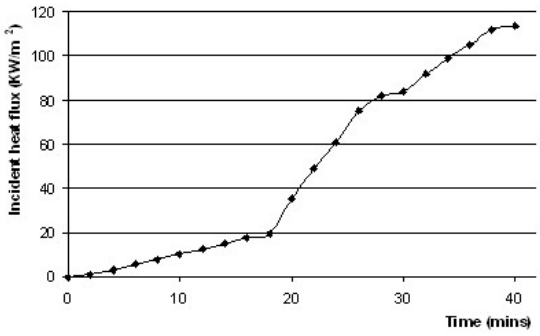

Figure 44: Corrected Incident Heat Flux Evolution in 'Old System' Fire Rating Test

3.3.8. LSF External Fire Rating Characterization

The modelling of the 'New System' was less tedious as the only heat transfer mechanism considered within the specimen is conduction. This means that the temperature rise in the exposed flange and the variation of the thermal time constant as a function of the incident heat flux can be assumed to be linear. Figure 45 and Figure 46 show the evolution of those

important parameters used to theoretically approximate the temperature growth in the exposed flange.

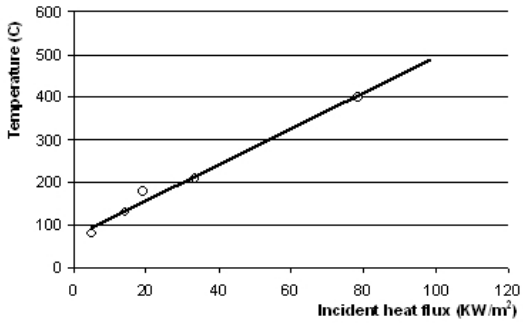

Figure 45: New System Experimental Exposed Flange Temperature Evolution

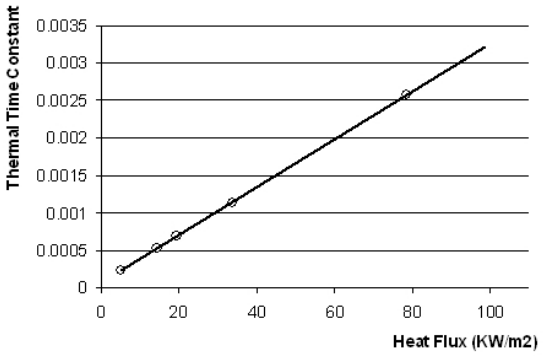

Figure 46: New System Thermal Time Constant

The analytical solution found for the New System that characterizes both the maximum critical temperature (exposed flange) and the thermal time constant for each characteristic incident heat flux is as follows:

$$Tcrit_{\max} = 4.206 \times Q_{inc} + 72.241$$

$$\tau = 3.188 \times 10^{-5} \times Q_{inc} + 6.884 \times 10^{-5}$$

Where,

$Tcrit_{max}$ is the maximum temperature to be reached in the exposed flange (steady state conditions) in $^{\circ}$C

Q_{inc} is the incident heat flux in KW/m^2

τ is the thermal time constant

A good agreement between the experimental and the analytical solutions is found and it is shown in Figure 47. The graph shows only the period of temperature growth as the decay period is omitted.

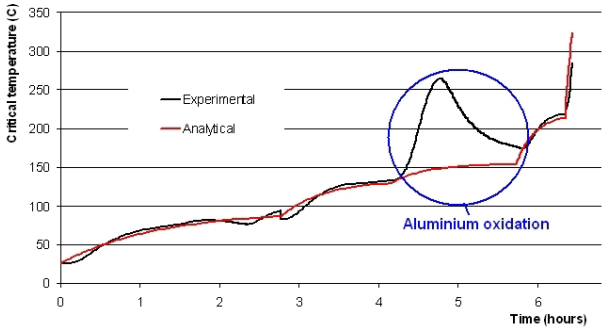

Figure 47: New System Exposed Flange Temperature - Experimental vs. Analytical Solutions

3.3.9. Aluminium Oxidation

One of the most noticeable phenomenon when subjecting the samples to the effect of variable heat fluxes is the oxidation process that happens in the aluminium forming the honeycomb layer. This oxidation is extremely exothermic and therefore, the heat generated by this source needs to be considered in further computer analysis. This alloy is initially covered by a thin layer of aluminium oxide that protects the metal from further oxidation. When subjected to a heat flux, this thin layer is altered and a larger area of aluminium is exposed to the effect of the surrounding air therefore oxidation occurs gradually as the element is heated up. The standard heat of formation of this compound is 1675.7 KJ/mol [84] and the formula that characterizes this chemical reaction is as follows.

$$4Al + 3O_2 \rightarrow 2Al_2O_3$$

From this, it can be deduced that 108 grams of pure aluminium (molar mass 27g/mol) produces 204 grams of aluminium oxide (molar mass 102 g/mol). The weight of the aluminium alloy per square metre of honeycomb is 2 kg/m^3. If the standard heat of formation is taken into account, a maximum heat release of 124.126 MJ can be expected from a square meter of honeycomb, which illustrates the importance of this phenomenon.

The fire rating prediction tests have shown that this oxidation is only noticeable when relatively high heat fluxes attack the aluminium alloy and therefore, it is only considered at elevated temperatures. However, at lower temperatures, the resins that keep the honeycomb and the fibre glass sheets together release heat when pyrolysis starts. Both of these effects are taken into consideration in further computer analysis.

3.3.10. Fire Rating Prediction Computer simulations

Computer simulations have been conducted to compare quantitatively the insulating properties between the reference system ('Old System' in this case) and any other ('New System' in this case). This comparison is done to calculate the incident heat flux evolution that is found in the full scale fire rating test for any assembly ('New System' in this case). A non dimensional parameter (U2/U1) that represents the rate of thermal transmittance variation between the systems studied is presented. The incident heat flux to be applied over the New System in order to get its fire rating results from multiplying that parameter by the incident heat flux imposed over the reference assembly ('Old System').

It is recommended that the software package used can incorporate non linear analysis (properties of constitutive materials change with time) to get a more accurate outcome. HEAT2 has been selected in this case for the computational modelling even though this programme does not account for non lineal analysis. The outcome is assumed to be very accurate as the type and quantity of materials involved in both of the assemblies studied are very similar and their properties will change accordingly. The results obtained from the computational analysis are presented in Table 17 and Figure 48.

Temp exposed face (˚C)	U-values		(U2/U1)
	Old System (U1)	New System (U2)	
100	0.3207	0.2314	0.7215
200	0.3338	0.2354	0.7052
300	0.3451	0.2391	0.6928
400	0.3552	0.2429	0.6838
500	0.3642	0.2466	0.6771
600	0.3723	0.2503	0.6723
700	0.3794	0.2540	0.6695
800	0.3858	0.2575	0.6674

Table 17: Qualitative comparison of thermal properties

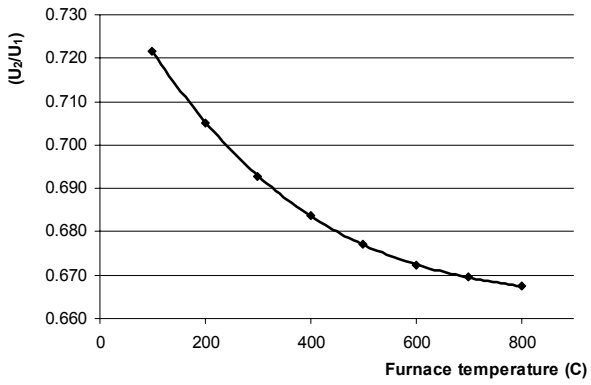

Figure 48: Qualitative comparison of thermal properties

As it was stated before, the thermal properties of the constitutive materials depend on the temperature. Figure 48 shows the dependence in terms of a non dimensional parameter (U2/U1) that represents the rate of thermal transmittance variation between the systems studied. The furnace temperature has been taken as a reference to determine that change in the properties. The corrected incident heat flux is to be applied over the New System in order to get its fire rating results from multiplying that value by the incident heat flux imposed over the reference assembly ('Old System'). The New System's exposed flange temperature evolution for the first 38 minutes can be closely calculated. At that particular moment in time, the critical temperature in the New System was 386 °C (temperature in the exposed flange) compared to 450 °C for the Old System. This clearly shows the better behaviour of the New System under fire conditions.

In order to predict the fire rating for the New System, the incident heat flux after 38 minutes must be approximated. There is an uncertainty about how that incident heat flux will evolve from then on and assumptions must be made in that respect. The approach taken assumes a logarithmic heat flux evolution after the first 38 minutes. This logarithmic heat flux growth is similar in terms of slope variation to the temperature rise imposed on the furnace temperature and it is plotted in Figure 49. The expected temperature in the exposed flange for that incident heat flux evolution has also been plotted for the approach considered in Figure 50.

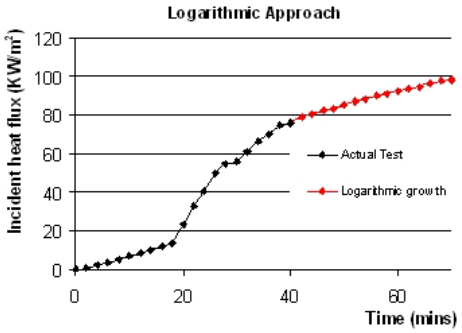

Figure 49: Incident heat flux evolution for New System

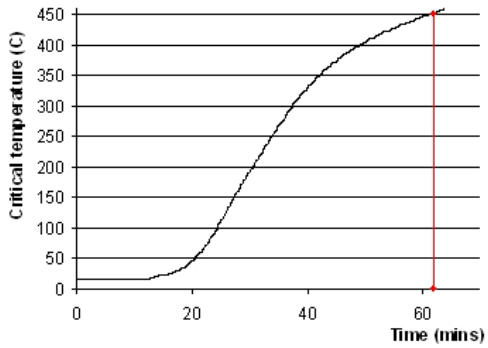

Figure 50: Exposed flange temperature evolution

As shown in Figure 50, this logarithmic approach gives a fire resistance of 62 minutes. Other approaches are shown in the following chapter when analyzing the thermal behaviour of the walling systems by means of computer models.

3.3.11. Infill walling systems

Infill walling systems do not carry any load. They are attached to the concrete slabs that form the floor and the ceiling by mechanical fixings. A gap is normally left between the top channel and the ceiling in order to allow thermal expansion therefore buckling induced by thermal expansion is normally not expected. In addition to that, there is no restriction for vertical expansion when subjected to the fire rating test. In conclusion, these systems do not fail because of load bearing capacity. For this reason the approach used in the previous section needs to be amended in order to cope with this variation. The main adaptation is based on swapping the critical temperature keeping the core of the mathematical approximation the same.

The critical temperature is no longer the temperature of the exposed flange as the failure mechanism is no longer the load bearing capacity. For infill

walls, the failure mechanism could either be insulation or integrity. Integrity can not be predicted with the methodology suggested. Therefore, insulation is the critical failure criteria and the temperature in the unexposed surface is the critical one. There are some uncertainties attached to this calculation method and the main one is the assumption concerning the temperature evolution after the first 38 minutes. For this reason, computer models are used to calculate the fire rating in infill walls. The results are presented in the chapter dedicated to structural behaviour.

3.3.12. Fire Rating Prediction Conclusions

The two systems analyzed in this report have shown a similar temperature rise in the critical sections when subjected to identical heat fluxes however due to their dissimilar thermal properties, the incident heat flux evolution when exposed to the fire rating test varies significantly. The new system is more insulating and none of its constitutive materials melt when subjected to the full scale fire performance test. That is why the fire rating is more satisfactory.

The outcome of this investigation is the time that any specimen would withstand when tested in the furnace used for our analysis. If any other furnace is used, corrections to the solution obtained need to be applied. In that case, it is recommended to understand the methodology and then apply it to the new furnace after obtaining the new governing equations.

One of the main criticisms of the fire performance test is the difference in the rating that dissimilar furnaces give when testing the same specimen. Even though the governing heat transfer mode within the furnace is convection, radiation also affects the outcome. Radiation depends on the characteristics of the furnace (size, ceramic walls, fuel, etc.), therefore it is

noted that there is a need for regulation with regards to the calibration of the existing furnaces in order to get universal ratings.

A measure was adopted by fire research organizations willing to homogenize fire ratings based on the use of plate thermometers. These reliable sensors are placed on the exposed surface allowing a gap between them and the specimen. Although more homogeneous results have been gathered, this approach has proved not to be enough and the need to account for heat fluxes has been identify if further improvement of this experiment wants to be achieved. If furnace calibration was carried out, heat flux evolution as a function of time and thermal insulating properties of the specimens could be drawn and be the basis for engineering based fire performance predictions.

3.4. LSF on Dalmarnock Fire Tests

Fire rating requirements are to be satisfied by all construction elements. However they do not fully represent the conditions encountered in real life scenarios. All methodologies involved in assessing real fire performance need to be validated for realistic fires. Tests involving full scale fires are not normally viable due to economical, environmental and safety reasons however an experiment of such a nature has been carried out in order to analyse the performance of LSF self contained infill walls under the action of severe fire conditions.

The full scale fire test took place in a 22 storey reinforced concrete residential council estate in Dalmarnock, Glasgow. The Glasgow Housing Authority had previously identified this building for demolition and when tenants were evacuated, the block was made available for fire testing. Three fire tests took place over a period of two days, from the 25th to the 26th of July 2006. These tests were done to assess the effect of an actual

fire in the structure. Light weight construction elements were fitted and satisfactory conclusions about their behaviour were drawn.

3.4.1. Experiment description

The first test carried out on Tuesday 25th July 2006 was an uncontrolled fire situated in Flat 19 on the fourth floor. The living room compartment was fully furnished as a lounge/office in a single-family two bedroom flat, with full monitoring by sensors to assess fire and structural behaviour. In this case the fire was allowed to reach flashover. The second test also took place on this day but was used to assess stairwell smoke management. The third and final test was carried out on Wednesday 26th July 2006 in Flat 7 on the 2nd floor. The apartment, furniture and its arrangement was identical as in Test 1. For this scenario some of the windows and doors were remotely controlled to influence the fire growth. This test was used to show how two situations with the same fire load but different and controlled ventilation patterns would produce extremely different outcomes.

For the purpose of this thesis only the data from Test 1 was used as the LSF walling system was selected to be in that compartment as it is the most effective at showing the effects of a fully developed fire on such a structure. The external walling stacking system used corresponds to the New System and it was fitted to separate the living room and the kitchen area of apartment 19 as it is shown in Figure 51 and Figure 52.

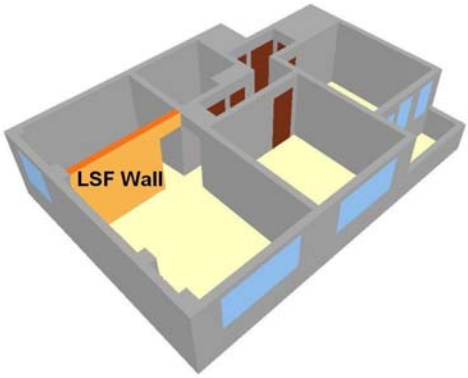

Figure 51: Apartment layout

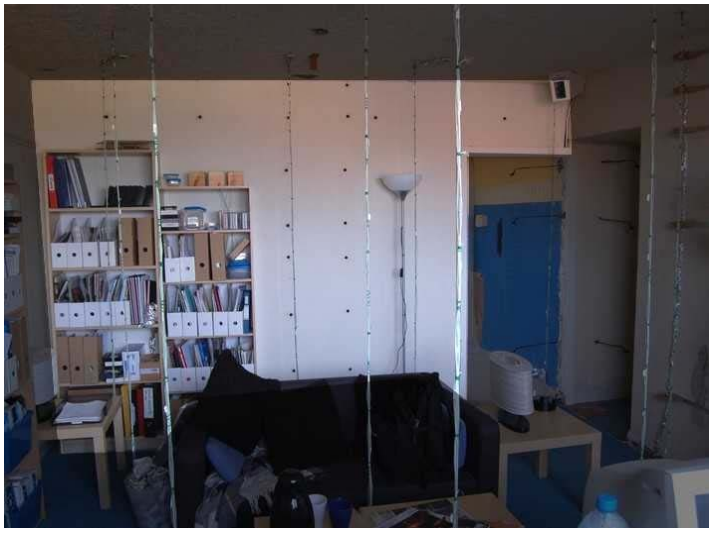

Figure 52: LSF System in Dalmarnock Fire Experiments

Although the insulating properties of the LSF system correspond to those of an external wall, this was fitted inside the apartment. The benefits of the location and geometry of the LSF walling system meant that the wall was attacked with fire from both sides. This replicates what would happen if fitted as an external wall with the advantage of more severe conditions being reached.

A doorway created by the walling system (connection of rectangular panel and beam) was built in order to facilitate ventilation and flame spread to both sides of the wall. This affects the temperatures obtained in the non

exposed face of the system (gypsum board). The external side of the walling system (render) was placed facing the fire (living room) for two reasons. One is that enough information is given by the manufacturers of gypsum board [85] with regards to its behaviour under fire conditions when sheathing LSF structures. The second is that external fire spread over LSF facades was being analysed and placing the render side facing the fire replicates this condition. In addition the existing external wall could not be knocked down, as this would create a structural weakness and a major risk of safety.

In any case, both sides were subjected to the action of the flames as the fire crept around the door opening and had an effect on the unexposed surface. It is of common knowledge that when there is an opening in the building envelope, the fire tends to rush towards it, creeps through the upper part of the gap and engulfs the outside surface with flames burning in a vertical direction at a faster rate than inside the compartment. This effect is shown in Figure 53 and it is intended to be approximated with the experiment by having the render side facing the fire. In doing so, the most representative side of the wall when having external flaming is affected by the fire. The plasterboard side is also affected by the fire as it would in external flaming conditions. The dimensions of the compartment (living room area) where the fire was started are shown in Figure 54 and the layout of the furniture is shown in Figure 55.

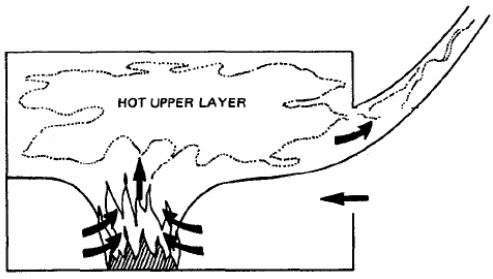

Figure 53: Fire Development on Facade Opening

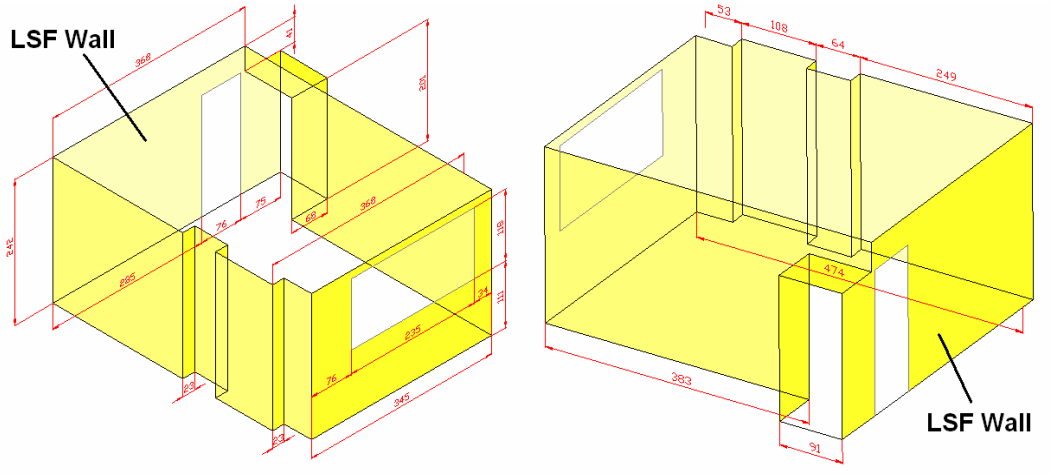

Figure 54: Compartment Dimensions (in cm)

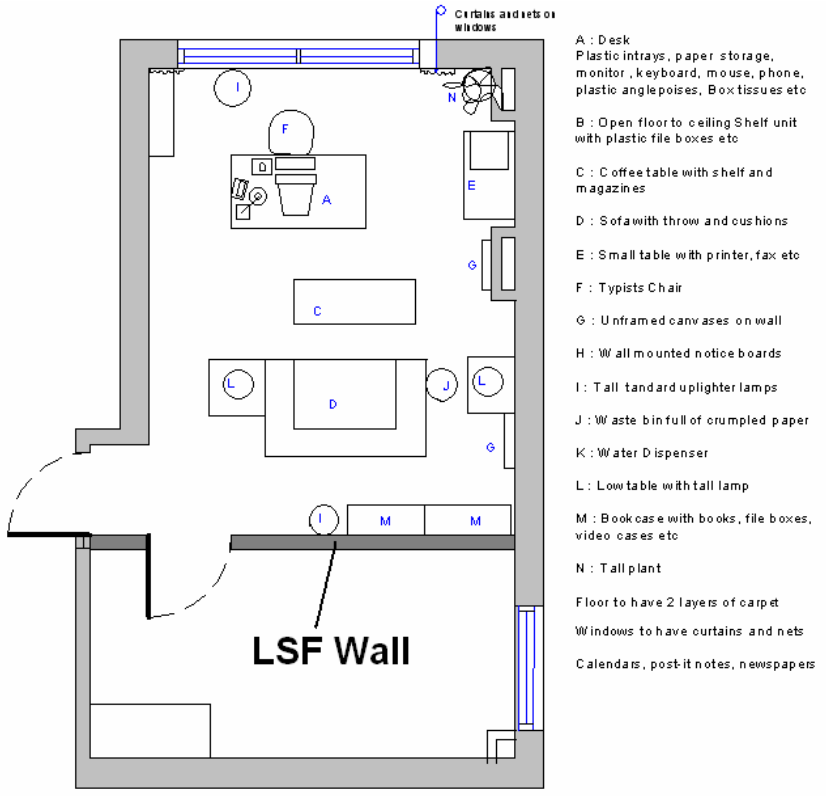

Figure 55: Furniture Layout

A basket (J) placed next to the sofa is initially ignited and a few seconds later, the fire starts spreading. The sofa (D) made from particleboard, polyurethane and polyester with dimensions of 1370 mm x 780 mm x 720

mm and a weight of 34 Kg is then ignited. Thereafter, the fire spreads to the bookcases (M). They are filled, as they would be in a regular house/office with books, files and videotapes. They are made of particleboard and acrylic paint with a weight of 21.3 Kg. These items are particularly relevant in this analysis due to their proximity to the LSF walling system. They are shown in Figure 56.

Figure 56: Dalmarnock Relevant Furniture (D & M)

The desk (A) and tables (E & C) take up a large percentage of the floor space as shown in Figure 57. Item (A) is a desk with typical office materials such as plastic trays, paper storage, computer, monitor, keyboard, mouse, phone, etc. It is made from solid wood and metal legs with dimensions 1200 mm x 755 mm x 730 mm. Article (C) is a low table in front of the sofa with magazines. It is made from particleboard and acrylic paint with dimensions 900 mm x 550 mm x 450 mm. Article (E) is a table with a printer, fax, etc. It is made from particleboard with dimensions 800mm x 550mm x 730 mm.

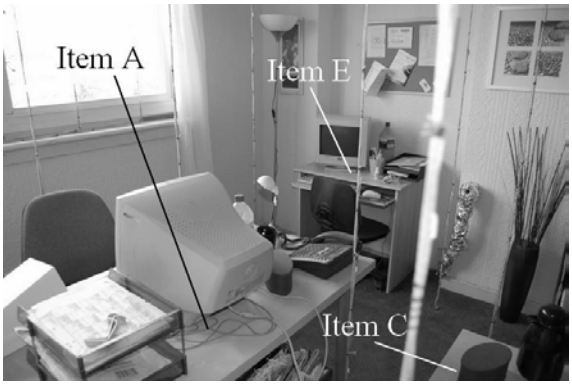

Figure 57: Dalmarnock Relevant Furniture (A & E)

Piece (L) is a low table with a lamp very close to the waste paper basket first ignited. It is made from particleboard and acrylic paint with dimensions 550 mm x 550 mm x 450 mm. The window was dressed with curtains made up of 65% polyester and 35% cotton, which remained open for the experiment. The polypropylene plastic box (O) was full of office items at a weight of 2.7 Kg and dimensions 350mm x 320mm x 61mm. The floor of the room had two layers of carpet. The above details best describe a regular set up in a living room/office, which aims to give realistic results. Some of these items are shown in Figure 58.

Figure 58: Dalmarnock Relevant Furniture (L, O & I)

3.4.2. Fire Timeline

The paper contained in the rubbish bin and some accelerant was initially ignited. Thereafter, the fire spread to a blanket draped over the sofa, where the cushions also caught fire. The sofa then caught fire and soon the bookcases placed in contact with the LSF wall (M) ignited. In 5:30 minutes the flash over phenomena took place and flames covered the whole living room area. The smoke layer descended to the ground so the cameras installed to record the fire evolution could no longer visualise the fire spread. The fire was allowed to burn for 19 minutes in total when the fire brigade decided to intervene and extinguish it. The total heat released by the fire was between 4 and 5 MW. Figure 59 shows two of the most

characteristic moments in the fire, ignition and flash over and Table 18 shows the timeline of the fire evolution.

Figure 59: Fire Ignition and Flash Over

Time from ignition (min:sec)	Event
00:00	Ignition
00:09	Cushions ignite
03:06	Smoke visible in main corridor
04:35	Bookcase ignites
05:30	Flash Over
13:21	Window Breakage (Assisted)
18:00	External Flaming
19:00	Extinction
22:00	Mostly Smouldering

Table 18: Fire Evolution Timeline

3.4.3. LSF Specimen Description

The LSF walling system comprised of a rectangular panel connected to a suspended beam. The consecutive steps in its construction are shown in Figure 60 and its dimensions and geometry in Figure 61. The walling

system was bolted to floor and the ceiling (concrete slab) to obtain a fixed end connection. Small gaps between the top and bottom horizontal steel channels and their respective concrete slabs have been allowed in order to facilitate the assembly of the walling systems and to allow differential thermal expansion to occur, which minimizes thermal stresses on the wall. These gaps are 20 mm thick on the top and 10 mm thick on the bottom. They have been filled with fire resistant foam. Another 15 mm gap has been allowed between the suspended beam and the existing concrete wall, which has been filled with similar fire resistant foam.

Figure 60: LSF Consecutive Construction Steps

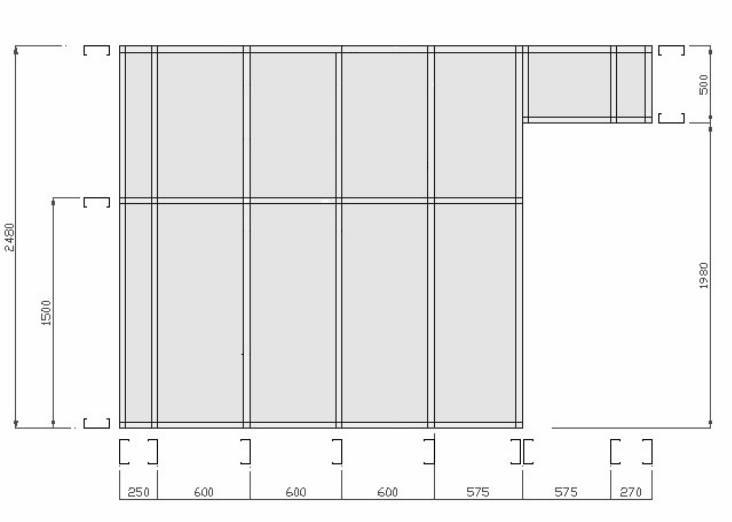

Figure 61: Dalmarnock LSF Geometry

The main rectangular panel of the walling system has been fixed to the floor and ceiling (concrete slab) using 3 bolts on top and another 3 on the bottom. The suspended beam has been bolted to the previous panel, the ceiling and the existing lateral wall, producing a doorway that facilitates fire spread. Their coordinates are shown in Table 19 and the reference system is the same as the one shown in Figure 61.

	Bolt N.	Coordinates		
		X	Y	Z
Top Three Bolts	1	140	124	2480
	2	1300	124	2480
	3	2350	124	2480
Bottom Three Bolts	4	140	124	0
	5	1300	124	0
	6	2350	124	0
Panel / Beam Connection	7	3050	124	2480
	8	3470	124	2480
	9	2625	124	2480

Table 19: Fixing Bolt Coordinates

This walling system has been heavily instrumented with thermocouples and heat flux meters in order to record the dynamic variation of temperature and heat flux respectively throughout the duration of the test. Table 2 and Figure 3 show the position of the sensors used in the experiment. As can be seen from Figure 3, the thermocouples and heat flux meters are more concentrated in the upper part of the wall. This is because as the fire progresses the smoke layer becomes denser and remains in the top of the room thus greater temperatures and heat fluxes are expected to be recorded in this area. Also, the flames from the bookcases were burning in the upward direction towards the top of the wall, this is therefore where the most extreme temperatures are experienced.

Thermocouples were made from a stock of calibrated wire certified by the supplier to comply with [89] to a tolerance of 0.4 %. Those fixed to steel members have been attached using silver soldering and their positions were selected to follow the logical heating pattern of any vertical member subjected to a conventional fire (initial high temperatures in the top part due to the smoke layer that develops downwards). Those placed in the exposed surface have been embedded under the render, to avoid damage and the effect of radiation from the smoke layer. Due to the thickness of the render layer, the temperature recorded by those thermocouples can be assumed to be the same as those in the solid/gas phase interface. Those placed in the unexposed surface have been taped over the plasterboard. In some areas of the walling system several thermocouples are placed across the whole thickness of the specimen. This indicates the temperature gradient as a function of the depth. They all appear grouped in Figure 62, Table 20 and Table 21.

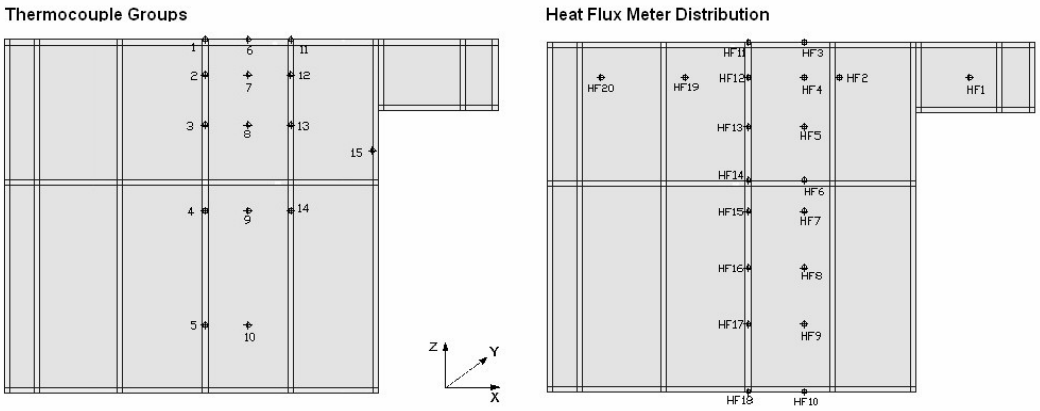

Figure 62: Sensor Position

TC Number	TC Group	Position (mm)			Comment	TC Number	TC Group	Position (mm)			Comment
		X	Y	Z				X	Y	Z	
TC1	2	1450	54	2230	A	**TC21**	4	1450	218	1280	E
TC2	2	1450	124	2230	B	**TC22**	5	1450	4	480	D
TC3	2	1450	194	2230	C	**TC23**	5	1450	218	480	E
TC4	3	1450	54	1880	A	**TC24**	6	1750	4	2480	D
TC5	3	1450	124	1880	B	**TC25**	7	1750	4	2230	D
TC6	3	1450	194	1880	C	**TC26**	7	1750	124	2230	B
TC7	4	1450	54	1280	A	**TC27**	7	1750	218	2230	E
TC8	4	1450	124	1280	B	**TC28**	8	1750	4	1880	D
TC9	4	1450	194	1280	C	**TC29**	8	1750	124	1880	B
TC10	12	2050	54	2230	A	**TC30**	8	1750	218	1880	E
TC11	13	2050	54	1880	A	**TC31**	9	1750	4	1280	D
TC12	14	2050	54	1280	A	**TC32**	9	1750	218	1280	E
TC13	15	2625	124	1700	B	**TC33**	10	1750	4	480	D
TC14	5	1450	54	480	A	**TC34**	10	1750	218	480	E
TC15	1	1450	4	2480	D	**TC35**	11	2050	4	2480	D
TC16	2	1450	4	2230	D	**TC36**	12	2050	4	2230	D
TC17	2	1450	218	2230	E	**TC37**	12	2050	218	2230	E
TC18	3	1450	4	1880	D	**TC38**	13	2050	4	1880	D
TC19	3	1450	218	1880	E	**TC39**	13	2050	218	1880	E
TC20	4	1450	4	1280	D	**TC40**	14	2050	4	1280	D

A=Exposed Flange, B=Flange/Mineral Wool Centre, C=Unexposed flange, D=Exposed Surface, E=Unexposed Surface

Table 20: Dalmarnock Thermocouple Coordinates (mm)

Heat Flux Number	Coordinates		Heat Flux Number	Coordinates	
	X	Z		X	Z
HF1	2970	2230	**HF11**	1445	2480
HF2	2050	2230	**HF12**	1445	2230
HF3	1745	2480	**HF13**	1445	1880
HF4	1745	2230	**HF14**	1445	1500
HF5	1745	1880	**HF15**	1445	1280
HF6	1745	1500	**HF16**	1445	880
HF7	1745	1280	**HF17**	1445	480
HF8	1745	880	**HF18**	1445	0
HF9	1745	480	**HF19**	950	2230
HF10	1745	0	**HF20**	350	2230

Table 21: Dalmarnock Heat Flux Meter Coordinates (mm)

The use of strain gauges was discussed to show deflections in the walling system. Their use was finally discarded as it was not possible to predict whether deformations were going to happen and where they would have happened. The most critical part of the wall section to cause loadbearing failure under fire conditions is the exposed flange, which is the nearest to the exposed surface. Local buckling induced by thermal expansion is the most frequent collapse mechanism although in this case no buckling was found as the structure was not loaded and insufficient temperatures were reached in the critical section.

3.4.4. Heat flux Measurements

The total heat flux imposed by the fire was estimated by means of Thin Skin Calorimeters [86]. The advantages of this method are numerous including dimensions that are relatively small compared to the size of the members analyzed, simple setting up and acceptable accuracy. A total of 20 thin skin calorimeters have been embedded in a LSF walling system in the Dalmarnock Fire Tests to map the heat flux distribution over the exposed surface throughout the duration of the fire.

The construction of these sensors is relatively simple and has been carried out to levels specified in international standards [86]. The geometry selected comprises a 20 mm diameter, 2 mm thick copper disc [87] tightly fitted into a flat bottomed hole, drilled into a 40 mm diameter, 12.5 mm thick circular section of gypsum plasterboard [88] to minimize lateral heat conduction effects as shown in Figure 63. A type K thermocouple [89] is embedded in the back of the copper disk to work as an electrical transducer from which heat flux measurements can be deduced. The exposed surface of the copper disk has been painted with matt black paint to get an emmisivity close to 1.

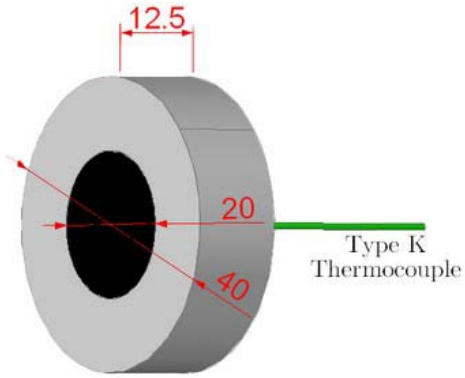

Figure 63: Thin Skin Calorimeter Geometry

The temperature gradients within the cooper disk are almost negligible, which produces a very short characteristic transient time compared to the phenomenon that is being measured. The characteristic term that describes the rapidity of the thin skin calorimeters to detect any changes in the external conditions is the initial response time [86]. It represents the time for the temperature of the rear, unexposed surface of the copper disk to come within 1% of the temperature of the exposed surface. Kidd [90] showed that if conduction into the type K thermocouple wire is ignored, the initial response time is expressed by the following equation.

$$\tau_f = 0.5\frac{\rho C_p \delta^2}{k} = 0.017\,s$$

Where:

τ_f is the initial response time in seconds

ρ is the density of copper equal to 8960 Kg/m^3

C_p is the specific heat capacity of copper equal to 380 J/Kg·K

δ is the thickness of the thin skin calorimeter equal to 0.002 m

k is the thermal conductivity of copper equal to 401 W/m·K

The response of the thin skin calorimeters is approximated by a lumped parameter analysis. The lumped capacitance method can be satisfactorily

applied to solve transient conduction problems when the Biot Number is bellow a certain characteristic value as expressed in the following equations [92]. The characteristic convective coefficient is assumed to be 25 W/mK for the fire and the characteristic length is the ratio of the solid's volume to surface area. It is therefore concluded that the copper disk acts as a thermally thin transducer and a good choice for steady-state measurements or rapidly developing fire environments.

$$Bi = \frac{hL_c}{k} = 0.00012 << 0.1$$

$$L_c = \frac{V}{A_s} = 0.002m$$

- Energy Balance

An energy balance based on the assumption of three dimensional heat transfer in the copper disc was conducted to characterize the various factors that influence the performance of these instruments [91]. The incident heat flux (cold wall heat flux) was deduced by accounting for the net heat flux and the heat losses according to the equations below. The left-hand side term of the first equation corresponds to the energy stored or heat build-up within the copper plate over a discreet time step calculated by multiplying the copper disk density in Kg/m^3, thickness in m, specific heat in J/Kg·K and the rate of change in temperature of the plate surface with respect to time in K/s.

$$\dot{q}''_{stored} = \rho \delta c_p \frac{dT}{dt} = \dot{q}''_{NET} - \dot{q}''_{loss}$$

$$\dot{q}''_{NET} = \dot{q}''_{inc} - \dot{q}''_{rad} - \dot{q}''_{conv}$$

$$\dot{q}''_{loss} = C\dot{q}''_{inc}$$

$$\dot{q}''_{inc} - \left[\varepsilon\sigma(T_S^4 - T_0^4) + h_{conv}(T_S - T_g)\right] = \dot{q}''_{NET} = \frac{1}{(1-C)}\left[\rho\delta c_p \frac{dT}{dt}\right]$$

$$\dot{q}''_{inc} = \frac{1}{(1-C)}\left[\rho\delta c_p \frac{dT}{dt} + \varepsilon\sigma(T_S^4 - T_0^4) + h_{conv}(T_S - T_g)\right]$$

Where:

T_S is the temperature recorded by the thin skin calorimeter in K

T_0 is the temperature of the surroundings in K

T_g is the temperature of the gas phase around the thin skin calorimeter in K

The first term on the right-hand side of the second equation represents the incident heat flux per unit area. The second is the radiation exchange between the copper plate and the surroundings and the third represents the convective heat flux per unit area. The next equation shows the heat lost by conduction to the back and sides of the copper disk. This term depends strongly on the thermal properties of the structural element into which the thin skin calorimeter is embedded and is expressed as a fraction of the incident heat flux. The last equation is a simplified form of the previous equations to assist the understanding of the energy balance in the copper disk.

- Conduction Factor

As stated earlier, the C-factor represents the proportion of incident heat flux that is lost via conduction through the back and sides of the copper disk. Conduction is strongly dependant on the thermal properties of the structural member over which the incident heat flux is being recorded. This factor changes as a function of the copper disk surface temperature and it is therefore recommended that the thin skin calorimeters are individually calibrated before being exposed to full scale fire conditions.

The convective coefficient that appears in the previous equations has been deduced from empirical correlations for external free convection flows [92]. The air velocity was assumed to be 0.5 m/s [91], and its properties have been evaluated for $T_f = (T_S+T_{lab})/2$.

$$h_{conv} = \frac{Nu_L \cdot k}{L}$$

$$Nu_L = \left\{ 0.825 + \frac{0.387 Ra_L^{1/6}}{\left[1 + (0.492/\mathrm{Pr})^{9/16}\right]^{8/27}} \right\}^2$$

$$Ra_L = \frac{g\beta(T_s - T_{lab})L^3}{\alpha\nu}$$

The calculation of the C-Factor for thin skin calorimeters embedded in a characteristic LSF walling assembly (New System) was conducted for varying heat fluxes. A Schmidt-Boelter radiometer [93] was used as a reference to assist the calculation of these characteristic parameters, as shown in Figure 64. The readings from each of the devices (Schmidt-Boelter radiometer and thin skin calorimeter) were recorded every second (far above the initial response time). Thereafter, the rate of change in temperature of the plate surface is calculated taking 10 second steps and it is then used to deduce the heat stored by the copper disk.

The convective heat flux has been calculated at every time step multiplying the temperature difference between the copper disk surface and the laboratory by a relatively constant value of the convective coefficient calculated from the previous equations. The radiation heat flux is deduced from the same temperatures to the power four multiplied by the Stefan-Boltzman constant and the emmisivity, which is assumed to be one as stated before.

The heat lost by conduction is a function of the copper disk surface temperature and it is calculated using trial and error based on the variation of the steady response of the thin skin calorimeter as a function of the C-factor. By matching the steady response of both the calibrated Schmidt-Boelter radiometer and the thin skin calorimeter, the C-Factor has been deduced for each of the heat fluxes and subsequently for each of the associated surface temperatures. Thereafter, the transient response, which is characterised by increasing temperatures, was compared in both of the meters for each of the heat fluxes using the previously calculated C-Factor trend line. The transient response was found to show a satisfactory agreement as illustrated by Figure 64.

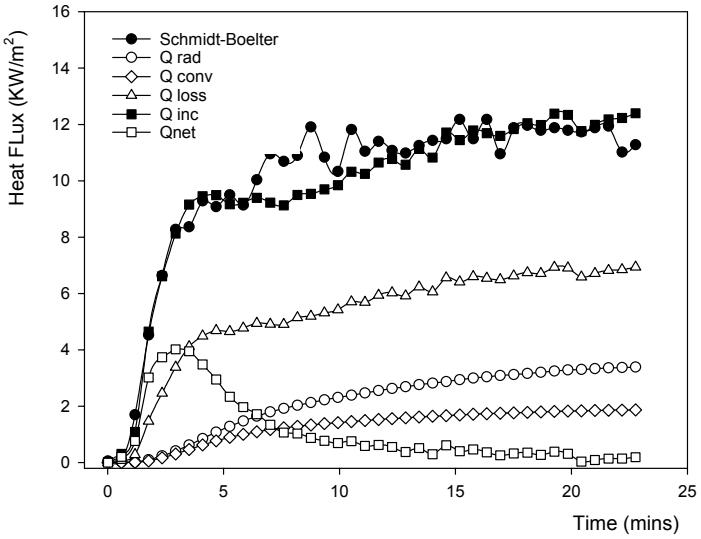

Figure 64: Incident Heat Flux Composition

The lines created from joining the white filled dots represent each of the individual heat fluxes (radiation, convective, stored and lost by conduction) that when summed, equal the incident heat flux measured from the thin skin calorimeter. The total incident heat flux obtained using the thin skin calorimeter is plotted using black filled squares and the readings from the Schmidt-Boelter radiometer are drawn using black filled circles. These two characteristic lines match closely throughout the

duration of the test and the agreement is found to be satisfactory except for situations in which noise from the sensors is transmitted to the data logger.

The experimentally obtained C-factor as a function of the copper disk temperature is plotted in Figure 65. This parameter is similar to the one obtained by Alston, J. [91], who reported a constant value of 0.2.

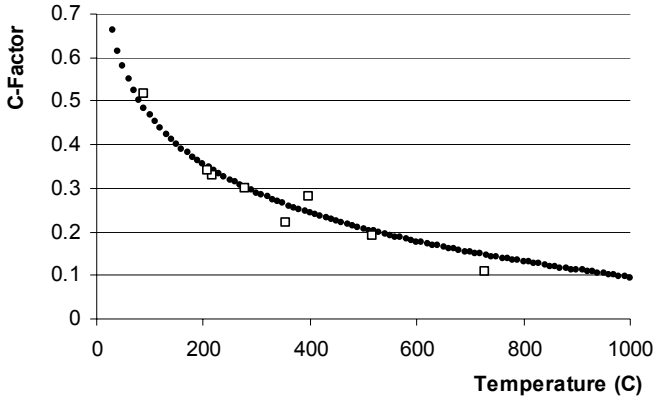

Figure 65: Thin Skin Calorimeter C-Factor

- Thin Skin Calorimeter Calibration

An analysis to ascertain the accuracy and potential errors of these instruments was carried out. The test comprised a sequence of experiments in which six thin skin calorimeters were subjected to a series of known constant heat fluxes. The sensors were not embedded in any structural member because the thermal conductivity of the plaster board is very low with respect to the structural element and so it is not expected that this will affect the results. The incident heat flux was accurately recorded by a calibrated Schmidt-Boelter radiometer [93], which was inserted in the centre of the thin skin calorimeters as shown in Figure 66.

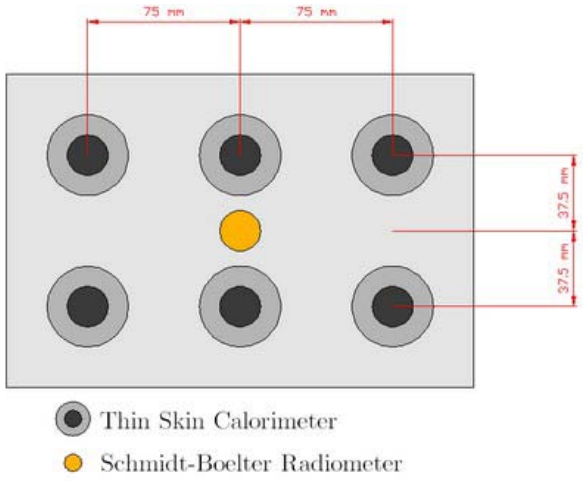

Figure 66: Thin Skin Calorimeter Calibration Arrangement

The previous energy balance has been applied to calculate the C-factor for each of the thin skin calorimeters used in this calibration experiment as shown in Table 22. Constant values of that parameter for each of the thin skin calorimeters are deduced and subsequently used as a comparison tool to determine the characteristic error bars. The source of error in the temperature reading is dependent on the method by which the junctions of the thermocouples are embedded in the copper disk. This could be reduced by attaching the thermocouples to the metal by spot, electron beam, or laser welding.

A similar pattern to the one shown in Figure 65 is observed for the C-Factors in Table 22. They tend to decrease as a function of the heat flux and consequently as a function of the disk surface temperature. However, the shape of their characteristic trend lines might differ due to the fact that the thin skin calorimeters used for the calibration are not embedded in a structural member, whereas those shown in Figure 65 are embedded in a LSF structure.

Copper Disk Position	C-Factor		
	Test 1 5.5 KW/m2	Test 2 12 KW/m2	Test 3 40 KW/m2
top left	0.30	0.29	0.29
top middle	0.33	0.28	0.26
top right	0.32	0.29	0.24
bottom left	0.30	0.26	0.25
bottom middle	0.27	0.24	0.22
bottom right	0.26	0.22	0.22
Average	0.296	0.263	0.247
Standard Error	0.011	0.012	0.011

Table 22: Thin Skin Calorimeter Error Bars

3.4.5. Full Scale Experiment Heat Flux Definition

Some of the assumptions previously made with regards to the utilization of thin skin calorimeters can no longer be applied to full scale fires due to the uncertainties found in some of the fields calculated. Ventilation patterns and convective coefficients in full scale fire experiments are significantly more unpredictable. The convective heat flux term is no longer generated by the increasing temperatures on the copper disk surface but instead is dependant on the turbulence of the gases around the flames and on the varying currents generated over the duration of the fire. For this reason, the convective heat flux term must be included together with the radiation heat flux term into a total heat flux.

The radiation from the disk to the surroundings in a full scale fire should consider the influence of the conditions around the thin skin calorimeter that might influence its output, such as flame distribution, smoke layer formation, soot concentration, temperature rise of surrounding surfaces etc. so a simplification must be applied to account for these effects. If the

initial radiation to the background is deducted from the subsequent measurements (after the fire is ignited), anything above this initial value takes into consideration the numerous effects. The equation for energy balance in the copper disc can therefore be simplified when considering these facts, which results in the following equation.

$$\dot{q}''_{inc} = \frac{1}{(1-C)}\left[\rho\tau c_p \frac{dT}{dt} + \varepsilon\sigma(T_S^4 - T_0^4)\right]$$

This equation characterizes the thin skin calorimeter heat balance for full scale experiments when the room is engulfed in fire and it accounts for the combination of convective and radiation heat fluxes from the fire to which the instruments are exposed.

3.4.6. Post Fire Visual Evaluation

Initial conclusions can be drawn post fire by visually inspecting the residuals of the LSF walling system. Figure 67 shows a series of pictures taken after the experiment which show no constitutive materials falling apart from the specimen analyzed. This is a very positive outcome as it shows that given a real fire to the wall performs well, minimizing accidents and fire spread.

The exposed side of the wall presents some render spalling and the remaining coating can be easily removed manually. The honeycomb is still in place but its constitutive aluminium channels can no longer stand any impact due to the epoxy resin melting and draining down the system. For the same reason, the fibre glass used in the honeycomb panels is no longer stuck to the aluminium although they have managed to resist the fire. The back of the wall (plasterboard) was blackened by the effect of the fire and some bowing has been noted. There has not been any cracking or falling of plasterboard and the most external layers have remained in place.

No buckling has been observed and deformations in the steel did not appear throughout the duration of the test. One effect observed is that the more external screws (those fixing the honeycomb) were loose after the experiment and could be unscrewed manually, whereas the more internal ones (fixing mineral wool) were still tightly in place. This indicates the importance of the fixings to keep the materials in place and to protect the steel work.

Figure 67: Post-fire Visual Evaluation

After the fire was extinguished, smoke was still emerging from the existing holes left on both sides of the walling system. This is due to the epoxy resins used to keep the honeycomb together melting and dripping down to the bottom of the walling system, where smouldering was occurring. They were still hot and releasing smoke for a few minutes after the test. Further more, the moisture within the insulation was still evaporating due to the

high temperatures reached during and after the experiment. In some sections of the walling system, heat conduction was greater than in others. Figure 68 shows a portion of 180 Kg/m^3 mineral wool being removed from the walling systems. It can be noted darker portions around the studs due to greater heat transmission.

Figure 68: Mineral Wool Thermal Bridging

Due to the same effect of excessive heat transfer through some sections, melted aluminium has been found around some of the heat flux meters. This is due to the fact that the copper discs of the thin skin calorimeters have conducted more heat to the surroundings producing this effect as shown in Figure 69.

Figure 69: Aluminium Melted Around Thin Skin Calorimeters

3.4.7. Dalmarnock Temperature Evolution

Figure 70 shows the air temperature evolution within the living room area. The average room temperature is represented in that figure. This value provides a qualitative estimation of how the temperatures around the room vary with time. However, this does not represent a good estimation of the actual average room temperature because the proximity between thermocouples is not accounted for when averaging. This graph only characterizes performance patterns.

As the ignition source and primarily ignited items are close to the LSF wall, the temperatures around it at the beginning of the experiment are higher than in any other parts of the room. It can be observed that after the flash over phenomenon, the temperature in the room becomes more homogeneous and the average room temperature converges with the temperature around the LSF wall. Temperatures around 950 °C have been reached in the gas phase around the LSF walling system.

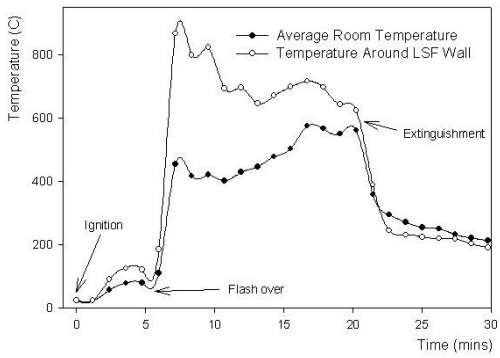

Figure 70: Room Temperature Evolution

Figure 71 and Figure 72 show the temperature evolution in several points within the walling system. At the beginning of the experiment, the radiation coming from the flames in the bin was not enough to significantly heat up the interior of the walling system. Little attention has been paid to the readings recorded post extinguishing, because the water

used for that purpose had damaged most of the thermocouples, introducing noise in the readings. There are missing readings from some thermocouples as they have been damaged either during the experimental set up or by the fire itself.

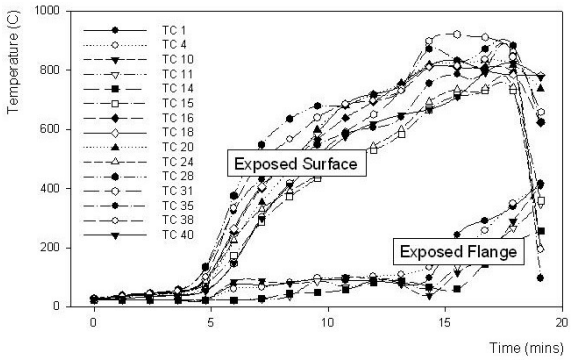

Figure 71: Temperature Evolution in Exposed Side

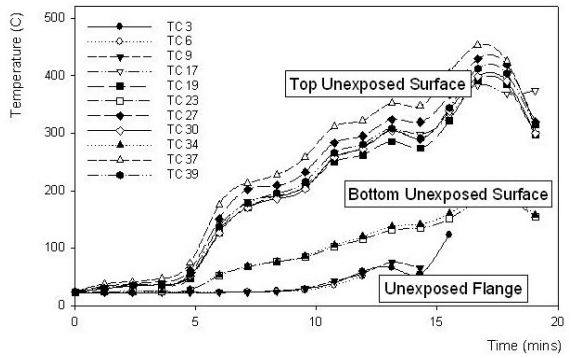

Figure 72: Temperature Evolution in Unexposed Side

Figure 73 and Figure 74 show the temperature evolution following vertical sensor distribution over the exposed and unexposed surface of the walling system (render and plasterboard respectively). They focus on the steel work to find any traces of temperature stratification due to the smoke layer.

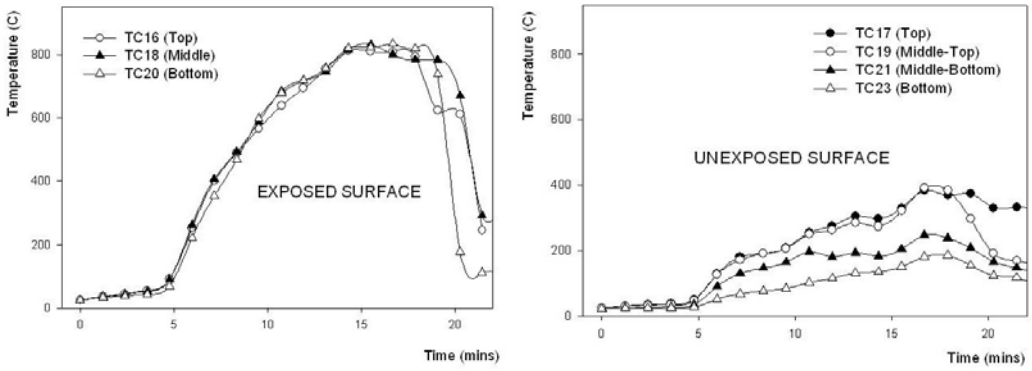

Figure 73: Left-Centre Stud Temperature Stratification

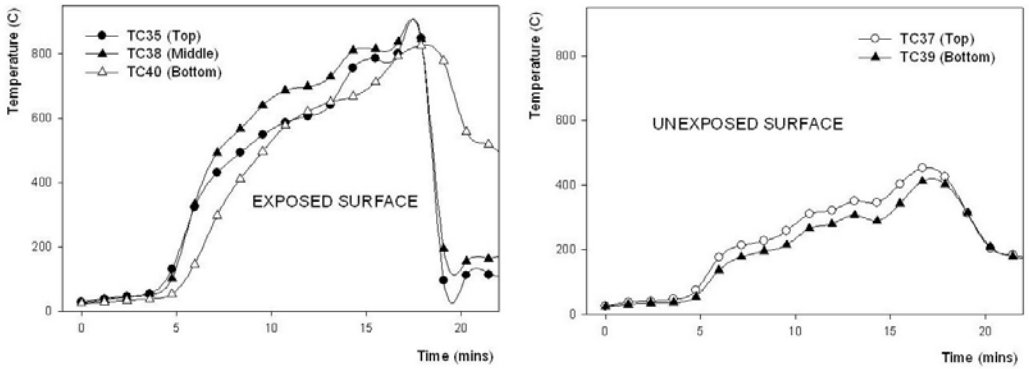

Figure 74: Right-Centre Stud Temperature Stratification

When analysing the previous figures, it is observed that the temperature distribution in the exposed surface (living room side) of the test sample is reasonably homogeneous (no stratification of temperatures) for two reasons, firstly due to the proximity of the sensors to the fire, and secondly due to a low density smoke layer created due to arbitrary ventilation patterns. On the other hand, the temperature distribution in the unexposed face (plasterboard) is more stratified. This is because the window situated in the kitchen broke several minutes into the fire facilitating the smoke in creating a noticeable smoke layer.

Figure 75 illustrates the temperature evolution across the steel stud and the mineral wool at two sections of the same height. These sections correspond to Thermocouple Group 2 and Thermocouple Group 7. The

same pattern has been observed in other sections of the wall when comparing the temperature in the steel and in the batt insulation for the same heights. The surface temperature is very similar in both cases, and it is noted that the temperature of the centre part of the steel web remains constant throughout the duration of the test and similar to the temperature of the mineral wool. It is in the later stages of the test when it starts to increase rapidly. This is due to the exothermic oxidation of the aluminium honeycomb. A generally good behaviour of the steel work is observed due to the way it is protected by the insulation. This again indicates the importance of the fixings to keep the constitutive materials in place.

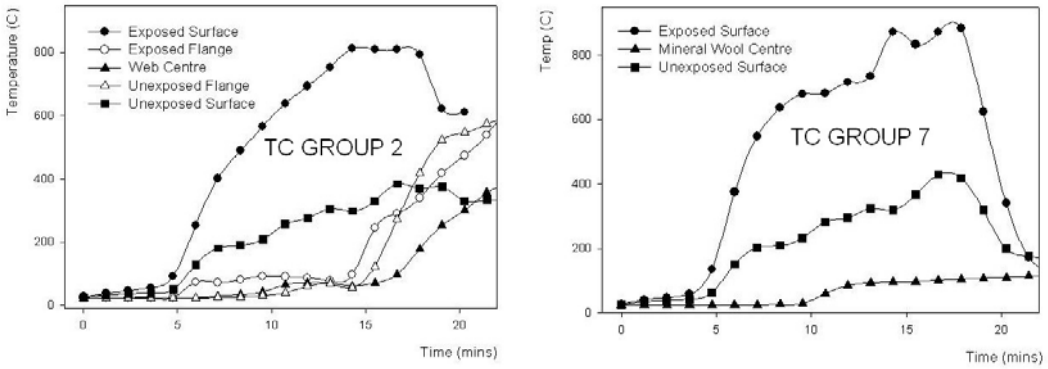

Figure 75: Temperature Evolution across Steel and Batt Insulation

3.4.8. Dalmarnock Heat Flux Evolution

The way the LSF Walling System is heated up by the fire is not regular and homogeneous. It depends on the location of the flames, the smoke distribution and the effect that those aspects have on radiation and convection therefore generalized heating patterns cannot be extracted from the data gathered. The arrangement of the furniture in the room and especially, the way the fire developed had an important impact on the heat flux distribution throughout the duration of the fire. The incident heat fluxes encountered in this experiment were calculated using analysis

presented before and are plotted in the following figures. Figure 76 shows the evolution of the incident heat flux on the exposed LSF surface for the duration of the fire and Figure 77 shows heat flux contour plots for the most significant events during the fire.

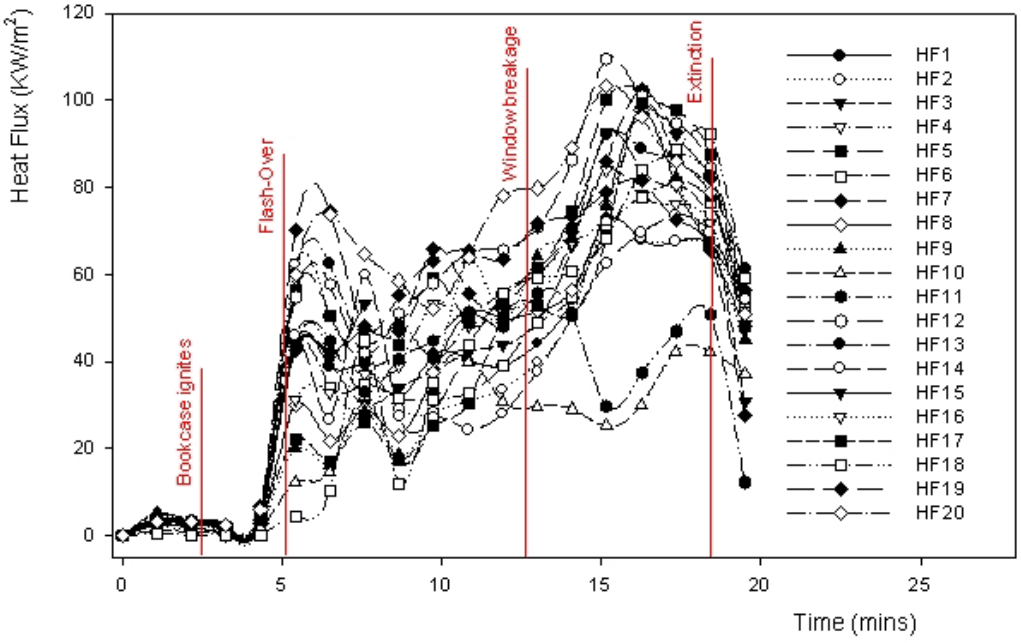

Figure 76: Dalmarnock Fire Tests Heat Flux Evolution

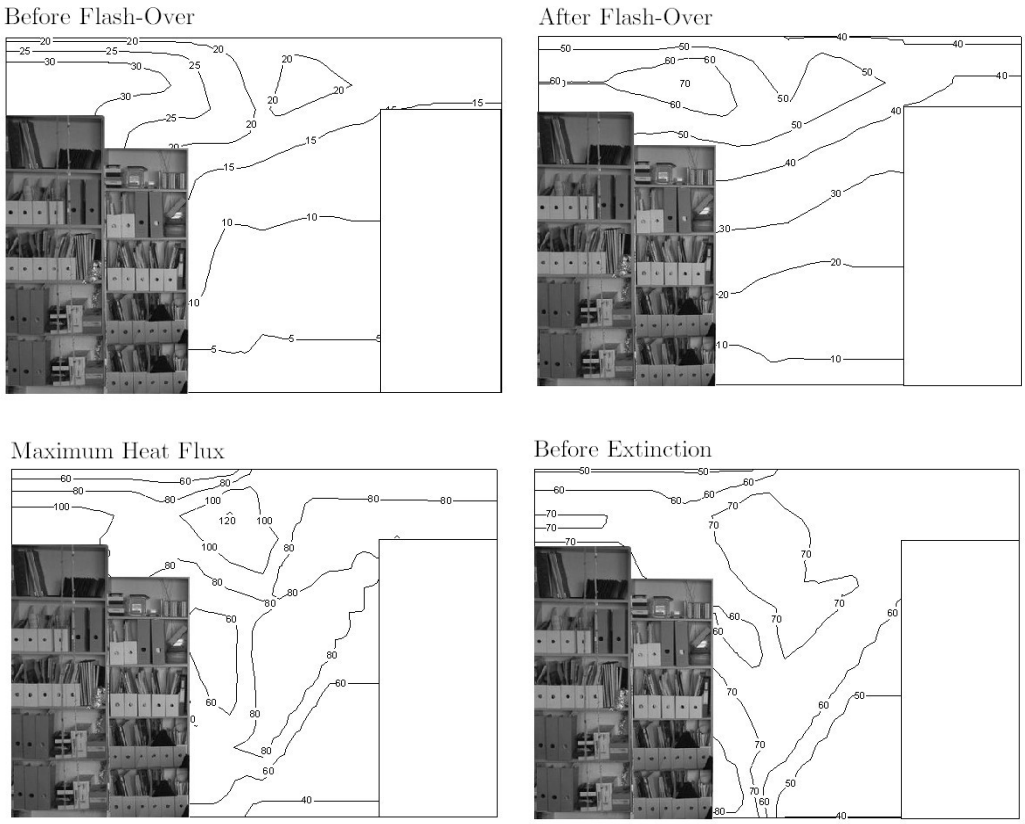

Figure 77: Heat Fluxes Spatial Distribution for Different Critical Times

The heat fluxes are presented as a function of time. All heat flux sensors show the same trends with time but with very different magnitudes, indicating a strong heat flux distribution. The sensors initially show close to zero heat fluxes. It is important to note that this is the case almost to flash-over. Flashover is characterized by a dramatic increase in the heat flux followed by an almost constant heat flux period. A second peak is observed after the windows break, but this peak is delayed by several minutes from the moment of breakage. Heat fluxes finally decay after the intervention of the fire fighters.

The magnitude of the heat flux shows significant spatial heat flux gradients after flashover. This is important because this is the period of interest for structural integrity. The iso-heat flux contours presented in

Figure 77 give a better indication of the heat fluxes. The region protected by the bookshelves will experience very weak heat fluxes. The rest of the wall will be initially subjected to a fairly homogeneous heat flux, but later clear stratification with areas of strong heat insult can be observed. These areas correspond mostly to the location of flame impingement. The flames were coming from the bookshelves indicated in the figures. As indicated in Figure 77, the gradients continue through the whole post-flashover period.

It was expected that the net heat flux over the steel members (HF11 to HF 18) were going to produce greater readings than those placed over the batt insulation (HF3 to HF 10 respectively), although this behaviour is only observed at the beginning of the experiment becoming rather arbitrary afterwards. The reason for this is the non regular heating distribution stated earlier. Eight critical heat flux meters have been selected to characterize the LSF behaviour in the experiment. Each critical heat flux reading is compared with their corresponding thermocouple measurements taken at the same or nearest point in the assembly. Table 23 explains the positions of heat flux meters and their related thermocouples. Table 24 shows the thermocouples grouped in terms of their location in the specimen, which helps to understand the heating patterns.

Heat Flux Meter Code	Nearest TC Group	Thermocouple Code
HF1	11, 12, 13, 15	TC35, TC10, TC36, TC37, TC11, TC38, TC39
HF2	12	TC10, TC36, TC39
HF3	6	TC24
HF4	7	TC25, TC26, TC27
HF5	8	TC28, TC29, TC30
HF6	8, 9	TC28, TC29, TC30, TC31, TC32
HF7	9	TC31, TC32
HF8	9, 10	TC31, TC32, TC33, TC34
HF9	10	TC33, TC34
HF10	10	TC33, TC34
HF11	1	TC15
HF12	2	TC1, TC2, TC3, TC16, TC17
HF13	3	TC4, TC5, TC6, TC18, TC19
HF14	3, 4	TC4, TC5, TC6, TC18, TC19, TC7, TC8, TC9, TC20, TC21
HF15	4	TC7, TC8, TC9, TC20, TC21
HF16	4, 5	TC7, TC8, TC9, TC20, TC21, TC14, TC22, TC23
HF17	5	TC14, TC22, TC23
HF18	5	TC14, TC22, TC23
HF19	2	TC1, TC2, TC3, TC16, TC17
HF20	2	TC1, TC2, TC3, TC16, TC17

Table 23: Heat Flux Meters and Corresponding Thermocouples

Code	TC Group	Comment	Code	TC Group	Comment
TC15	1	Exposed Surface	TC25	7	Exposed Surface
TC1	2	Exposed Flange	TC26	7	Flange / MW Centre
TC2	2	Flange / MW Centre	TC27	7	Unexposed Surface
TC3	2	Unexposed Flange	TC28	8	Exposed Surface
TC16	2	Exposed Surface	TC29	8	Flange / MW Centre
TC17	2	Unexposed Surface	TC30	8	Unexposed Surface
TC4	3	Exposed Flange	TC31	9	Exposed Surface
TC5	3	Flange / MW Centre	TC32	9	Unexposed Surface
TC6	3	Unexposed Flange	TC33	10	Exposed Surface
TC18	3	Exposed Surface	TC34	10	Unexposed Surface
TC19	3	Unexposed Surface	TC35	11	Exposed Surface
TC7	4	Exposed Flange	TC10	12	Exposed Flange
TC8	4	Flange / MW Centre	TC36	12	Exposed Surface
TC9	4	Unexposed Flange	TC37	12	Unexposed Surface
TC20	4	Exposed Surface	TC11	13	Exposed Flange
TC21	4	Unexposed Surface	TC38	13	Exposed Surface
TC14	5	Exposed Flange	TC39	13	Unexposed Surface
TC22	5	Exposed Surface	TC12	14	Exposed Flange
TC23	5	Unexposed Surface	TC40	14	Exposed Surface
TC24	6	Exposed Surface	TC13	15	Flange / MW Centre

Table 24: Dalmarnock Thermocouple Groups

HF1 was situated above the door on the suspended constitutive beam of the LSF wall. This area was subject to flames as the door acts as a ventilation gap in which the flames rushed through towards the kitchen at an increasing rate. The heat fluxes encountered in this section were not extreme due to the direction of those flames, with a maximum incident heat flux recorded of 74.2 KW/m^2. HF1 corresponding thermocouple groups are too away far to be representative of the local temperature evolution therefore no heat flux/temperature correlations are drawn.

HF5 experienced very high incident heat fluxes throughout the experiment. The position of HF5 was between the shelves and the door opening, near the top of the walling system, which explains why the recorded incident heat flux was so high. The flames from the shelves were rushing towards

the door, past HF5 at a very fast rate with a constant increase in temperature until the fire was extinguished. Also, the smoke layer influenced the data recorded by HF5 producing high heat fluxes. The maximum incident heat flux recorded was 112.8 KW/m^2 and from Figure 78 it can be seen that the closest match lies with thermocouple 28, which was on the exposed surface. It can also be seen in the graph that the temperature in the unexposed surface has some influence in the recorded heat fluxes. This is because during the calibration of the thin skin calorimeters, the unexposed side worked as a heat sink. In this case it is being heated and a correction is needed. However, due the impracticability of doing it and the small variations expected in the recorded heat fluxes, this has been neglected.

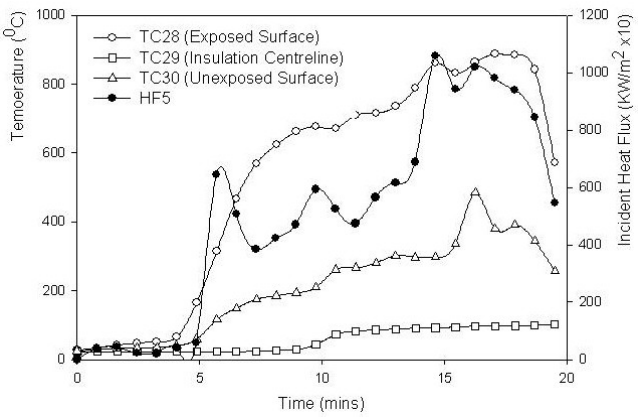

Figure 78: Heat Flux / Temperature Distribution around HF5

HF7 shown in Figure 79 also appears to be one of the critical meters as it is situated at a mid height in the wall next to the shelves but not to the same extreme as some of the others. It does however measure the highest incident heat fluxes at various times throughout the experiment, which implies that during the test, this area was subject to severe flames from the shelves as the fire grew. The overall maximum incident heat flux recorded was 106.2 KW/m^2. The corresponding Thermocouple Group 9 and within this, TC31 representing the exposed surface, gives the closest

correlation to HF7. The heating pattern and its corresponding temperatures show a similar path which assures the reliability of the experimental data.

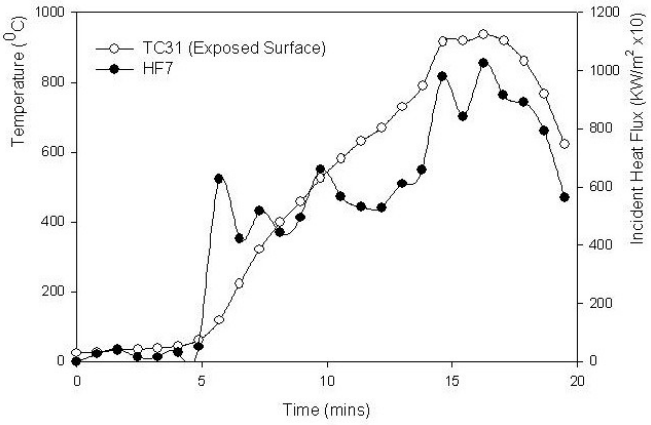

Figure 79: Heat Flux / Temperature Distribution around HF7

A comparison between HF10 and HF18 has been made to illustrate how distance and shadow effects might affect the heat fluxes recorded as shown in Figure 80. F10 and HF18 are situated at floor height, in-between the burning shelves and the doorway. They are 795 mm apart, with HF18 being the closest to the shelves. The maximum incident heat flux recorded by HF10 and HF18 was 49.2 KW/m^2 and 91.6 KW/m^2 respectively. This is a major difference considering the small distance apart, but this confirms that a small distance in a fire might result in a large difference in temperature. This is caused by the lowest section of the sofa blocking the radiation reaching HF18.

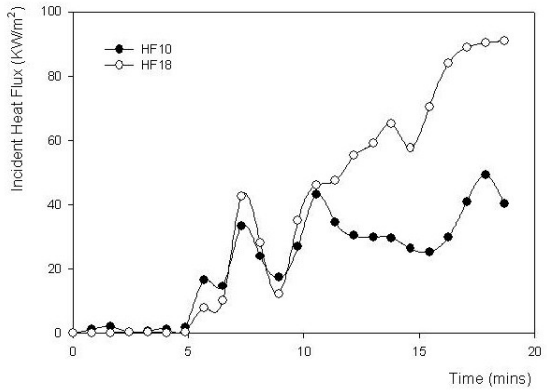

Figure 80: Floor Height Heat Flux Evolution

HF12 recorded the highest incident heat flux with a maximum of 120.4 KW/m^2. HF12, HF19 and HF20 run along the top of the burning shelves so they are grouped together in Figure 81. HF20 is also critical as it recorded the second largest incident heat flux of 112.0W/m^2. The high readings provided by these sensors are due to the fire evolution and the way it spread as explained previously

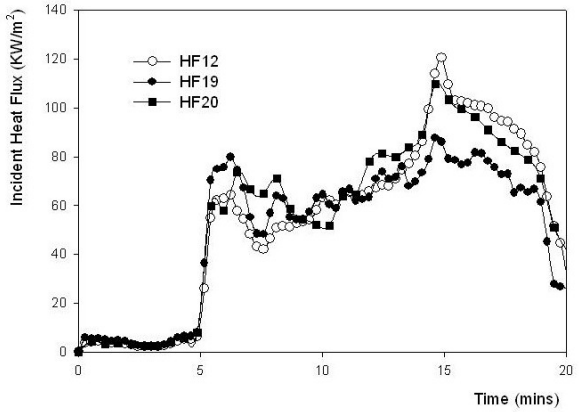

Figure 81: Heat Flux Evolution in HF12, HF19 and HF20

Similar heat flux gradients have been observed in the past. The heat fluxes observed in the Cardington tests [94] were larger to those found for the Dalmarnock fire tests due to the difference in the fire load, the openings and the ventilation patterns. However, a similar characteristic pattern is

observed for both cases as shown in Figure 82. That figure also includes the heat flux evolution recorded by Sultan [95] in the Fire Rating Test [10] when testing fire bricks. If the pre-flashover period is ignored, the heat flux evolution encountered in the furnace is very similar to the one found in the Dalmarnock Fire tests. The heat flux evolution predicted for the New System when subjected to the fire rating test is below the one recorded by Sultan due to the strong dependency of this parameter with the insulating properties of the specimen tested.

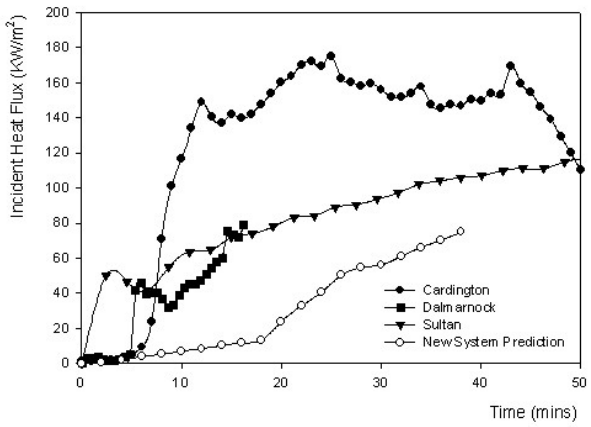

Figure 82: Heat Flux Evolution Comparison

3.4.9. Dalmarnock Fire Tests Computer Simulations

Although no deformation of the LSF walling system has been observed in the Dalmarnock fire tests, a thermal/structural characterization of the experiment is conducted in the following chapter. This is an uncoupled analysis where the thermal field is calculated first and subsequently inputted into a structural model to map the stresses and strains that appear in the experiment for several sections of the structure. The software package ABAQUS [28] is selected for that purpose.

3.5. LSF Fire Performance Conclusions

The prediction of fire ratings for LSF structures using bench scale experiments is feasible by applying the methodology presented in the first section of this chapter. This is a novel methodology that has proved to be sound and robust. Information about the insulating properties of the system analyzed (thermal efficiency) is inputted into the method and predictions about fire performance can be concluded. This explains the integral approach that the research aims for, because by applying the methodology suggested, information about both thermal efficiency and fire performance is being gathered and comprehensive solutions can be found.

These methods can be implemented over any lightweight construction system using a small scale furnace as long as incident heat fluxes are recorded in the specimen exposed surface. It is important to understand the concept of critical section and critical temperature because they cause failure. Once this is determined and its evolution studied, final conclusions can be drawn. By incorporating the aid of software packages even more extensive conclusions can be drawn.

In addition, fire rating methodologies involved in assessing real fire performance are validated for realistic fire scenarios (Dalmarnock Fire Tests). One reference LSF walling system has proved to successfully withstand the effects of a severe post-flashover fire with no symptoms of deformation or collapse. The fixings have successfully held the constitutive materials in place and the deterioration encountered was not enough to propagate the fire or to cause any accident. The outcome is very positive and opens the possibility to further research into potential improvements to this type of construction systems.

Chapter Four

4. Lightweight Building Systems Structural Behaviour

4.1. Background to Structure Behaviour

The structural behaviour of lightweight structures at ambient temperatures has been studied extensively by many research organizations. There are also a number of existing protocols [14; 15] that facilitate the design process of LSF assemblies. Their validity is not questioned by this research but their influence over the aspects analyzed is considered. In addition, there is a lack of knowledge about structural performance of lightweight construction systems under fire conditions and the need to understand their behaviour has been identified. The main focus of this research has been on steel framed structures and extensive computational work to support the existing empirical results has been conducted.

4.2. LSF Structural Behaviour Project Objective

The objective of this research is to determine the validity of computer based methodologies to assess the structural behaviour of lightweight construction systems in fire. Due to the nature of this research, the methodologies mentioned previously have been implemented on light steel framing (LSF) structures, and extensive conclusions have been drawn such as the possibility to apply these methodologies to any other lightweight construction technology.

When analyzing complex lightweight construction systems, it is of vital importance to begin with a well defined thermal analysis, from which subsequent structural examination might be carried out. Other studies conducted in the past [73; 78] analyze the behaviour of isolated cold formed steel members when subjected to fire by heating up whole elements uniformly around the perimeter. They also study the behaviour when interacting with a limited number of traditional insulating and sheathing materials. The results obtained from these studies are the basis of further

computational models. Due to the way construction technologies are evolving, the nature of the constitutive materials and their interactions are becoming more and more complex. The way heat is conducted within the construction systems is therefore an important issue to address before any structural analysis is conducted, in which those interactions must also be taken into account.

A decoupled thermal/structural computer analysis is undertaken to assess the fire performance of complex LSF systems such as those mentioned in previous chapters. The software package ABAQUS [28] has been selected for that purpose. Both the Dalmarnock Fire Test [13] and the Fire Rating Test [10] are modelled and general conclusions about LSF structural behaviour in fire are drawn. As explained previously, an initial thermal analysis must be carried out using the most realistic thermal properties of the constitutive materials. ABAQUS is capable of predicting the temperature field in the solid phase corresponding to the boundary conditions encountered in those experiments. Thereafter, by incorporating the structural properties, a full analysis is carried out to draw extensive conclusions about LSF structural behaviour in fire.

The qualitative nature of the structural analysis carried out in this research is imposed due to the fact that in real life conditions, the existence of imperfections will influence the behaviour of LSF systems. The simulations carried out in this research only represent loaded vertical members where readings about structural behaviour have been gathered. The effect of bracings, service holes, material imperfections, etc is not considered. As identified in the literature review as vital when simulating real life scenarios, these imperfections produce different types of local buckling. These failure mechanisms are rarely found in our analysis and only global buckling imposed by the thermal gradients in the steel frame is encountered.

4.3. LSF Structural Behaviour Literature Review

This section contains a literature review of the structural behaviour of LSF at ambient temperatures. Information about structural behaviour at elevated temperatures can be found in the previous chapter. Although some of the studies mentioned in this chapter are meant to analyze structural behaviour under fire, they also provide information about ambient conditions. Therefore, the loads and failure modes at ambient temperatures gathered from those papers are included in the literature review.

Previous research focuses mainly on the structural analysis of isolated cold-formed lightweight steel beams and columns, ignoring the complexity of complete steel frame structures. By analysing only certain sections of the walling system, the interactions between insulation, sheathing materials, connexions, fixings and bracing components with the studs are not accounted for. The most relevant studies analyzing beam sections are the ones testing the complete failure of specimens without restraining failure modes.

When analyzing isolated LSF member behaviour, the following research studies have been considered. Chu *et al* [96] and Young *et al* [97] look at the critical loading of steel stud beams reaching failure. These are relevant to the top stud tracks of LSF walling systems, which are used as floor joists in multi-storey buildings. Schafer *et al* [98; 99] and Pi *et al* [100] take this testing further and develop guidelines based on Finite Element models, where a number of critical parameters to understand the behaviour of LSF beams are identified. Schafer [101] also analyses the main buckling modes of columns. Feng *et al* [63; 68; 73] studies the performance of cold-formed thin walled steel members in fire conditions.

Although this is not directly related to LSF behaviour at ambient temperatures, they also test these same systems under ambient conditions to establish comparative parameters.

Some research studies discussed in the following lines consider the structural behaviour of LSF framing systems as a whole including plasterboard sheathing and cross bracing. The effects of these are not traditionally included in the load capacity design of LSF walls. Veljkovic and Johansson [18] has quantified the addition of plasterboard to the overall wall strength. They conclude that plasterboard on its own is enough to resist any structure lateral deflections, which would result in not using bracing members.

The main existing protocol to design LSF structures in Europe is Eurocode 3 [102]. Due to a lack of detail when prescribing the design of LSF structures, other standards can be applied. BS 5950 [15] is a document that combines codes of practice to cover the design, construction and fire protection of steel structures. It also covers the prescribed specifications for materials, workmanship and erection. Part 5 is responsible for the design of lightweight cold-formed members. A supplementary document created to assist with the design of beams, columns, roof trusses and their connections is also included in this national standard. By 2010 it is thought that Eurocode 3 will totally replace the corresponding British Standards mentioned here.

It is common in building construction in North America to attach plasterboard to both sides of the steel stud frames. Telue and Mahendran [103; 104] studied the effect of having two sides of plasterboard sheathing on the axial compressive strength of certain frame panels. They also produced a finite element model [105], which was validated by theoretical and experimental results, to facilitate the design of LSF structures with

plasterboard attached to both sides. This research paper took the results from their previous studies, which looked at different grades of unlipped steel stud and different frame configurations. The model also includes geometric imperfections and residual stresses of the frames, which are vital to obtain realistic results.

Salhab and Wang [106] tested LSF frames under compression with small perforations in their webs and the results were compared to frames with no perforations. It was concluded that the perforations only have a minor effect on the failure load of the steel frame because they work as stiffeners. ABAQUS modelling was also carried out to prove the reliability of computer models. Other studies have looked at the structural performance of perforated stud columns. Kesti and Makelainen [107] found that the perforations led to a reduced shear and buckling strength using both finite element methods and experimental results.

As mentioned previously, Feng *et al* [73] conducted tests on frame panels in fire conditions, but they also analysed the structural behaviour of some of the frames at ambient temperatures. The standard vertical studs had horizontal noggins attached to them for lateral stability and plasterboard was fixed to both sides of the frame. The two frames at ambient temperature were axially loaded, until failure of all the vertical steel channels occurred. Local buckling at the service hole of the studs caused flexural buckling failure, which points out the importance of imperfection when calculating the failure load.

Studies have been carried out to investigate different types of sheathing boards and the difference between using it on one or both sides of the steel stud frame. Tian *et al* [108] proved that when weak sheathing boards (Calcium Silicate) are added to the frame it increases the load carrying capacity of any steel stud by between 26 and 56%. If the spacing of the

screws attaching the sheathing board to the frame is then reduced, the outer studs become slightly weaker, and the middle stud doubles in strength. The type of sheathing was also found to have an effect. Different sizes and grades of steel stud were also tested, but Torsional-flexural buckling was the main failure mode in the middle stud of the frames, and mainly flexural buckling occurred in the side studs. As plasterboards made out of gypsum are a derivative similar to Calcium Silicate mentioned above, they could be assumed to have similar properties.

Tian *et al* [109] also looked at the stress/strain distributions in the studs of a typical frame panel. The same loading arrangements were used as indicated previously, and three types of sheathing board fixed to one side of the frame were again tested. As well as the failure loads and strains in the studs, vertical displacements were measured. The screws attaching the sheathing boards to the studs were found to restrain the lateral displacement, and also re-distribute some of the vertical load onto the sheathing board and down onto the foundation below the frame panel. The sheathing board was found to act as a shearing member to also steady the panel against lateral loads. It was also found to enhance the overall performance of the steel studs against buckling, and finally, it helped support part of the vertical load on the frame panel.

Pham *et al* [110] analysed boxed steel studs as well as the more common C section studs, which are being developed in an attempt to reduce the number of studs needed for a given wall area. Boxed studs do in fact have a higher ultimate failure load than the conventional C sections, found by assessing sixteen stud framed panels tested under combined axial and bending. Connection of the plasterboard with the steel studs is also better with the boxed sections, leading to a larger overall panel strength. The research paper calls for the additional strength offered by the plasterboard to be incorporated into modern design codes, as it also proves the axial

failure load increases for frames with the plasterboard attached to the interior side.

Tian *et al* [111] studied the shear resistance and lateral displacement of ten frames under horizontal loading with various types of bracing. Computer models based on the slope-deflection method were validated with the experiments. Their failure modes were observed for various bracing methods (no bracing, sheathing board, cross bracing on one side and double cross bracing on the frame panel). BS EN 594 [112] states the maximum allowable deflection limit for wall panels. The maximum deflection load and the residual lateral deflection once the load is removed were calculated for the previous bracing configurations.

Non-linear analysis is also developing due to the advances in computer simulation software. Schafer *et al* [113] have experimentally tested sixteen steel frames with random yield strengths under random gravity loads. Non-linear analysis simulations have then been used to replicate those results as best they can. A current analytical tool for estimating experimental results is Load and Resistance Factor Design (LFRD), which was compared to the non-linear computer analysis, and first plastic hinge strengths were determined for both methods. It was found that these sets of experimental results were simulated well using non-linear computer analysis, but conclusions may not be representative for other structures.

4.4. LSF Structural Behaviour Computer Modelling

Thermal and structural analyses of the solid phase in fire using ABAQUS are generally a simultaneous process for most of the models implemented using this software package. However, concurrent analysis for LSF walling systems can not be carried out due to the need to model cavity radiation when considering the systems as a whole. Cavity convection normally has

little effect on the overall outcome due to the proximity of the boundary cavity surfaces that minimize internal air movement due to friction. Even when this heat transfer mechanism is neglected within the cavity, accurate results are expected.

A decoupled analysis is conducted when cavity radiation needs to be modelled and two separate analyses of both the thermal and structural aspects need to be performed. The temperature evolution on each of the nodes in the model is first calculated, which depend on the geometry, thermal properties, boundary conditions and thermal loads. Thereafter, that information is inputted into the structural model and results about stresses, strains and deformations can be computed.

2D and 3D models have been developed to simulate some of the scenarios presented in the previous chapters. As was stated before, it is very important to begin with a well defined thermal analysis because the way the steel frame is heated will influence the final structural behaviour. Information about isolated members being heated is the starting point in any research but the need to account for the interactions between constitutive materials is relevant. Therefore, the prediction of temperature fields in the steel work and the definition of the weaknesses are vital to assess lightweight construction designs.

2D models are based on planar and deformable parts to which partitions that represent the constitutive materials are applied. Thereafter, section and material properties are assigned. The mesh is then generated minimizing computer effort without compromising the reliability of the results. This is feasible in 2D models due to the fact that even fine meshes do not signify important computer efforts. The cell size in the 3D models is also selected to minimize computational time without compromising the quality of the results obtained. 3D models are produced in a similar way to

the previous ones, using 3D deformable parts that are extruded and partitioned to represent the materials and sections involved.

The cell size and the time step used in the simulations have been used as a tool to reduce computational effort. The mesh is finer in areas of increasing heat transfer such as those where thermal bridges are found (around the steel work). This is shown in Figure 83. The number of cells used in the analyses varies from 18000 to 24000. Increasing those numbers was found not necessary to get better results. The lower limit (18000 cells) was found representative enough to provide accurate results and its used was extended through the execution of the computer models.

By limiting the maximum and minimum duration of any time step, the time domain has been discretized according to an imposed criterion. This limits the duration of any simulation to a maximum of 24 hours. The results obtained are assumed to represent the phenomena studied in great detail. Symmetry and repeatability is taken into consideration to simplify the models that are meant to replicate the behaviour of the LSF systems analyzed. The elements modelled have a width representative of the stud separation expected in real life conditions (600 mm). 2D simulations have been used initially to get a good understanding of the thermal behaviour of the LSF systems and 3D structural analyses have been carried out subsequently.

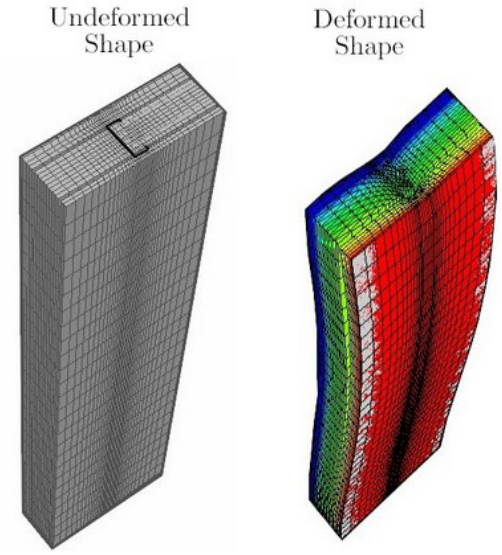

Figure 83: 3D LSF ABAQUS Mesh

The boundary conditions are temperature/time curves for the gas phase that represent the scenarios analyzed. Heat generation due to internal reactions within the constitutive materials is not considered in the computer models, however, they are accounted for when drawing conclusions. Incident heat fluxes as boundary conditions have been applied to predict structural performance. However, the temperature approach has proved to be more accurate and that is the reason why most of the simulations are carried out on that basis.

The variations of the temperature as a boundary conditions correspond to those recorded in actual tests and therefore, the outcome represents reality closer. Because fire severely affects only one of the sides of the specimen the temperature distribution within the test element is unsymmetrical. This causes a redistribution of stresses and strains that will cause eventual deformations in the weaker parts, such as the exposed flange.

Different degrees of freedom have been allowed for top and bottom sections of the systems modelled. The bottom part was modelled as a fixed

end and has been constrained in all the directions. The top part was model allowing vertical deflexions to happen. Rotations have been allowed both in the top and bottom to represent the conditions encountered in real life conditions.

4.5. LSF Material Properties in Fire

A transient analysis has been carried out to characterize the conditions encountered in the Dalmarnock Fire Tests [13] and in the Fire Rating Tests [10]. This is because the boundary conditions and the material properties change throughout any fire experiment due to large variations in temperature. The most important thermal properties required to characterize transient material behaviour are the specific heat (C_p), the thermal conductivity (k) and the density (ρ) of each of the individual materials that comprise the wall. Information about how these properties change as a function of the temperature, for the reference LSF systems presented in previous pages, has been gathered from experiments and the existing literature.

The thermal conductivity of the shell elements used in the assemblies have been calculated experimentally using a Guarded Heat Flow meter Dynatech TCHM-LT C-Matic. This applies to the plasterboard sheathing and the aluminium honeycomb. The values collected from those tests have been kept constant throughout the simulations. This is because the thermal conductivity of plasterboard and honeycomb does not change significantly for the range of temperatures found in the experiments. This is shown by the analysis carried out by Benichoun & Sultan [114]. The same research has been used to determine the thermal conductivity evolution of mineral wool, which is used in the reference assemblies. Eurocode 3 Part 4.3 [14] is used to characterize the thermal conductivity of steel. The thermal conductivity of the coating elements was initially

taken from the manufacturer and has been modified according to the information provided by Harmathy [115] and Wright *et al* [116].

The specific heat for most of the materials used in LSF constructions tends to vary when the members are heated up in a fire, as some materials self react at high temperatures. This is characteristic for insulating materials (mineral wool, aluminium honeycomb) comprising combustible bonding agents, which might combust by smouldering producing a heat generation source. The water contained within some LSF materials such as plasterboard or external coating evaporates internally. This contributes to the favourable behaviour of these materials in fire as most of the initial heat transferred to the wall is used to evaporate the water and does not conduct through the wall.

The specific heat evolution of LSF materials has been gathered from the literature and used in the computer simulations. The information provided by Benichoun & Sultan [114] has been used as a basis for the analysis. The specific heat evolution of mineral wool found in that study has negative values due to the ignition of the bonding agents. This presents a problem in ABAQUS analysis; therefore an average value for this property in the temperate range of interest has been selected. Plasterboard presents a peak in the specific heat at around 100 $^{\circ}$C as shown in the previous research paper. The most conservative approach (lowest peak heat flux) has been selected for the simulations providing accurate results. Eurocode 3 Part 4.3 [14] is used to characterize the specific heat of steel. Incropera [92] and Harmathy [115] provided information about the specific heat of render and coating materials.

The density of most of the materials used in LSF remains constant when heated. The slight variations encountered in density do not imply important differences in the outcome obtained from the computer models.

They have been measured experimentally with the aid of a calibrated scale and compared to the values provided by the Catalogue of Material Properties [117].

The steel frame provides the strength to the structure when framing with LSF. Although the rest of the constitutive materials provide extra stiffness to the system, this effect has been neglected for the purpose of the simulations. The main structural properties and the way they change with temperature are the Young Modulus (E), the Coefficient of Expansion (α) and the Yield Stress (σ_y) for each characteristic plastic strain and temperature. The way these properties change with temperature has been taken from the research paper by Zhao *et al* [78].

4.6. Dalmarnock Fire Test Computer Modelling

An initial thermal analysis is carried out to replicate the event of fire and its effects. A subsequent structural analysis is conducted where deformations in the steel work are recorded and compared to draw conclusions about structural behaviour of LSF in real life fire conditions.

4.6.1. Dalmarnock Fire Test Computational Thermal Analysis

The temperature evolution over the exposed and unexposed surfaces of the test element in the Dalmarnock Fire Tests is very irregular. The top of the specimen was heated up significantly more than the bottom part due to the impingement of the flames and the formation of the smoke layer. A characteristic section of the walling system, which corresponds to the one shown in Figure 84 has been selected to characterize the behaviour of a reference LSF structure under real fire conditions. The gas phase temperature evolution around the exposed surface was recorded. The temperature was also recorded over the unexposed surface.

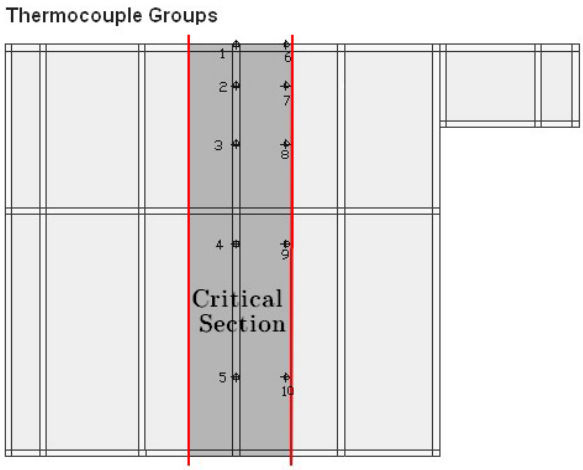

Figure 84: Dalmarnock LSF Critical Section

The convective coefficient in the exposed surface was approximated using trial and error techniques to match experimental and computational temperatures. This has been kept constant throughout the simulations and it was found always to be below 100 W/m^{2}K. There is no need to approximate this value on the unexposed surface because gas temperature readings were not recorded and the surfaces temperatures are therefore inputted. Figure 85 shows consecutive time steps of the computer model output where the temperature field is represented. It can be noted how the top of the specimen heats up faster than the bottom as mentioned before.

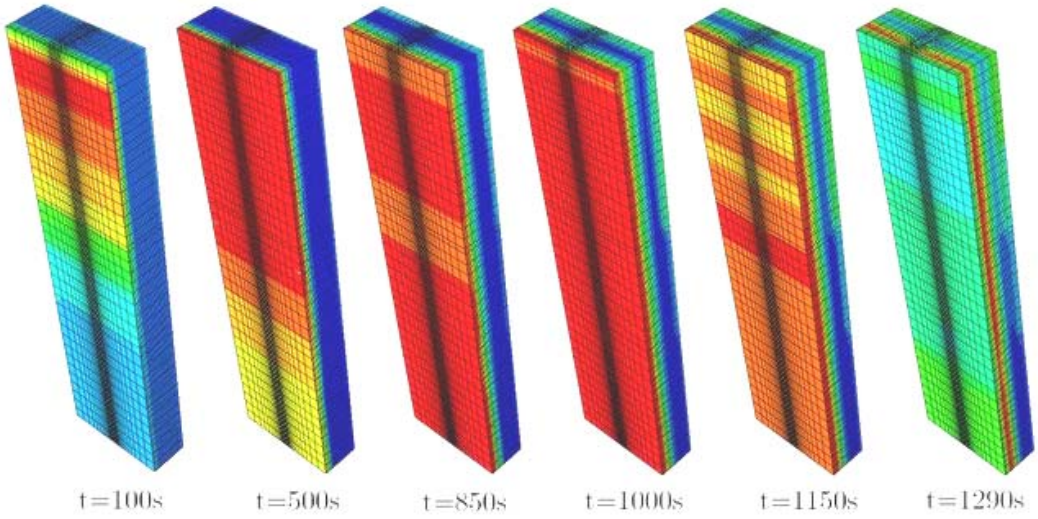

Figure 85: 3D Model Consecutive Steps

The temperatures obtained from the computer models in some characteristic points have been compared to the experimental ones. Good agreement has been found as shown in Figure 86 and Figure 87 . The temperature evolution of the exposed surface is slightly overestimated by the computer models due to constant values being taken for the convective coefficient and the emmisivity. A conservative approach to approximate these parameters is taken so subsequent structural analyses provide a higher safety factor. The flange temperatures recorded in the Dalmarnock Fire Test seem to change suddenly due to the rapid changes in the boundary conditions. The computational model however, shows constant thermal behaviour patterns and represents temperature tendencies.

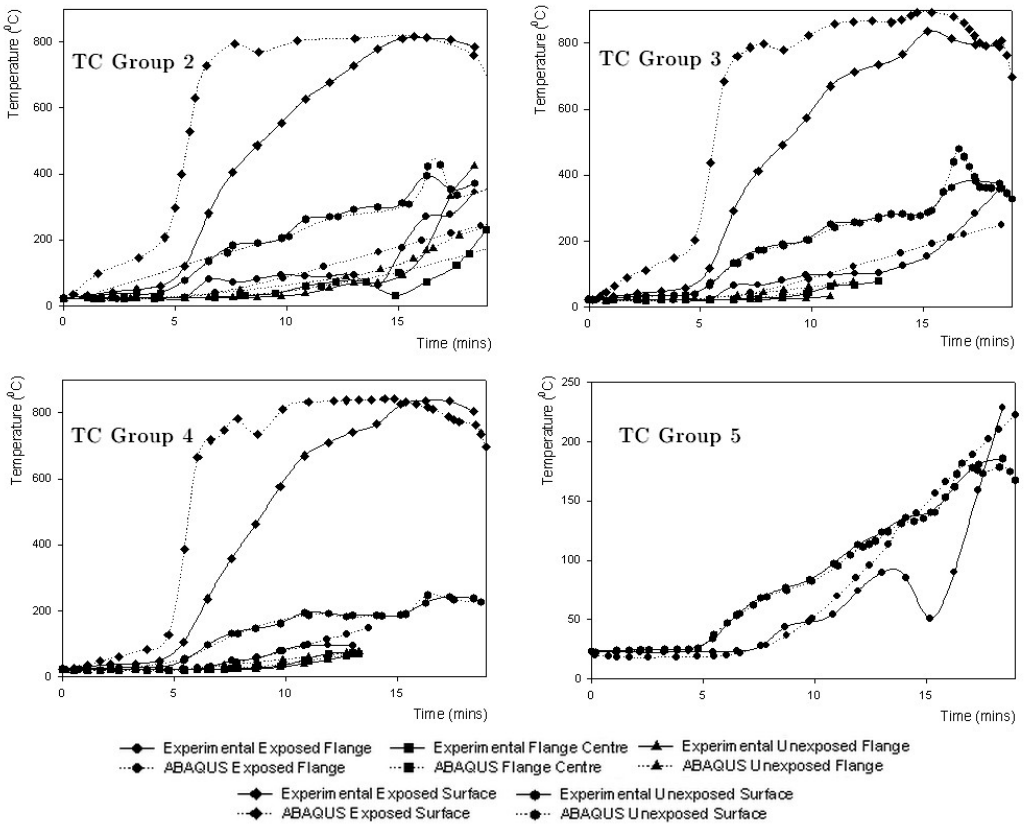

Figure 86: TC Groups over Steel Studs - Experimental Vs Model Temperatures

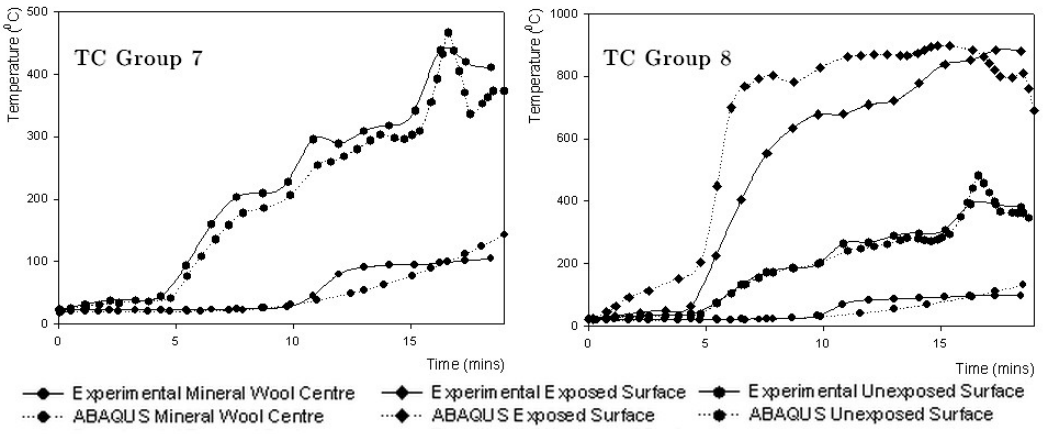

Figure 87: TC Group over Batt Insulation - Experimental Vs Model Temperatures

There is a good agreement between experimental and modelled temperatures for the steel section in TC Group 2. It is noted however that in the last 5 minutes of the test, the experimental temperatures tend to rise faster than the computed ones. This is because the model does not account for the heat generated by the oxidation of the aluminium honeycomb and the combustion of the bonding agents of the batt insulation. In spite of this, the computer models are found to realistically represent the temperature evolution. Some of the experimental flange temperatures in TC Group 3 and TC Group 4 present distortions in the readings after the first 13 minutes. These therefore have only been plotted up to the limit when irregularities began. The agreement in the temperature evolution up to that point shows a good agreement between experiment and computer models.

TC Group 7 and TC Group 8 show a good agreement in the temperature evolution for both the exposed and unexposed surfaces. The temperatures experimentally recorded in the centre of the mineral wool follow a characteristic evolution pattern that is not found in the computer model. That is due to the assumptions made when approximating the specific heat of the mineral wool. However, the final and intermediate temperatures gathered from the computer model present an acceptable error bar. It can be concluded therefore that the assumption was accurate and the models can be trusted.

4.6.2. Dalmarnock Fire Test Computational Structural Analysis

The temperature evolution for each of the nodes in the vertical steel stud is used as an input for the structural analysis. Although the system tested in the Dalmarnock Fire Tests is an infill wall, this can be loaded in the computer models to get information about behaviour under load bearing conditions for a system with the same characteristics. Due to the nature of

the analysis, the conclusions to be drawn are qualitative. This is because imperfections, bracings, sheathing influence, fixings, etc are not accounted for.

The boundary conditions imposed to the walling system are a fixed end on the unloaded cross section and one degree of freedom (vertical translation) is allowed for the loaded one. Any lateral movement of the bottom cross section is disabled and the top part is only allowed to move vertically. The intermediate points however between the top and bottom of the steel member are allowed to rotate and moved horizontally and vertically in any direction.

Loads are applied to the top end of the steel stud in the form of distributed pressures to avoid local deformations produced by point loads. Figure 88 shows the vertical translation of the top end of the stud when it is loaded. This deformation has been recorded in the centre of the web. It can be noted that the more the load is increased, the lower the vertical deformation is, due to the inability of the steel member to expand freely. The magnitude of the load therefore is proportional and represents the constraint to expand vertically. The stresses caused from this inability are redistributed horizontally and therefore, the horizontal deformations encountered are larger when the load is increased as shown in Figure 89.

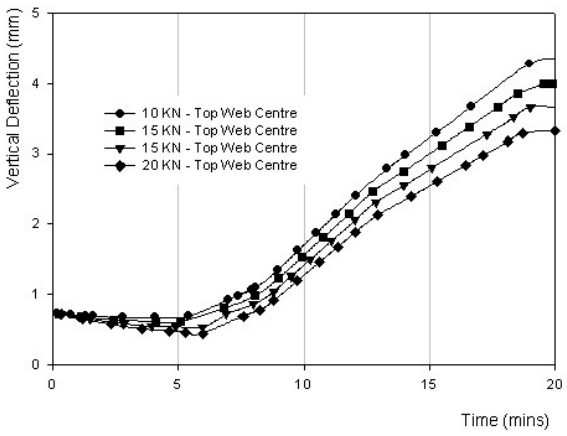

Figure 88: Vertical Deflection for Various Loading Scenarios

Figure 89 shows horizontal deflections for some characteristic points in the steel member. These have been selected to be on the exposed flange, where the larger thermal gradients are encountered. Horizontal deflections represent both buckling and the hypothetical fracture of sheathing elements, which gives an idea of failure. The horizontal deflections plotted in Figure 89 represent translations of the steel member inwards and outwards the fire location and it is perpendicular of the sheathing materials. This deflection therefore represents potential cracking of sheathing materials and local buckling. Positive values represent bowing of the steel studs towards the fire and negative, bowing away from it.

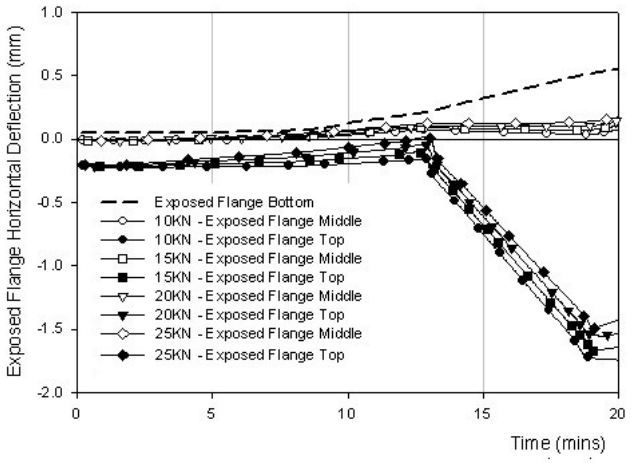

Figure 89: Horizontal Deflection for Various Loading Scenarios

The bottom part of the exposed flange in the Dalmarnock Test is not heated drastically by the fire as shown in Figure 85. That is why the horizontal deflections at that point, which are represented in Figure 89 with a dashed line, are independent of the load. The change in horizontal deflection is therefore a function of the temperature at that node and not of the load itself. It is shown by Figure 89 that the stresses caused from the impossibility to expand vertically are redistributed horizontally when the load is increased, which causes larger horizontal deflections.

4.7. Fire Rating Test Computer modelling

An initial thermal analysis is carried out to replicate the event of the Fire Rating Test and its effects. A subsequent structural analysis is conducted where deformations in the steel work are recorded and compared to draw conclusions about structural behaviour of LSF in Fire Rating Test conditions.

4.7.1. Fire Rating Test Computational Thermal Analysis

The thermal properties of the constitutive materials of the LSF system used for the Dalmarnock Fire Test is used for further analysis such as the fire rating test computer modelling. Both of the systems explained and analyzed in previous chapters have been modelled and conclusions about structural performance have been drawn. A similar loading has been used as in the previous section (distributed pressure in top end cross section). The support conditions selected for this analysis are the same as those in the Dalmarnock Fire Tests and the main difference lies in the temperature evolution of the gas phase.

The temperature evolution in the exposed flange has been identified as critical to influence the structural behaviour of load bearing LSF systems. This is not the case for infill conditions as explained later, where the critical temperature is the one found in the unexposed surface. The predicted and computed temperature evolutions in the exposed flange for load bearing conditions are compared in Figure 90. There is a good agreement between the temperatures calculated by the computational model and the predicted ones that would be found in a full scale experiment. It should be noted that the temperature in the flange presents a gradient and the temperatures selected for the analysis are those in the

centre of the exposed flange, where thermocouples are more likely to be found in full scale experiments.

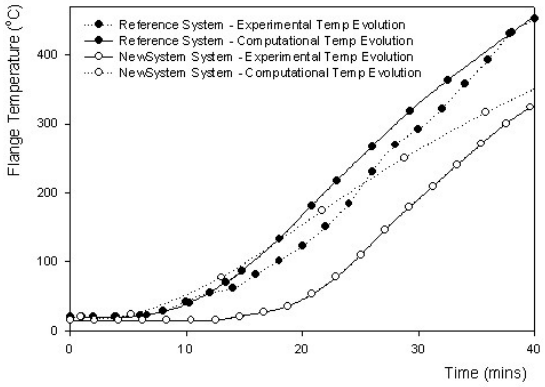

Figure 90: Computer Vs Experimental Exposed Flange Temperature Evolution

The temperature evolution predicted by the model matches closely with that encountered for the actual fire rating test in the reference system. This is due to the corrections applied in the emmisivity of the honeycomb, which radiated over the exposed surface through the cavity left by the melted polystyrene channels. This corrected emmisivity intends to represents the actual one plus the effect of the convective heat losses that occur when the channels have melted. In the New System, the cavity is substituted by mineral wool, therefore correction to the emmisivity is not needed. The results show a good agreement although it is noted that the model overestimates the exposed flange temperatures at the beginning of the test and homogenizes afterwards.

Infill walls do not carry any external load. The only internal load they take is gravity, which is not enough to produce any deformations at the encountered steel temperature range for the fire rating test. Therefore, the temperature in the unexposed surface is identified as critical and this is plotted in Figure 91. None of the systems described in that figure would

present insulation failure after 2 hours. This fact is unrealistic because it is based on the assumption that all the constitutive elements are kept in place throughout the duration of the experiment. In reality, it is expected to see unpredictable local failure of some of the constitutive materials, which will affect the thermal model used. However, it is clear that failure of LSF infill walls happen at later times than in load bearing conditions.

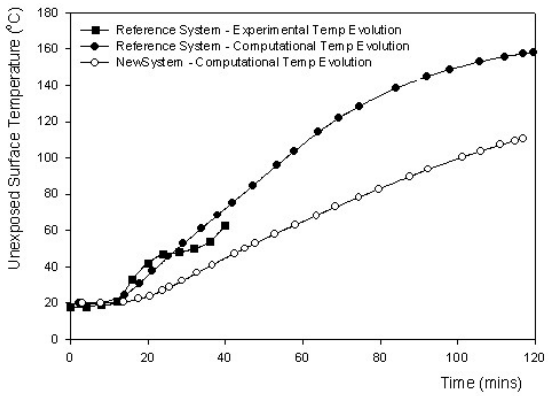

Figure 91: Unexposed Surface Temperature Evolution

4.7.2. Fire Rating Test Computational Structural Analysis

The temperature evolution for each of the nodes in the vertical steel stud is used as an input for the structural analysis. This is then loaded in the computer models to get information about behaviour under load bearing conditions and qualitative conclusions are drawn. The same analysis as in the Dalmarnock Fire Test has been conducted to understand the behaviour of LSF systems in the Fire Rating Test. The horizontal deflections have been plotted for the top of the stud and for the centre point (half of the height). The bottom part deflections are very similar to those encountered on the top because the system is heated uniformly through the exposed surface. This causes the temperature distribution in the steel work to be constant vertically throughout each point of the stud

cross section. Figure 92 and Figure 93 show the deflections computed for both the LSF reference system (Old System) and for the New System.

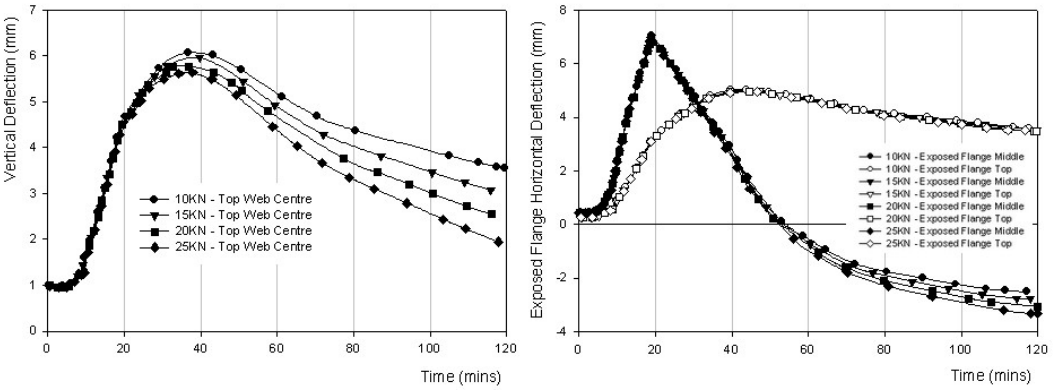

Figure 92: Reference System Deflections in Fire Rating Test

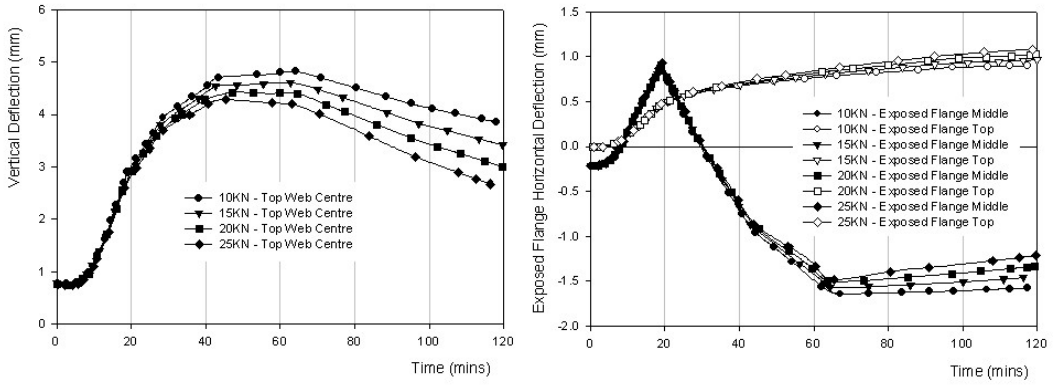

Figure 93: New System Deflections in Fire Rating Test

The same pattern seen in the Dalmarnock Fire tests is encountered in the way vertical and horizontal deflections are affected by the magnitude of the load applied to the steel section. Horizontal deflections however, swap from positive to negative for both systems, which represents some initial bowing of the steel work towards the furnace followed by global buckling away from it. Figure 94 compares the structural data produced for the reference and the New Systems. The deformations plotted are those encountered for a 10 KN load.

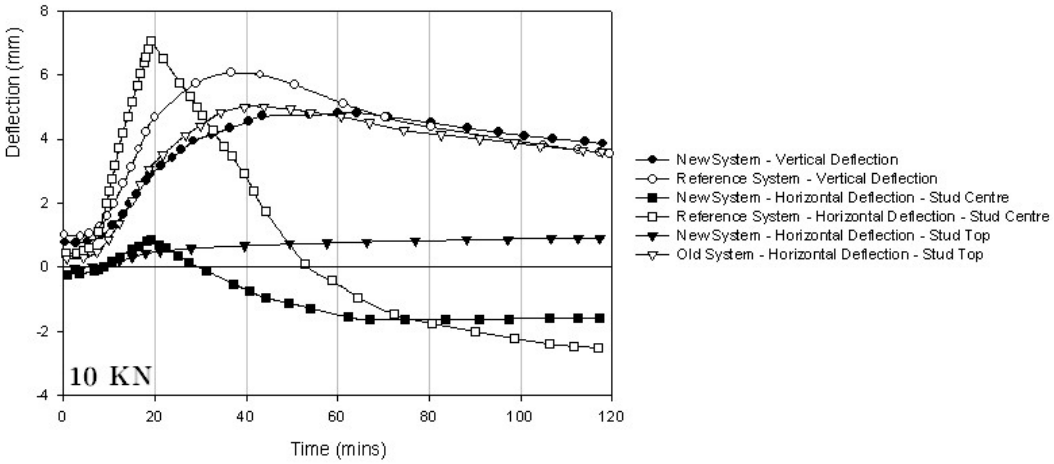

Figure 94: Comparison of Deflections for Two LSF Designs

The vertical deflection is larger in the Reference system. This might produce stress concentration due to the restriction on movement imposed by the floor and ceiling slabs (load bearing conditions). Infill walls however are assembled leaving a gap between themselves and the structural slabs to allow thermal expansion, which reduces the likelihood of stress concentrations. The horizontal deflections are also larger for the Reference systems, which facilitate buckling and hypothetical fracture of the sheathing elements. The differences encountered in the structural behaviour are due to the different design of the systems analyzed and the thermal behaviour that they present.

4.8. Real Fire and Fire Rating Test Structural Behaviour Comparison

The same LSF System has been tested under the fire conditions found in both the Dalmarnock Fire Tests and the Fire Rating Test. The comparative analysis is presented in Figure 95. The deformations plotted are those encountered for a 10 KN load.

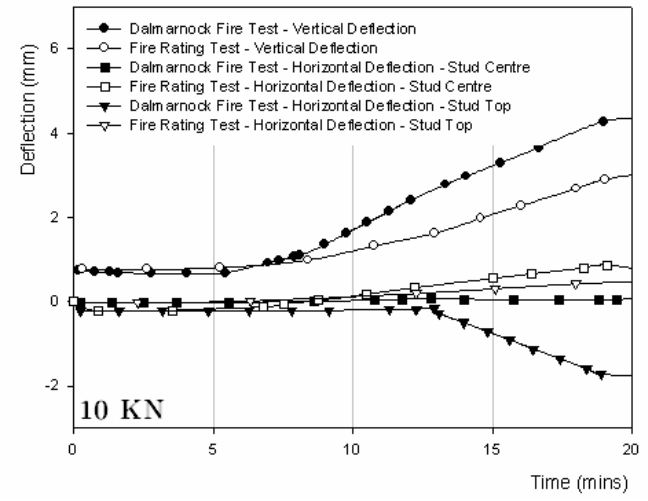

Figure 95: Comparison of Deflections between Fire Rating Test and Dalmarnock Fire Tests

It is observed that the most significant deflections are encountered during the Dalmarnock fire Test. This is due to the greater thermal gradients recorded in the second part of the test (fire attacking both sides of the specimen). The more severe boundary conditions in that test caused the steel to heat more rapidly, which produces larger deflections. Vertical deflections are not important in infill conditions but need to be accounted for when designing complete LSF buildings. It can also be noted that the centre of the system remains rather immobile due to the overlapping deflections encountered in the top and bottom of the stud. The more severe the external conditions are, the larger the deformations expected and the likelihood of failure.

4.9. LSF Structural Behaviour Conclusions

The use of computer models to predict fire performance has been analyzed with the aid of actual experimental results. Limitations in the way models are produced have been identified and the effect that they might have in

the solutions is commented on. Further work however should be carried out to determine the effect of irregularities such as section imperfections, bracings, sheathing influence, fixings, etc. Qualitative conclusions have however been drawn from the general analysis carried out in this study. LSF deflections in the steel frame have been recorded and compared in two different scenarios, the Fire Rating Test [10] and the Dalmarnock Fire Tests [13]. Although satisfactory structural behaviour has been observed, design optimization is expected to improve the way these systems behave at ambient and elevate temperatures.

When analyzing complex lightweight construction systems, it is of vital importance to begin with a well defined thermal analysis, from which subsequent structural examination might be carried out. Due to the way construction technologies are evolving, the nature of the constitutive materials and their interactions are becoming more and more complex. The way heat is conducted within the assembly is therefore an important issue to address before any structural analysis is conducted, in which those interactions must also be taken into account.

One of the key aspects to produce a reliable thermal analysis is to use the most realistic thermal properties of the constitutive materials. These have been gathered from the existing literature in this study. Complementary experimental testing however is also recommended. Boundary conditions also are important when producing accurate computer models. This are normally approximated and constant values tend to be used. Although this is the case for this study, the outcome is satisfactory when experimental and computational results are compared.

Only axially compressed steel sections have been studied in this analysis and the deflections recorded have been used as a comparative tool between different systems and external conditions. In real life conditions, the way

the load is applied and the torque they might produce effects the outcome. One limitation observed in the ABAQUS models is the impossibility to couple thermal and structural analysis. This is due to the existence of internal cavities in which radiation needs to be modelled. In addition, only temperature/time curves have been used as boundary conditions in the analysis. This is because of the limitations that software packages present to input heat flux/time curves as boundary conditions.

Chapter Five

5. Discussion of Results, General Conclusions and Further Work

5.1. Discussion of Results, General Conclusions and Further Work

The integral assessment of lightweight construction systems is now possible through the implementation of the methodologies presented in this paper also described in the following figure. In isolation these methodologies provide information about thermal efficiency, fire performance and structural behaviour and when combined, global and integral information about particular designs can be obtained. This can aid decision making in the design process of lightweight construction systems as quantitative information can now be compared.

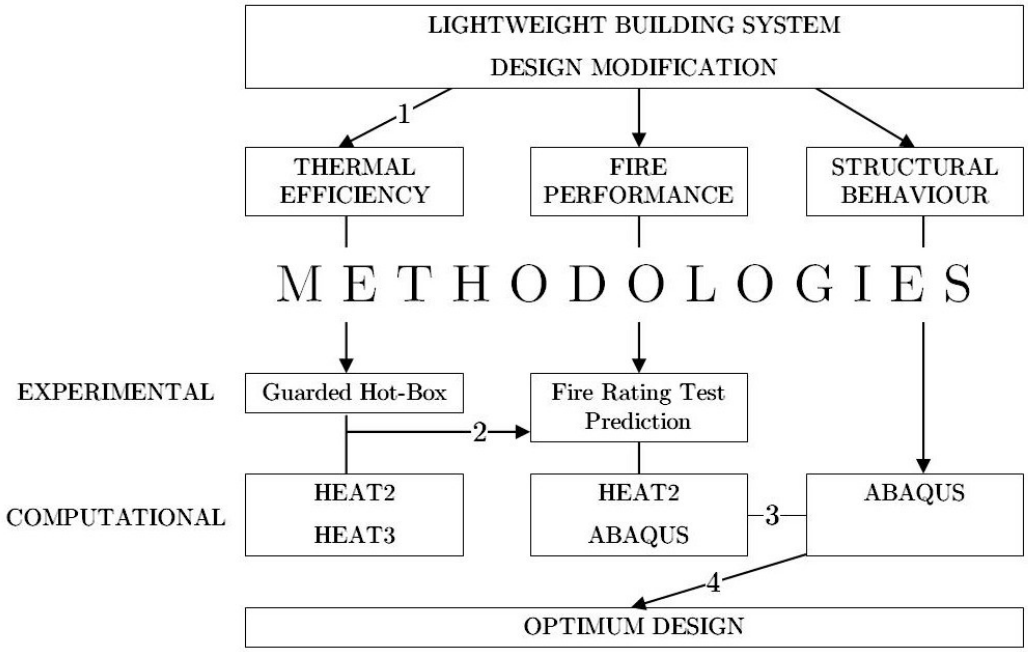

The methodologies presented in this project to analyze thermal efficiency of lightweight construction systems have proved to be robust and it is concluded that building designers can rely on computer models to calculate realistic U-Values for lightweight construction systems although it should be noted that slight corrections and a good definition of the thermal properties are necessary if these computer models are to lead to

representative results. It is recommended that the initial design modifications are assessed computationally so general conclusions about performance can be drawn. Thereafter, prototypes might be built and can be tested in the Guarded Hot-box apparatus designed, constructed and calibrated for that purpose.

Building regulations are becoming more restrictive and are targeting U-Values. Prescribing slight reductions in this parameter is a synonym of large savings in the residential energy bill and a decrement in the CO_2 emissions to the atmosphere. It has been proved by this research that using the correct methodologies and software packages lead to improved designs. This study however, does not account for other aspects such as assembly imperfections or reduced material qualities that are very influential for the thermal performance of the building system as a whole.

A more strict approach to be taken by building control authorities is necessary to tackle the problem of increasing CO_2 emissions every year. Integral measures need to be taken by the regulatory bodies, if more sustainable construction techniques are aimed. Controlling the assembly process and the thermal properties of the materials used in the construction of residential buildings will increase the quality of the final product reassuring the user and the environment.

The Hot-box experiment has proved to be a sound technique to determine experimentally the thermal transmittance of external walling specimens. It is also an experimental procedure recommended to analyze the interaction between the systems assessed with windows, doors, ceilings, corner configurations, etc. It is however not prescribed by building regulations the execution of such a test and compliance with current prescriptions is demonstrated by computational means. These have proved to underestimate U-Values and therefore, it is recommended a redefinition of

those regulations. The number of testing facilities around the world capable of conducting Hot-box experiments is rather limited and governments should be encouraged to increase those numbers.

In addition, national and international standards that apply to this type of measuring equipments are far too strict to be fully satisfied. A revision of their contents is recommended to lead to improved empirical tests. There are aspects included within these standards that are not highly relevant for the definition of the thermal transmittance. These aspects should be neglected or altered to simplify the experiments and facilitate their execution. Good examples of this are the prescribed laboratory conditions, the error bar suggested, etc.

Some other relevant aspects are omitted by the standards and their revisions should account for them in the modifications. For instance, the calibration of a Guarded Hot-box is not compulsory but recommended in the standards. This action is however extremely important to understand the existing errors of every particular apparatus and they can be accounted for in further tests. The calibration of these apparatus should be compulsory.

The execution of Hot-box experiments is rather time consuming. Their cost however is marginal and prescribing the execution of these tests would not be an economical difficulty, which could be assumed by the construction companies. The opposite happens with the fire rating test that is explained in the following chapter. In that case, cheaper and reliable methodologies capable of approximating the outcome obtained from the full scale test are necessary and they are developed and recommended.

The final outcome of the thermal efficiency methodologies is the value of the thermal transmittance (U-Value) that indicates heat loss for any lightweight construction configuration. In addition, and more importantly, this property is inputted into subsequent methodologies to analyze the performance of these systems in fire. This contributes to an integrated approach to design lightweight construction systems, which is the main goal of the project.

The prediction of fire ratings for lightweight construction systems using bench scale experiments is feasible by applying the methodology presented in this thesis. This is a novel methodology that has proved to be sound and robust. Information about the insulating properties of the system analyzed (thermal efficiency) is inputted into the method and predictions about fire performance can be concluded. By applying the methodology suggested, information about both thermal efficiency and fire performance is gathered and comprehensive solutions can be found.

These methods can be implemented over any lightweight construction system using a small scale furnace so long as incident heat fluxes are recorded in the specimens exposed surface. It is important to understand the concept of critical section and critical temperature as they cause failure. Once this is determined and its evolution studied, final conclusions can be drawn. By incorporating the aid of software packages, more extensive conclusions can be drawn.

The two systems analyzed in this report have shown a similar temperature rise in the critical sections when subjected to identical heat fluxes however due to their dissimilar thermal properties, the incident heat flux evolution when exposed to the fire rating test varies significantly. The new system is more insulating and none of its constitutive materials melt when subjected

to the full scale fire performance test. That is why the fire rating is more satisfactory.

The outcome of this investigation is the time that any specimen would withstand when tested in the furnace used for our analysis. If any other furnace is used, corrections to the solution obtained need to be applied. In that case, it is recommended to understand the methodology and then apply it to the new furnace after obtaining the new governing equations.

One of the main criticisms of the fire performance test is the difference in the rating that dissimilar furnaces give when testing the same specimen. Even though the governing heat transfer mode within the furnace is convection, radiation also affects the outcome. Radiation depends on the characteristics of the furnace (size, ceramic walls, fuel, etc.), therefore it is noted that there is a need for regulation with regards to the calibration of the existing furnaces in order to get universal ratings.

A measure was adopted by fire research organizations willing to homogenize fire ratings based on the use of plate thermometers. These reliable sensors are placed on the exposed surface allowing a gap between them and the specimen. Although more homogeneous results have been gathered, this approach has proved not to be enough and the need to account for heat fluxes has been identify if further improvement of this experiment wants to be achieved. If furnace calibration was carried out, heat flux evolution as a function of time and thermal insulating properties of the specimens could be drawn and be the basis for engineering based fire performance predictions.

In addition, fire rating methodologies involved in assessing real fire performance are validated for realistic fire scenarios (Dalmarnock Fire Tests). One reference LSF walling system has proved to successfully

withstand the effects of a severe post-flashover fire with no symptoms of deformation or collapse. The fixings have successfully held the constitutive materials in place and the deterioration encountered was not significant enough to propagate the fire or to cause any accidents. The outcome is very positive and opens the possibility to further research into potential improvements to this type of construction system.

The use of computer models to predict structural behaviour in fire has been analyzed with the aid of actual experimental results. Limitations in the way models are produced have been identified and the effect that they may have in the solutions is commented on. Further work should however be carried out to determine the effect of irregularities such as section imperfections, bracings, sheathing influence, fixings, etc. Qualitative conclusions have been drawn from the general analysis carried out in this study. LSF deflections in the steel frame have been recorded and compared in two different scenarios, the Fire Rating Test and the Dalmarnock Fire Tests. Although satisfactory structural behaviour has been observed, design optimization is expected to improve the way these systems behave at ambient and elevated temperatures.

When analyzing complex lightweight construction systems, it is of vital importance to begin with a well defined thermal analysis, from which subsequent structural examinations might be carried out. Due to the way construction technologies are evolving, the nature of the constitutive materials and their interactions are becoming more and more complex. The way heat is conducted within the assembly is therefore an important issue to address before any structural analysis is conducted, in which those interactions are taken into account.

Only axially compressed steel sections have been studied in this analysis and the deflections recorded have been used as a comparative tool between

different systems and external conditions. In real life conditions, the way the load is applied and the torque they might produce effects the outcome. One limitation observed in the ABAQUS models is the impossibility to couple thermal and structural analysis. This is due to the existence of internal cavities in which radiation needs to be modelled. In addition, only temperature/time curves have been used as boundary conditions in the analysis. This is because of the limitations that software packages present to input heat flux/time curves as boundary conditions.

LSF systems such as those referenced in this study have proved to be a suitable replacement for traditional construction techniques. They comply with current building regulations and can easily adapt to prescriptive changes due to the versatility that their design presents. Further work however is needed to improve the characteristics and to add value to these modern construction technologies.

References

[1] Stephen Emmitt. Architectural Technology. Blackwell Publishing 2002. 264 pages. ISBN 063206403X

[2] M D Heywood. Benefits of off-site steel construction in urban locations. The Steel Construction Institute. Technical Information Sheet (2006)

[3] Ulrich Bogenstatter. Prediction and optimization of life-cycle costs in early design. Volume 28, Number 5 - 6 / Journal of Building Research & Information. Pages 376 – 386 (2000)

[4] Warwick District Action 21. Sustainable˙construction. Existing buildings 2006. Available from: http://www.action21.co.uk

[5] Consortium for Advance Residential Building. Case Study, Dearbought Townhouses, Frederick, Maryland, USA (1997)

[6] Aitor Amundarain, Jose L. Torero, Asif Usmani, Ahmad M. Al-Remal. Thermal Efficiency and Fire Performance of Light Steel Framing: Challenges for a New Technology. WCAEBE Conference, Birmingham, 2006.

[7] BS 874-1:1986. Methods for determining thermal insulating properties. Introduction, definitions and principles of measurement.

[8] Building Regulations for England and Wales 2006. Part L. Conservation of fuel and Power. Department of Trade and Industry.

[9] BS 874-3.1:1987. Methods for determining thermal insulating properties with definitions of thermal insulating terms

[10] BS 476. Fire tests on building materials and structures

[11] Farid Alfawakhiri and Mohamed A. Sultan (October 2000). Fire Resistance of Loadbearing LSF Assemblies. Institute for Research in Construction, National Research Council Canada. 15th International Specialty Conference on Cold-Formed Steel Structures, St. Louis, MO, U.S.A.

[12] D. B. Moore, T Lennon (2003). Building Research Establishment (February 2003) ODPM Building Regulations Division Project Report : Fire Safety of Light Steel Framed Houses - Test results and observations. Project report number 202-999.

[13] G. Rein, C. Abecassis Empis, A. Amundarain, H. Biteau, A. Cowlard, A. Chan, W. Jahn, A. Jowsey, P. Reszka, T. Steinhaus, S. Welch, J.L. Torero, J. Stern-Gottfried, A. Coles, M. Lazaro, D. Alvear, J.A. Capote,

N.L. Ryder, F. Mowrer, C. Lautenberger, S. Desanghere, D. Joyeux, S. Kumar; Round-Robin Study of Fire Modelling Blind-Predictions using the Dalmarnock Fire Experiments. 5th ISFEH Conference, Edinburgh, April 2007.

[14] BS EN 1993-1-13. Eurocode 3. Design of steel structures. General rules - Supplementary rules for cold-formed members and sheeting.

[15] BS 5950-5:1998. Structural use of steelwork in building - Part 5: Code of practice for design of cold formed thin gauge sections

[16] Powerwall Systems Limited Technical Brochures. Applications. Web Page: http://www.powerwall.co.uk

[17] NHBC Standards. National House-Building Council. 2006 Technical Standars. Chapters 6.9 and 6.10

[18] Milan Veljkovic, Bernt Johansson; Light steel framing for residential buildings. Thin-Walled Structures. Thin-Walled Structures, In Press, Corrected Proof, Available online 23 February 2007

[19] British Standard BS EN 520: 2004. Gypsum plasterboards: Definitions, requirements and test methods

[20] prEN 14566 CEN WI 00241013. Mechanical fasteners for gypsum plasterboard systems - Definitions, requirements and tests methods

[21] BS EN 10147-S350 G. Continuously hot-dip coated strip and sheet of structural steels. Technical delivery conditions

[22] BS EN 13162: 2001. Thermal insulation products for buildings. Factory made mineral wool (MW) products. Specification

[23] BS EN 13163: 2001. Thermal insulation products for buildings. Factory made products of expanded polystyrene. Specification

[24] Asif Usmani, Huang Hou-Cheng. Finite element analysis for heat transfer. London : Springer-Verlag, 1994

[25] HEAT2. A PC-program for heat transfer in two dimensions. Manual with brief theory and examples. Version 5.0. Lund-Gothenburg Group for Computational Building Physics. 2000

[26] HEAT3. A PC-program for heat transfer in three dimensions. Manual with brief theory and examples. Version 4.0 Lund-Gothenburg Group for Computational Building Physics. 2001

[27] TRISCO Manual. Edited and Published by Physibel. http://www.physibel.be/

[28] ABAQUS Theory Manual. Edited and Published by ABAQUS. http://www.abaqus.com/

[29] Kyoto Protocol Reference Manual on Accounting of Emissions and Assigned Amounts. UNFCCC secretariat. February 2007

[30] DTI. Department of Trade and Industry. Energy Consumption in the United Kingdom, Final energy consumption by final user 1970 to 2004. (2006)

[31] American Iron and Steel Institute - Steel in Residential Construction Advisory Group. Thermal Design Guide for Exterior Walls, Publication RG-9405, Appendix, 1995

[32] ASHRAE 1997 - 1997 ASHRAE Handbook of Fundamentals. Atlanta - pp. 24.11 and 14.12

[33] U. S. Department of Housing and Urban Development Office of Policy Development and Research. Design for a Cold-Formed Steel Framed Manufactured Home:Technical Support Document. Final Report (2002)

[34] Jan Kosny, Jeffrey E Christian. Reducing the uncertainties associated with using the ASHRAE zone method for R-value calculations of metal frame walls. ASHRAE TRANS. Vol. 101, Pt 2, pp. 779-788. 1995

[35] Edward Barbour, John Goodrow. Thermal performance of steel-framed walls. ASHRAE TRANS. Vol. 101, Pt 2, pp. 766-777. 1995

[36] J. Kosny, A. Desjarlais, and J. Christian; Whole Wall Rating/Label for Structural Insulated Panels: Steady-State Thermal Analysis. Oak Ridge National Laboratory. Buildings Technology Center (1999)

[37] Williams R. G., Gatland S.D., Goss W. P., Baumgardner R. L., Miller R. G. A wall and edge guarded hot box for thermal transmittance measurements, ASTM special technical publication, n 1320, pp. 46-60 (1997)

[38] Bipin Shah, Dragan Curcija; A Pilot Project to Establish the Technical Basis and Institutional Framework for Assuring the Energy Efficiency of Fenestration Building Products in Certain Transitional Economy Countries - Phase 0 Results. Technical Report. Centre for Energy Efficiency and Renewable Energy University of Massachusetts (2000)

[39] Paul Fazio, Andreas K. Athienitis, Cedic Marsh and Jiwu Rao. Environmental Chamber for Investigation of Building Envelope Performance. Jorunal or Architectural Engineering, Volume 3, Issue 2, pp. 97-102 (June 1997)

[40] Goufeng Mao; Laboratory Measurements and Modelling of the Dynamic Thermal Performance of a Thermal Bridge. Nordic Journal of Building Physics Vol 1, (1998)

[41] Rose J.; Validating Numerical Calculations against Guarded Hot Box Measurements. Nordic Journal of Building Physics Vol.4 (2004)

[42] Canadian Sheet Steel Building Institute. Energy Efficiency of Steel Framed Homes Confirmed, Vol. 5/No.1, July 1999

[43] BS EN ISO 8990:1996 - Thermal insulation. Determination of steady-state thermal transmission properties. Calibrated and guarded hot box

[44] BS 7501:1989 EN 45001:1989. General criteria for the operation of testing laboratories

[45] J. Kosny and J.E. Christian. Thermal evaluation of several configurations of insulation and structural materials for some metal stud walls . Eergy and Buildings. Number 2, 1995, pp. 157-163(7)

[46] J. Kosny and P. Childs. Accuracy of hot box testing of steel stud walls, ASTM Special Technical Publication, Issue 1426, 2002, Pages 147-158

[47] J. Kosny, J. E. Christian and A. O. Desjarlais. Improving Energy Performance of Steel Stud Walls. Steel Framing Can Perform As Well As Wood. Oak Ridge National Laboratory / Buildings Technology Centre Internal Report

[48] T. Hoglund, H. Burstrand. Slotted steel studs to reduce thermal bridges in insulated walls. Thin-Walled Structures 32 (1998) Pg 81-109

[49] Nader R. Elhajj. Development of Cost-Effective, Energy-Efficient Steel Framing. Thermal Performance of Slit-Web Steel Wall Studs. Steel Framing Alliance Washington. September 2002

[50] Kesti J., Makelainen P.; Design of Gypsum-Sheathed Perforated Steel Wall Studs . Journal of Constructional Steel Research, Volume 46, Number 1, pp. 215-216(2) (1998)

[51] Suda N., Uno N., Shimizu J., Kanno R., Sugita K.; Thermal Insulation and Thermal Bridge of Steel-Framed Walls, Nippon Steel technical report No.79, op. 35-40 (1999)

[52] S. M. Doran and M. T. Gorgolewski. U-Values for Light Steel Frame Constructions. BRE Digest 465, CI 38/19/229, February 2002

[53] BS EN ISO 6946 (1997). Building components and building elements. Thermal resistance and thermal transmittance. Calculation method

[54] BS EN ISO 10211-1 (1996). Thermal bridges in building construction. Heat flows and surface temperatures. General calculation methods

[55] J. Kosny and A.O. Desjarlais. Performance of Residential Wall Systems Influence of Architectural Details on the Overall Thermal. Journal of Building Physics 1994. 18; 53

[56] Nader Elhajj. Steel Framing Alliance. Steel Recognized in Green-Building Guidelines. Framework Journal. Mar/Abr 2005.

[57] RUUKKI. Steel-Framed House for the Housing Fair, Kotka, Finland. Internal Report (2006)

[58] Steel construction institute. Light Steel Framing in Residential Housing, Issue No. 33, Technical Information Sheet (1999)

[59] M D Heywood. Benefits of off-site steel construction in urban locations. The Steel Construction Institute. Technical Information Sheet (2006)

[60] BS 4937-30:1993. International thermocouple reference tables. Extension and compensating cables. Tolerances and identification system

[61] BS EN 13163:2001. Thermal insulation products for buildings. Factory made products of expanded polystyrene (EPS). Specification

[62] BS EN ISO 6946:1997. Building components and building elements - Thermal resistance and thermal transmittance - Calculation method

[63] Feng, M., Wang, Y.C., and Davies, J.M. Thermal performance of cold-formed thin-walled steel panel systems in fire. Fire Safety Journal 38 p365-394, 2003

[64] Sultan, M.A. A Model for Predicting Heat Transfer Through Noninsulated Unloaded Steel-Stud Gypsum Board Wall Assemblies Exposed to Fire. National Fire Laboratory, Institute for Research in Construction, National Research Council Canada, Ottawa, Ontario, Canada. 1996

[65] Kodur V.K.R. & Sultan M.A. Factors Influencing Fire Resistance of Load-bearing Steel Stud Walls. Fire Technology Journal, 42, pp 5-26, 2006

[66] Lee, J.H., Mahendran, M., Makelainen, P. Prediction of mechanical properties of light gauge steels at elevated temperatures. Journal of Constructional Steel Research 59, p1517-1532. 2003

[67] Ramberg, W. & Osgood, W.R. Description of stress-strain curves by three parameters. NACA. Technical Note 902. 1943

[68] Feng, M., Wang, Y.C., and Davies, J.M. Axial strength of cold-formed thin-walled steel channels under non-uniform temperatures in fire. Fire Safety Journal 38, p679-707. 2003

[69] BS EN 1993-1-2:2005 . Eurocode 3. Design of steel structures. General rules. Structural fire design

[70] Lawson R M. Building Design Using Cold Formed Steel Sections: Fire Protection. The Steel Construction Institute, Publication P129. 1993

[71] Buchanan, A.H., Collier, P.C.R., Gerlich, J.T. Design of Light Steel-Framed Walls for Fire Resistance. Fire and Materials, Vol 20. 79-96. 1996

[72] ISO 834-1:1999. Fire-resistance tests. Elements of building construction. Part 1: General requirement

[73] Feng, M. & Wang, Y.C. An analysis of the structural behaviour of axially loaded full-scale cold-formed thin-walled steel structural panels tested under fire conditions. Thin -Walled Structures Journal 43 pp. 291-332. 2005.

[74] BS DD ENV 1993-1-2:2001. Eurocode 3. Design of steel structures. General rules. Structural fire design (together with United Kingdom National Application Document)

[75] Alfawakhiri, F. and Sultan, M.A. Fire Resistance of Loadbearing LSF Assemblies, Institute for Research in Construction, National Research Council Canada. 2000

[76] Alfawakhiri, F., Sultan, M.A. and MacKinnon, D. H. Fire Resistance of Loadbearing Steel-Studs Walls Protected with Gypsum Board: A Review. Fire Technology Journal. Vol 35, No. 4. 1999

[77] Moore, D. B. and Lennon, T. Building Research Establishment (BRE) ODPM Building Regulations Division Project Report: Fire Safety of Light Steel Framed Houses - Test Results and Observations, Project Report Number 202-999, 2003.

[78] Zhao B., Kruppa J., Renaud C., O'Connor M., Mecozzy E., Azpiazu W., Karlstrom P., Jumppanen U., Kaitila O., Oksanet T., Salmi P. Calculation Rules of Lightweight Steel Sections in Fire Situation. ECSC PROJECT N. 7210 PR 254. 2003

[79] American Iron and Steel Institute. Steel Framing Alliance. Design Guide 9. Fire Resistance Ratings of Load Bearing Steel Framed Walls. 1981.

[80] U.S. Department of Housing and Urban Development (Office of Policy Development and Research) and the Steel Framing Alliance. Residential Steel Framing. Fire and Acoustic Details. 2002

[81] Steel Framing Alliance Report. A Guide to Fire & Acoustic Data for Steel Floor & Wall Assemblies. 2005

[82] The Steel Construction Institute. Building Design using Cold Formed Steel Sections for Fire Protection. ISBN 1 870004 97 3. 1993

[83] BS EN 1365-1:1999. Fire resistance tests for loadbearing elements - Part 1: Walls

[84] NIST Chemistry WebBook. NIST Standard Reference Database Number 69, June 2005 Release. http://webbook.nist.gov/chemistry/

[85] Fire Resistance Ratings of Load Bearing Steel Stud Walls. Design Guide 9. Published by the Steel Framing Alliance

[86] ASTM E459 - 05: Standard Test Method for Measuring Heat Transfer Rate Using a Thin-Skin Calorimeter

[87] BS EN 12164:1998. CW 004A. Copper and copper alloys. Rod for free machining purposes.

[88] BS EN 520: 2004. Gypsum plasterboards: Definitions, requirements and test methods.

[89] BS EN 60584-1:1996, IEC 60584-1:1995. Thermocouples. Reference tables

[90] Kidd, C. T., Thin-Skin Technique Heat-Transfer Measurement Errors Due to Heat Conduction into Thermocouple Wires, ISA Transactions, Vol 24, No. 2, 1985.

[91] Jarrod John Alston. Room/Corner Fire Calibration Data: Marine Composite Screening Specimens (Page 160 - 164). Degree of Master of Science Thesis. Worcester Polytechnic Institute (USA). May 2004

[92] Incropera and DeWitt. Fundamentals of Heat and Mass Transfer, Willey 2001. 5th Edition. ISBN: 0471386502

[93] P.F. Lennon and G.W.H.Silcock, A Preliminary Investigation into the Partitioning of the Convective and Radiative Incident Heat Flux in Real Fires. Fire Technology Journal, 42, 109-129, 2006

[94] Jowsey A., Fire Imposed Heat Fluxes for Structural Analysis. PhD Thesis, The University of Edinburgh. 2006

[95] Sultan, M.A. Incident heat flux measurements in floor and wall furnaces of different sizes. Fire and Material Journal 30:383-396. 2006

[96] Chu, X., Ye, Z., Kettle, R. & Li, L. Buckling behaviour of cold-formed channel sections under uniformly distributed loads, Thin-Walled Structures 43, pp. 531-542, 2005

[97] Young, B. & Hancock, G. J. Cold-Formed Steel Channels Subjected to Concentrated Bearing Load, Journal of Structural Engineering, pp. 1003-1010, 2003

[98] Schafer, B. W. & Pekoz, T. Computational modeling of cold-formed steel: characterizing geometric imperfections and residual stresses, Journal of Constructional Steel Research 47, pp. 193-210, 1998

[99] Cheng, Y. & Schafer, B. W. Simulation of cold-formed steel beams in local and distortional buckling with applications to the direct strength method, Journal of Constructional Steel Research 63, pp. 581-590, 2007

[100] Pi, Y. L., Put, B. M. & Trahair, N. S. Lateral Buckling Strengths of Cold-Formed Channel Section Beams, Journal of Structural Engineering, pp. 1182-1191, 1998

[101] Schafer, B. W. Local, Distortional, and Euler Buckling of Thin-Walled Columns, Journal of Structural Engineering, pp. 289-299, 2002

[102] BS EN 1993-1-2:2005 . Eurocode 3. Design of steel structures. General rules. Structural fire design

[103] Telue, Y. K. & Mahendran M. Buckling behaviour of cold-formed steel wall frames lined with plasterboard, In Proceedings of the 4th International Conference on Steel and Aluminium Structures, Espoo Finland, pp. 37-44, 1999

[104] Telue, Y. K. & Mahendran M. Behaviour of cold-formed steel wall frames lined with plasterboard, Journal of Constructional Steel Research 57, pp. 435-52, 2001

[105] Telue, Y. K. & Mahendran M. Behaviour and design of cold-formed steel wall frames lined with plasterboard on both sides, Engineering Structures 26, pp. 567-579, 2004

[106] Salhab, B. & Wang, Y.C. An experimental study of the compressive performance of structural panels with cold-formed thin-walled perforate steel channels, 17th International Specialty Conference on Cold-Formed Steel Structures: Recent Research and Developments in Cold-Formed Steel Design and Construction, pp. 209-223, 2005

[107] Kesti, J. & Makelainen, P. Design of Gypsum-Sheathed Perforated Steel Wall Studs, J. Construct. Steel Res. Vol. 46, Nos. 1-3, pp. 215-216, paper number 116, 1998

[108] Tian, Y. S., Wang, J., Lu, T. J. & Barlow, C. Y. An experimental study on the axial behaviour of cold-formed steel wall studs and panels, Thin-Walled Structures 42, pp. 557-573, 2004

[109] Wang, J., Tian, Y. S. & Lu, T. J. The role of frame members and sheathing in partition wall panels subjected to compression, Thin-Walled Structures 43, pp. 983-1002, 2005

[110] Pham, M. M., Mills, J. E. & Zhuge, Y. Experimental Capacity Assessment of Cold-Formed Boxed Stud and C Stud Wall Systems Used in Australian Residential Construction, Journal of Structural Engineering, pp. 631-635, 2006

[111] Tian, Y. S., Wang, J. & Lu, T. J. Racking strength and stiffness of cold-formed steel wall frames, Journal of Constructional Steel Research 60, pp. 1069-1093, 2004

[112] BS EN 594:1996. Timber structures. Test methods. Racking strength and stiffness of timber frame wall panels

[113] Buonopane, S. G. & Schafer, B. W. Reliability of Steel Frames Designed with Advanced Analysis, Journal of Structural Engineering, pp. 267-276, 2006

[114] Benichoun, N. & Sultan, M.A. Thermal properties of lightweight-framed construction components at elevated temperatures. Fire and Materials journal 29:165-179, 2005.

[115] Harmathy, T.Z. Properties of Building Materials at Elevated Temperatures. Internal report National Research Council of Canada, Division of Building Research. 1983

[116] Wright, C., Gorgolewski M. T., Couchman G. H. & Lawson R. M. Steel Construction Institute Publication P343. Insulated Render Systems Used With Light Steel Framing. 2007

[117] Catalogue of Material Properties, International Energy Agency, report Annex XIV, Volume 3.